ALEX SANTOS DA SILVA

APLICAÇÃO DO RISCO POTENCIAL DE FOGO DA VEGETAÇÃO EM ESCALA GLOBAL

Tese apresentada à Universidade Federal de Viçosa, como parte das exigências do Programa de Pós-Graduação em Meteorologia Aplicada, para obtenção do título de *Doctor Scientiae*.

VIÇOSA
MINAS GERAIS – BRASIL
2019

Ficha catalográfica preparada pela Biblioteca Central da Universidade Federal de Viçosa - Câmpus Viçosa

T
S586a
2019

Silva, Alex Santos da, 1987-
Aplicação do risco potencial de fogo da vegetação em escala global / Alex Santos da Silva. – Viçosa, MG, 2019.
xiii, 120f. : il. (algumas color.) ; 29 cm.

Texto em português e inglês.
Orientador: Flávio Barbosa Justino.
Tese (doutorado) - Universidade Federal de Viçosa.
Inclui bibliografia.

1. Avaliação de risco de incêndio. 2. Zonas temperadas. 3. Vegetação e clima. 4. Modelos matemáticos. I. Universidade Federal de Viçosa. Departamento de Engenharia Agrícola. Programa de Pós-Graduação em Meteorologia Agrícola. II. Título.

CDD 22. ed. 628.925

ALEX SANTOS DA SILVA

APLICAÇÃO DO RISCO POTENCIAL DE FOGO DA VEGETAÇÃO EM ESCALA GLOBAL

Tese apresentada à Universidade Federal de Viçosa, como parte das exigências do Programa de Pós-Graduação em Meteorologia Aplicada, para obtenção do título de *Doctor Scientiae*.

APROVADA: 24 de junho de 2019.

Joana Nogueira Brockmeyer

Nelson Jesus Ferreira

Paulo José Hamakawa

Alberto Waingort Setzer
(Coorientador)

Flávio Barbosa Justino
(Orientador)

Dedico,

Ao Senhor Jesus Cristo, coroado de glória e de honra, que pela Graça de Deus, deu-me vida e vida com abundância.
Aos meus amados pais: Florêncio e Imaculada.

“Portanto, quer comais, quer bebais, ou façais outra coisa qualquer, fazei tudo para a glória de Deus.” Fonte: Bíblia Sagrada (1 Coríntios 10.31).

SUMÁRIO

LISTA DE FIGURAS

LISTA DE TABELAS

RESUMO

SILVA, Alex Santos da, D.Sc., Universidade Federal de Viçosa, junho de 2019. **Aplicação do risco potencial de fogo da vegetação em escala global**. Orientador: Flávio Barbosa Justino. Coorientador: Alberto Waingort Setzer.

O fogo em vegetação tem um papel fundamental no sistema climático global. Um passo importante para a redução de seus impactos é por meio de investigação da suscetibilidade à ocorrência de queimadas em vegetação, devido às condições atmosféricas. Portanto, o objetivo deste estudo é aprimorar o Índice de Risco Potencial de Fogo, "PFI" (JUSTINO et al., 2010) em escala global, particularmente nas regiões extratropicais. A nova versão do índice (PFIv2) inclui uma função de crescimento logístico ajustada para as três camadas atmosféricas do Índice de Haines (HAINES, 1988) e um fator de ajuste da temperatura devido à variação da latitude. Em sua formulação, o risco de fogo na vegetação aumenta com o aumento da duração de períodos secos, tipo e ciclo natural da fenologia da vegetação, convecção e estabilidade da atmosfera. Os dados atmosféricos da Reanálise ERA-Interim e de precipitação do CPC/NOAA (*Climate Prediction Center / National Oceanic and Atmospheric Administration*) foram aplicados como dados de entrada do modelo. As validações das análises foram realizadas com o auxílio dos dados de fogo ativo do satélite Terra do projeto MODIS/NASA (*Moderate Resolution imaging Spectrometer / Natonal Aeronautics and Space Administration*). Em condições atuais de tempo e da vegetação, o PFIv2 representou as principais áreas de risco de fogo de ambos os hemisférios. Na região tropical, o PFIv2 apresentou, em média, eficiência superior a 5% na detecção dos focos de queimadas, em relação ao PFI. Já nas regiões extratropicais, essa diferença atinge valores de até 15% nas principais classes dos índices. Nas avaliações da influência das variabilidades climáticas El Niño Oscilação Sul e Oscilação do Atlântico Norte no risco de fogo, correlações positivas e estatisticamente significativas a 95% foram obtidas na América do Sul e Europa, respectivamente. A confiabilidade do PFIv2 para a reprodução de áreas com alta atividade de fogo indica que este índice é uma ferramenta útil para os tomadores de decisões, em previsões de ocorrências globais de fogo em vegetação.

ABSTRACT

SILVA, Alex Santos da, D.Sc., Universidade Federal de Viçosa, June, 2019. **Application of the potential risk of vegetation fire on a global scale**. Adviser: Flávio Barbosa Justino. Co-adviser: Alberto Waingort Setzer.

Fire in vegetation plays a fundamental role in the global climate system. An important step towards reducing its impacts is by investigating the susceptibility to the occurrence of vegetation fires due to atmospheric conditions. Therefore, this study aims to improve the Potential Fire Index, "PFI" (JUSTINO et al., 2010) on a global scale, particularly in the extratropical regions. The new version of the index (PFIv2) includes a logistic growth function adjusted for three atmospheric layers from the Haines Index (HAINES, 1988) and a temperature adjustment factor due to latitudinal variation. On its formulation, the fire risk in vegetation increases with the increase in the duration of dry periods, type and natural cycle of the phenology of vegetation, convection and stability of the atmosphere. The atmospheric data of the ERA-Interim reanalysis and precipitation of the Climate Prediction Center (CPC / NOAA) were applied as input data of the model. The validations of the analyses were performed by the active fire data of the Terra satellite from Moderate Resolution Imaging Spectrometer / National Aeronautics and Space Administration (MODIS / NASA) project. In current conditions of weather and vegetation, the PFIv2 represented the main areas of fire risk in both hemispheres. In the tropical region, PFIv2 showed an average efficiency up to 5% in the detection of fire occurrences in relation to the PFI. In the extratropical regions, this difference reaches values of up to 15% over main classes of indices. In the evaluations of the influence of the climatic variabilities El Niño South Oscillation and North Atlantic Oscillation in the risk of fire, positive and statistically significant correlations at 95% were obtained in South America and Europe, respectively. The reliability of PFIv2 for the reproduction of areas with high fire activity indicates that this index is a useful tool for decision makers, in forecasting global fire occurrences in vegetation.

CAPÍTULO 1
INTRODUÇÃO GERAL

Um dos maiores responsáveis pelas mudanças climáticas é o incêndio em vegetação (GIGLIO et al., 2013). Este atua como um condutor de mudanças no ambiente natural. Impactos do fogo na vegetação são questões proeminentes que envolvem mudanças do clima passado e futuro (LYNCH et al., 2007; SCOTT, 2012).

De acordo com Laturner e Scherer (2004), na história evolutiva do homem este utiliza o fogo desde as eras mais remotas, todavia, nas últimas décadas cresceu a preocupação de vários setores da sociedade com o uso indiscriminado do fogo. Embora destrutivo, o poder das queimadas pode ser vital na saúde de alguns ecossistemas, ajudando a manter um equilíbrio entre as muitas variedades de vida vegetal e animal.

Em condições florestais, o fogo limpa o solo e permite que a vegetação restante prospere. Mantém a continuidade das pastagens, melhora os nutrientes e retarda a introdução de espécies de plantas lenhosas (CARROL et al., 2018). Em muitos ecossistemas, algumas espécies tornaram-se adaptadas ao fogo, onde este pode se propagar e sobreviver.

No entanto, variações ocorreram com a advento da agricultura. O homem passou a usar o fogo para limpar grandes extensões de terra para a agricultura. Ao longo do tempo, o fogo de origem antrópica rompeu o delicado equilíbrio nos ecossistemas tolerantes ao fogo e dizimou os ecossistemas que não eram tolerantes. Segundo Collins e Stephens (2010), neste processo, a vegetação apresenta quantidades crescentes de matéria orgânica disponíveis para queimar quando o fogo retorna, criando conflagrações mais intensas e mais destrutivas.

Associadamente, o efeito imediato da queima da vegetação é a produção e liberação de gases, como o dióxido de carbono (CO_2), monóxido de carbono (CO), hidrocarbonetos e outros, que retornam para a atmosfera em questão de horas. Em geral, estes gases são quimicamente ativos e interagem com as hidroxilas (OH) presentes na atmosfera, alterando a eficiência da oxidação e modificando a quantidade de ozônio troposférico (GALANTER et al., 2000).

As queimadas possuem um papel significante no balanço de CO_2 global (TOSCA et al., 2013; LI et al., 2014). Os gases do efeito estufa, oriundos da combustão nas vegetações intensificam o aquecimento da Terra e as mudanças climáticas globais. Sazonalmente, os impactos das queimadas, mesmo de intensidades equivalentes podem diferenciar-se amplamente dependendo do período fenológico em que ocorrem. Em grande parte dos trópicos, os incêndios predominantemente antrópicos, são geralmente limitados à estação seca ou períodos de seca incomum (períodos de El Niño ou La Niña nas mesmas regiões; HOFFMANN et al., 2009).

De acordo com o relatório da FAO "*Fire Management – Global Assessment 2006"*, a quantidade de biomassa queimada anualmente considerando todas as fontes é de cerca de 9,2 x 10^9 toneladas. Incêndios globais em vegetação consomem aproximadamente 5,1 x 10^9 toneladas; 42 % delas somente na África. Tais queimadas liberam cerca de 3,4 x 10^9 toneladas de CO_2 e outras emissões. Contudo, há sequestro de carbono atmosférico para a rebrota da biomassa vegetal e assim, em caso de desmate, o CO_2 gerado pelo incêndio contribui efetivamente para uma emissão líquida de carbono na atmosfera.

Segundo Costa e colaboradores (2007), a queima de biomassa nos ecossistemas devido à expansão da fronteira agrícola, à conversão de florestas e cerrados em pastagens, e à renovação de cultivos agrícolas são alguns dos mais importantes fatores que causam impactos sobre o clima e a biodiversidade. As queimadas ainda provocam o empobrecimento do solo, a destruição da vegetação, problemas de erosão e estão ligadas a alterações na composição química da atmosfera (YORK et al., 2012).

Sabe-se que a ocorrência de fogo depende da quantidade, volume e espaçamento dos materiais combustíveis no local, temperatura, velocidade e direção do vento. Estes estão relacionados com a transmissão de calor concomitante da condução, convecção e radiação (McRAE and SHARPLES, 2013). Contudo, existe um grande debate sobre a importância das forçantes climáticas e antropogênicas na contribuição para ignição de incêndios em vegetação. Nos extratrópicos, por exemplo, os incêndios representam o perigo antrópico mais importante principalmente na região Euro-Mediterrânea (EU-MED), onde uma média de 4,5 x 10^3 km^2 de áreas arborizadas e de mata

queimam anualmente (SAN-MIGUEL-AYANZ et al., 2013), causando consideráveis danos econômicos, ambientais e perda de vida.

A principal causa do fogo natural procede das atividades de raios. Globalmente, no entanto, a atividade humana é a que causa mais queimadas (WHITLOCK, 2004). A taxa média de queimadas em gramíneas e savanas gira em torno de 522,8 Mha ano^{-1}, principalmente na África, Austrália, América do Sul e sul da Ásia, enquanto que o remanescente ocorre em regiões florestais da Terra (MOUILLOT and FIELD, 2005).

De fato, a distribuição e as propriedades ecológicas de muitos biomas do mundo são afetadas significativamente pelos regimes de fogo (BOND et al., 2005). Weisse e Goldman (2018) mostraram que as perdas anuais de florestas verdes atingiram níveis de 29,7 x 10^9 hectares em 2016. Todavia, o desmatamento mostrou tendências de redução para o período compreendido entre agosto de 2016 e julho de 2017, devido às áreas de preservação ambiental e de planejamento ecológico.

Resumidamente, a ocorrência de incêndio na vegetação pode ser descrita como qualquer atividade de fogo sobre a paisagem que consome recursos naturais, independentemente da origem de ignição. Ele tem a capacidade de causar danos significativos a um ecossistema ou pode ajudar a mantê-lo, torná-lo mais resiliente. Contudo, o fogo florestal gerido é amplamente determinado pelas condições em que o fogo existe e os resultados esperados ou desejados dos esforços de gestão. Sistemas de classificação de risco de fogo permitem a avaliação das condições ambientais que contribuem para o perigo de incêndio (ou potencial) e distribuição do fogo (FOSBERG et al., 1996; STOCKS et al., 1996; JUSTINO et al., 2013).

Avanços recentes na modelagem de circulação acoplada atmosfera-oceano conduziram ao desenvolvimento de modelos numéricos de previsões climáticas (DOBLAS-REYES et al., 2013). O potencial de tais sistemas de previsão para informar aos tomadores de decisões, em diferentes setores econômicos, é enorme devido à provisão de um grande número de variáveis fisicamente consistentes, em uma escala temporal sub-diária de um a vários meses de antecedência (MANZANAS et al., 2014). Em se tratando de experimentos de sensibilidades, Whitlock et al. (2006) atribuíram às variações

do regime de fogo nos Andes argentinos o aumento interanual da variabilidade climática e a intensificação do El Nino Oscilação Sul (ENOS).

Apesar de ainda relativamente escassos na literatura, alguns estudos de modelagem foram conduzidos baseados no regime de fogo acoplado às dinâmicas da vegetação (SCHEITER & HIGGINS, 2009; THONICKE et al., 2010; JUSTINO et al., 2013). A maior parte deles usam muitos parâmetros que incluem métodos avançados para os cálculos da interação entre as características do solo, alocação de carbono, combustíveis e quantidade de umidade na liteira. Devido à necessidade de vários parâmetros, estes modelos complexos podem incluir também um nível considerável de incertezas em simular a biomassa combustível e a competição entre as plantas, o que levaria a uma falha na precisão entre os incêndios observados e previstos (HICKLER et al., 2006).

Assim, propõe-se o aprimoramento do Índice de Risco Potencial de Fogo (PFI) particularmente frente às regiões extratropicais. Essa é a segunda versão do PFI (PFIv2), que também se enquadra entre os modelos de complexidade intermediária. A calibração do PFIv2 foi regida pelos dados atmosféricos da Reanálise ERA-Interim (DEE et al., 2011) e pelos dados de precipitação do CPC (XIE et al., 2010). Já as validações, foram realizadas pelos focos de calor do satélite Terra MODIS (*Moderate Resolution Imaging Spectroradiometer*) da NASA (*National Aeronautics and Space Administration*).

1.2 Objetivo Geral

O objetivo geral da tese é aprimorar o Índice de Risco Potencial de Fogo, “PFI” (JUSTINO et al., 2010) em escala global, particularmente nas regiões extratropicais.

1.2.1 Objetivos específicos

- Identificação e aplicação de novas variáveis com potencial de melhora do desempenho do PFI;
- Verificação do impacto do uso do tradicional Índice de Haines implementado ao PFI;

- Análise da variabilidade climática global em relação ao PFI;
- Análise de acerto espacial do PFIv2 para as seis subregiões globais da Organização Meteorológica Mundial;
- Análise sazonal dos resultados do PFIv2.

1.3 Estrutura da Tese

Este trabalho é constituído de uma primeira parte, com introdução e objetivos apresentados no capítulo 1; o capítulo 2 contém a revisão de literatura sobre a dinâmica do clima, ocorrência do fogo na vegetação e seus impactos. O capítulo 3 descreve os dados utilizados, o Índice de Risco Potencial de Fogo (PFI) e, as modificações necessárias para melhoria do PFI nas regiões extratropicais (PFIv2). Esta parte conclui com as referências utilizadas em sua elaboração.

A segunda parte, que compõe os capítulos 4, 5 e 6 são os resultados, em termos comparativos e de artigos para publicação em revistas científicas, visando atender exigência do Programa de Pós-graduação em Meteorologia Aplicada da UFV. Ambos os artigos estão estruturados em estilo convencional para tais contextos: introdução, dados e metodologia, resultados e discussão, conclusões, agradecimentos e referências.

A terceira e última parte é constituída pelo capitulo 7, que aborda as conclusões e perspectivas do uso do PFIv2.

CAPÍTULO 2
ESTIMATIVAS DO RISCO DE FOGO EM VEGETAÇÃO

Um passo importante para a redução das queimadas é o uso da modelagem na investigação da suscetibilidade da vegetação ao fogo. No Hemisfério Norte, os Estados Unidos, Canadá e Rússia apresentam avanços nos métodos desde o início da década de 70. Seus avanços decorrem a partir das bases de temperatura e umidade relativa do ar a modelos complexos que calculam interações entre as características do solo, alocação de carbono, e o conteúdo de umidade na liteira (ARCHIBALD et al., 2009; BRADSTOCK, 2010).

Na América do Sul e Caribe, a equipe do Projeto Queimadas do Instituto Nacional de Pesquisas Espaciais (INPE) desenvolveu, com base na análise de ocorrência de centenas de queimadas, uma metodologia que relaciona as condições atmosféricas (temperatura, umidade e precipitação) e os tipos de vegetação na área de cada evento (SETZER et al., 2002). Atualmente, seus produtos e documentação são livremente obtidos em *http://www.inpe.br/queimadas/portal/risco-de-fogo-meteorologia*.

2.1 Índice logarítmico de Telicyn

Desenvolvido na União das Repúblicas Socialistas Soviéticas (URSS), este índice tem como variáveis as temperaturas do ar e do ponto de orvalho, ambas medidas às 13 horas. O índice é acumulativo, isto é: seu valor aumenta gradativamente, como realmente acontece com as condições de risco a incêndios, até que a ocorrência de uma chuva o reduza a zero, recomeçando um ciclo de cálculos, conforme a equação 2.1.

$$I = \sum_{i=1}^{n} \log\left(T_i - r_i\right) \qquad \text{(eq. 2.1)}$$

em que:

I = Índice de Telicyn;
r = temperatura do ponto de orvalho (°C);
T= temperatura do ar (°C);
log = logaritmo na base 10.

Neste índice, sempre que ocorrer uma precipitação igual ou superior a 2,5 mm, elimina-se a somatória e recomeça-se o cálculo no dia seguinte, ou quando a chuva cessar. Na presença de precipitação, o índice é nulo. Quanto ao grau de risco de fogo, o índice acumulativo apresenta 4 classes (Tabela 2.1).

TABELA 2.1. Grau do risco de fogo de Telicyn.

Valor de I	Grau de Risco
≤ 2,0	Nenhum
2,1 a 3,5	Pequeno
3,6 a 5,0	Médio
> 5,0	Alto

2.2 Índice de Nesterov

O sistema de taxa de risco de fogo mais utilizado na Rússia é um índice de ignição relativamente simples, denominado Índice de Nesterov (IN). Ele fornece um índice geral de ignição potencial (FOSBERG et al., 1996; STOCKS et al., 1996), baseia-se principalmente na inflamabilidade dos combustíveis, e não na velocidade de propagação do fogo. As variáveis atmosféricas para este índice são:

- ✓ Temperatura do bulbo seco;
- ✓ Temperatura do ponto de orvalho (extraída da umidade relativa e temperatura);
- ✓ Precipitação.

O índice é inicializado a zero e é determinado tomando-se a diferença entre as temperaturas diárias do ar (bulbo seco) e do ponto de orvalho, multiplica-se esta diferença pela temperatura do ar e então, cumulativamente somam-se os valores sobre o número de dias, desde que a precipitação tenha sido inferior a 3 mm. Na ocorrência de precipitação diária de 3 mm ou mais, o índice retorna a zero (BUCHHOLZ e WEIDEMANN, 2000). Este índice é expresso matematicamente por:

$$IN = \sum_{i=1}^{W} (T_i - D_i) \times T_i \qquad \text{(eq. 2.2)}$$

onde:

IN = Índice de Nesterov;

W = número de dias com precipitação até 3 mm;

T = Temperatura (°C);

D = Temperatura do ponto de orvalho (°C).

Em dias com chuva, onde a precipitação pluviométrica é igual ou maior a 3 mm, a inflamabilidade dos combustíveis se reduz substancialmente e o valor de $T_i - D_i$ é quase nulo. Segundo Pyne e colaboradores (1996), o IN é usado para agendar operações de queimadas diárias na Federação Russa. Posteriormente, o IN foi aperfeiçoado na Polônia. Mantendo-se o padrão acumulativo do índice, seu ajuste deu-se na consideração direta do DPV das 13 horas, mesmo horário das coletas da temperatura do ar (equação 2.3).

$$IN = \sum_{i=1}^{n} DPV_i \times T_i \qquad \text{(eq. 2.3)}$$

sendo:

IN = Índice de Nesterov;

DPV = déficit de pressão de vapor do ar (milibares);

T = temperatura do ar (°C).

O DPV, por sua vez, é igual a diferença entre a pressão máxima de vapor d'água e a pressão real de vapor d'água, sendo calculado neste caso, pela equação 2.4.

$$DPV = E \times \left(1 - \frac{H}{100}\right) \qquad \text{(eq. 2.4)}$$

em que:

E = pressão máxima de vapor d'água (milibares);

H = umidade relativa do ar (%).

Na adaptação polonesa, a continuidade da somatória do Índice de Nesterov é limitada pela ocorrência de uma série de restrições (Tabela 2.2).

TABELA 2.2. Restrições na continuidade da somatória do Índice de Nesterov.

Chuva (mm)	Modificação no cálculo (diário)
≤ 2,0	Nenhuma.
2,1 a 5,0	Abater 50% no valor de IN calculado na véspera e somar IN do dia.
5,1 a 8,0	Abater 50% no valor de IN calculado na véspera e somar IN do dia.
8,1 a 10,0	Abandonar a somatória anterior e recomeçar o cálculo.
> 10,0	Quando a chuva cessar.

A Tabela 2.3 apresenta a variação do grau de risco deste índice, mantidas as considerações originais.

TABELA 2.3. Classes e graus de risco de incêndios de Nesterov.

Classes de Perigo	Valores de Nesterov	Graus de Risco
I	≤ 300	Nulo
II	301 a 500	Pequeno
III	501 a 1000	Moderado
IV	1001 a 4000	Alto
V	> 4000	Extremo

2.3 Sistema de previsão de risco de incêndios florestais dos Estados Unidos

O sistema nacional de previsão de risco de incêndios florestais dos Estados Unidos (NFRDS) foi desenvolvido em 1972 e revisado em 1988, para incluir respostas quanto às condições de seca, sensibilidade sazonal, materiais combustíveis, condições do tempo e do clima (BURGAN, 1988). Os parâmetros observados do tempo que conduzem a formulação do NFDRS são:

- ✓ Temperatura do ar (F);
- ✓ Umidade Relativa (%);
- ✓ Cobertura de nuvem e tipo de precipitação;
- ✓ Velocidade média do vento a 6 metros (mph);
- ✓ Umidade do combustível;
- ✓ Duração da precipitação (horas);

- ✓ Quantidade de precipitação (polegadas);
- ✓ Temperaturas mínima e máxima do ar (F);
- ✓ Umidade relativa mínima e umidade relativa máxima (%).

No NFDRS, vinte modelos de combustíveis que representam os tipos de vegetação e combustível são derivados usando-se uma combinação de umidade do combustível morto (1 hora, 10 horas, 100 horas, e 1000 horas). O teor de umidade de combustível vivo e quatro classes de tamanho de combustível morto são calculados a partir dos dados meteorológicos e valores de umidade. De modo que o combustível inoperante é determinado pelo diâmetro da madeira ou do intervalo de queima. Vale destacar que a variável de velocidade do vento influencia diretamente o componente de espalhamento, mas não o de energia liberada (Figura 2.1).

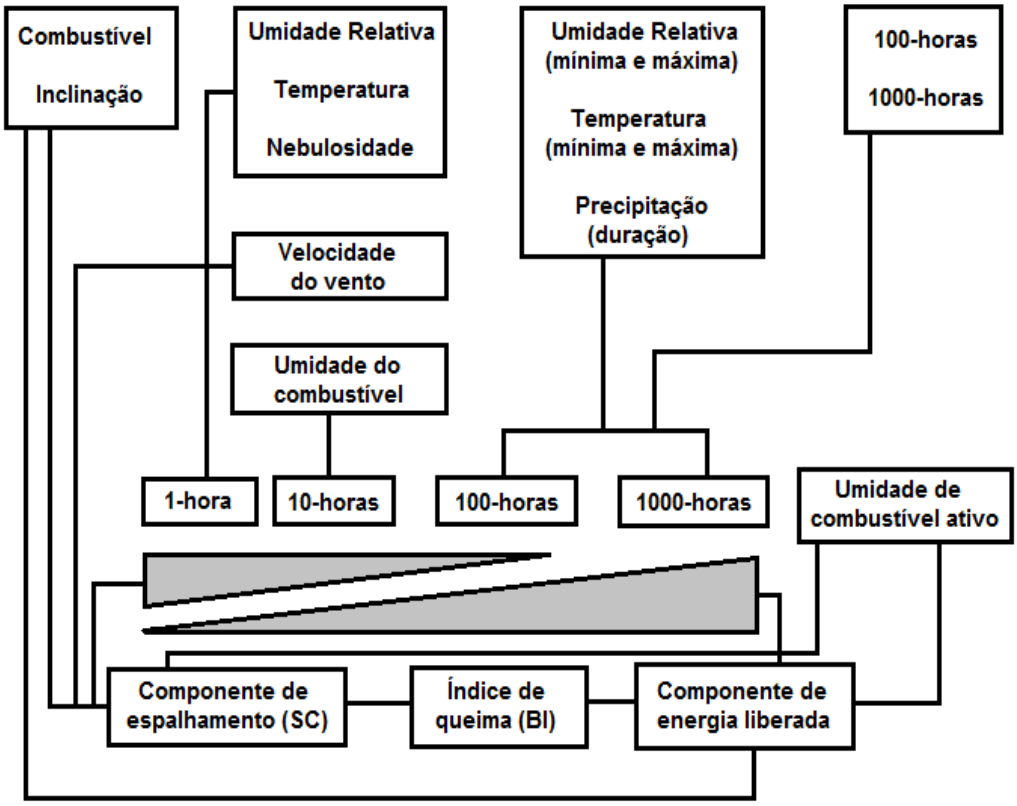

Figura 2.1. Fluxograma da estrutura do NFDRS. Os triângulos cinzas indicam as contribuições ponderadas das classes de combustíveis nos componentes de espalhamento e de energia liberada. Fonte: adaptado de Andrews e Bradshaw (1991).

Esse índice também possui os seguintes componentes de controle: queimadas antrópicas (MCOI); ocorrência de queimadas devido às atividades de raios (LOI) e; um índice de queima do material combustível por 0,3 m^2 (FLI). Uma descrição detalhada da evolução deste sistema de risco de fogo pode ser obtido em Hardy e Hardy (2007).

2.4 Índice de tempo e incêndios florestais do Canadá

De acordo com Stocks e colaboradores (1989), este sistema consiste de dois módulos: o índice de tempo e incêndios florestais canadenses (FWI, em inglês) e o sistema de previsão da evolução do fogo (FBP, em inglês). Possui um conjunto de tabelas que permitem estimar o perigo de incêndio correspondente a cada um dos principais tipos de combustíveis, com base nas observações de pluviosidade, umidade relativa do ar e velocidade do vento ao meio dia local. Algumas dessas tabelas permitem introduzir correções correspondentes a variações sazonais do estado da vegetação e da insolação. Embora existam tabelas para cada um dos principais tipos de combustíveis, a estrutura geral das tabelas para cada um dos principais tipos de combustíveis é a mesma. Tabelas especiais permitem correções relativas a regiões montanhosas, onde existem condições de grande secura, associadas à baixa umidade relativa noturna.

O módulo FWI é utilizado no Canadá desde 1970 e consiste de seis códigos detalhados de umidade e distribuição do fogo que contabilizam para com os efeitos de umidade de combustível e vento na evolução do fogo em um tipo de combustível padronizado (pinheiro maduro). Os componentes do sistema FWI são obtidos diariamente, considerando-se os seguintes parâmetros atmosféricos de entrada:

- ✓ Temperatura do Bulbo seco;
- ✓ Umidade Relativa (%);
- ✓ Velocidade do Vento (10 m);
- ✓ Precipitação acumulada (24 horas)

Os valores do índice apresentam uma relação direta com o grau de perigo de incêndios. O FWI consiste de dez tabelas que são agrupadas em seis blocos. Nos três primeiros blocos é analisado o efeito das condições meteorológicas sobre o conteúdo de umidade dos vários tipos de combustíveis orgânicos. Nos três últimos blocos são analisadas a quantidade de umidade acumulada e as características do comportamento do incêndio. No que tange a umidade, os componentes do FWI são:

- ✓ Quantidade de umidade de combustível (FFMC): refere-se à classificação numérica do conteúdo de umidade da camada orgânica e dos combustíveis finos existentes na floresta; (passo de tempo de 2/3 de um dia);
- ✓ Quantidade de umidade de turfa (DMC): refere-se à classificação numérica para a umidade média existente na camada orgânica não compacta com 2 a 4 polegadas de profundidade (passo de tempo de 12 dias);
- ✓ Grau de secura (DC): refere-se à classificação numérica da umidade média existente nas camadas orgânicas compactas e profundas. Esta quantificação deve ser utilizada como um guia nas atividades de supressão e preparação de longo prazo, em grandes áreas (passo de tempo de 52 dias).

Em se tratando dos três últimos blocos, tem-se:

- ✓ Índice de propagação inicial (ISI): refere-se à classificação numérica da velocidade do incêndio (taxa de propagação), imediatamente após a ignição, em um determinado tipo de material combustível;
- ✓ Ajuste da quantidade de umidade da turfa (BUI): refere-se à classificação numérica da quantidade de material combustível disponível para a combustão. Esta quantificação é adequada para uso como um guia nas atividades de preparação de curto prazo;
- ✓ Índice meteorológico de incêndios (FWI): refere-se à classificação numérica da intensidade potencial do incêndio em um determinado

tipo de combustível. Esta quantificação é um guia para as atividades diárias de preparação e supressão.

O constituinte orgânico avalia a camada húmus na superfície da floresta, que consiste da decomposição da liteira (folhas e outras vegetações mortas) e do solo mineral. Combustível na superfície inclui árvores maiores do que 2 metros; vegetação de gramíneas; liteira da superfície da floresta, e material de madeira. Os três componentes de umidade adicionam umidade para chuva e subtraem umidade para seca. Apesar dos três códigos possuírem diferentes escalas de tempo, taxas, e quantidades de precipitação necessárias para a saturação, qualquer um deles pode ser alto ou baixo em ralação aos outros.

O FWI surge da combinação entre o ISI e o BUI (Figura 2.2), que representa uma medida relativa da intensidade potencial de uma única propagação do fogo com uma fonte de combustível padrão, no nível do terreno. Cada um dos componentes do sistema FWI precisa ser examinado por uma interpretação adequada dos efeitos das queimadas passadas e presentes na inflamabilidade do combustível. Os componentes transmitem individualmente, informações diretas sobre o fogo potencial florestal.

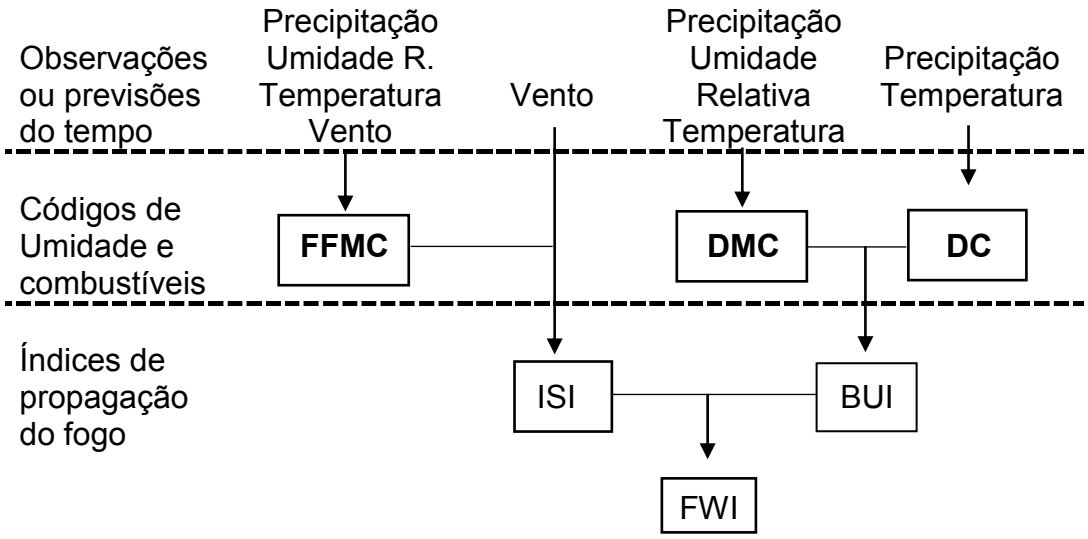

Figura 2.2. Estrutura do Índice de tempo e incêndios do Canadá (FWI).

O FWI atua com uma escala numérica de intensidade do fogo e possui as seguintes classes de risco: baixo, moderado, alto, muito alto e extremo

(Tabela 2.4). Ele combina o índice de propagação inicial e o índice de crescimento do fogo. Paralelamente, o risco de fogo é um índice relativo de quão fácil ocorre a ignição na vegetação, quão difícil o incêndio pode ser controlado, e quantos danos a queimada pode causar.

TABELA 2.4. Classes, escala numérica e características do FWI.

Classes	**Escala**	**Características**
Baixo	0 a 5	Focos auto extintos; fraca ignição
Moderado	6 a 10	Queimadas superficiais; fácil controle
Alto	11 a 20	Fogo vigoroso em superfície
Muito Alto	21 a 30	Carece de suporte aéreo para a contenção
Extremo	> 30	Rápida propagação; controle improvável

Na última década, modelos conceituais que levam em conta o tipo do ecossistema, e modelos de fogo baseados nas equações de balanço de energia e combustível, incluindo físicas de combustão detalhadas e dados de assimilação também foram empregados aos modelos de risco de fogo (MEYN et al., 2007; MANDEL et al., 2008). Quase sempre, contudo, tais modelos exigem um alto custo computacional. Semelhantemente, essa exigência seria necessária no uso do FWI devido à quantidade de variáveis envolvidas, o que também poderia gerar incertezas cumulativas. Já o IN, cuja dinâmica é mais simples, falharia com pequenas variações espaciais.

Por isso, a motivação de se propor um aprimoramento do PFI com características exponenciais, contínuas e orbitais, que também considere limiares específicos do IH para as diferentes latitudes, inclusive nas regiões extratropicais. A vantagem de utilizá-lo está no fato de se tratar de um modelo de complexidade intermediária, que representa a suscetibilidade ao fogo com variáveis atmosféricas e da vegetação acessíveis globalmente.

CAPÍTULO 3
DADOS UTILIZADOS E DESCRIÇÃO DO MODELO DE RISCO DE FOGO

3.1 Reanálise e dados observados

Dados de temperatura do ar e de umidade relativa da reanálise ERA-Interim, de precipitação do Centro de Previsões Climáticas (CPC/NOAA), classificação dos tipos de ocupação do solo do IGBP (*International Geosphere-Biosphere Programme*) e produtos de fogo da sexta coleção de imagens espectrômetras de resolução moderada do sensor Terra/*MODIS* foram utilizados para calibrar e validar as simulações diárias do risco de fogo (2001-2018):

(i) ERA-Interim (DEE et al., 2011), versão recente de reanálise atmosférica produzida pelo Centro Europeu de Previsão do Tempo de meso-escala (ECMWF, em inglês). A resolução espacial dos dados é a grade Gaussiana reduzida N128, que é simétrica em torno do equador, com um espaçamento aproximadamente uniforme na direção norte-sul, girando em torno de 0,703° entre as latitudes. Contabilizam-se 128 pontos alinhados ao longo do Meridiano de Greenwich, desde o equador até o polo em ambos os hemisférios. Já o número de pontos na direção leste-oeste varia com a latitude, com o espaçamento de grade uniforme de 0,703125° somente nas regiões dos trópicos. Os dados e todos os detalhes intrínsecos estão disponíveis em httpd://apps.ecmwf.int/datasets/data/interim-full-daily/levtype=pl/.

(ii) A resolução espacial do CPC (XIE et al., 2010) é de 0,5° de latitude e longitude, na superfície da Terra. Essa análise inclui assimilação de dados observados de precipitação diária, usando registros de aproximadamente 30.000 estações que são administradas por múltiplas agências. Registros históricos, observações independentes de estações vizinhas, radares e satélites, assim como previsões de modelos numéricos são aplicados no controle de qualidade dos dados.

(iii) Classificação dos tipos de ocupação da terra do IGBP (CHANNAN et al., 2014), dados reprojetados nas coordenadas geográficas de latitude e longitude do sistema de referência EPSG: 4326. São espacialmente agregados no período 2001-2012 em duas resoluções: 5'x5' (1776 linhas x 4320 colunas; aproximadamente 0,083°) e; 0,5° (296 linhas x 720 colunas). Detalhes e tabela de classificação do método podem ser obtidos em http://glcf.umd.edu/data/lc/.

(iv) Terra / MODIS (*Moderate Imaging Spectroradiometer*) (GIGLIO et al., 2016), produtos de fogo da sexta coleção de imagens espectrômetras de satélite com resolução moderada. No processamento destes dados, incluem-se algoritmos para eliminação de alarmes falsos, causados pelos desmatamentos de pequenas florestas, precisão na detecção de incêndios de escala espacial reduzida, ajuste quanto à presença de nebulosidade e rejeição expandida de brilho do sol. Seus produtos são definidos em uma grade senoidal da Terra às escalas espaciais de 250-m, 500-m, ou 1-km. Pelo fato das grades serem grandes em sua totalidade (43.200 x 21.600 píxeis a 1 km, e 172.800 x 86.400 píxeis a 250 m), elas são divididas em células fixas de aproximadamente 10° x 10° de dimensões. A cada célula é atribuída uma coordenada horizontal e uma coordenada vertical, variando de 0 a 35 e 0 a 17, respectivamente. A célula no canto superior a esquerda (mais a noroeste) é numerada por (0,0). Fonte disponível em https://earthdata.nasa.gov/earth-observation-data/near-real-time/firms/active-fire-data.

Para a viabilização dos cálculos nas células de grade, um ajuste nos dados de entrada do modelo (reanálise e vegetação) foi realizado através de interpolação bilinear, alterando as resoluções espaciais para 1° de latitude e longitude. As variáveis meteorológicas diárias utilizadas foram: precipitação, temperatura do ar, temperatura do ponto de orvalho e umidade relativa.

3.2 Índice de Risco Potencial de Fogo (PFI)

O PFI foi desenvolvido internamente no Centro de Previsão do Tempo e Estudos Climáticos (CPTEC), com base na análise de ocorrência de centenas de queimadas nos principais biomas (tipos de vegetação) do Brasil, em função

das condições e históricos meteorológicos na área de cada evento (SETZER et al., 2002). Toda a documentação do método está disponível no Portal do Monitoramento de Queimadas e Incêndios do Instituto Nacional de Pesquisas Espaciais (INPE), em *http://www.inpe.br/queimadas*.

O princípio do PFI é que quanto mais dias sem chuva, maior o risco de queimada da vegetação; adicionalmente, são incluídos no cálculo o tipo e o ciclo natural de desfolhamento da vegetação, temperatura máxima e umidade relativa mínima do ar, assim como a presença do fogo na região de interesse. A referência dos cálculos está nos "Dias de Secura" (DS), que é um número hipotético de dias sem nenhuma precipitação durante os últimos 120 dias (JUSTINO et al., 2010), respeitando as seguintes etapas:

1. Determina-se diariamente para a área geográfica de abrangência, o valor da precipitação, em milímetros (mm), acumulada para onze períodos imediatamente anteriores a 1; 2; 3; 4; 5; 6 a 10; 11 a 15; 16 a 30; 31 a 60; 61 a 90; e 91 a 120 dias.
2. Calculam-se os "fatores de precipitação" (FPs), cujos valores variam de 0 a 1 para cada um dos 11 períodos, utilizando-se uma função exponencial empírica de precipitação, em milímetros, para cada período. As respectivas equações são:

$$FP_1 = exp(-0,14Prec) \quad \text{(eq. 3.1)}$$
$$FP_2 = exp(-0,07Prec) \quad \text{(eq. 3.2)}$$
$$FP_3 = exp(-0,04Prec) \quad \text{(eq. 3.3)}$$
$$FP_4 = exp(-0,03Prec) \quad \text{(eq. 3.4)}$$
$$FP_5 = exp(-0,02Prec) \quad \text{(eq. 3.5)}$$
$$FP_{6-10} = exp(-0,01Prec) \quad \text{(eq. 3.6)}$$
$$FP_{11-15} = exp(-0,008Prec) \quad \text{(eq. 3.7)}$$
$$FP_{16-30} = exp(-0,004Prec) \quad \text{(eq. 3.8)}$$
$$FP_{31-60} = exp(-0,002Prec) \quad \text{(eq. 3.9)}$$
$$FP_{61-90} = exp(-0,001Prec) \quad \text{(eq. 3.10)}$$
$$FP_{91-120} = exp(-0,0007Prec) \quad \text{(eq. 3.11)}$$

3. *Calculam –se os "Dias de Secura" (DS):*

$$DS = 105 \times (FP_1 \times FP_2 \ldots \times FP_{61\text{-}90} \times FP_{91\text{-}120}) \qquad \text{(eq. 3.12)}$$

4. Determinar o risco de fogo potencial básico (RB) para cada um dos tipos de vegetação considerada, usando a seguinte equação:

$$RB_{n\text{-}0,16} = 0,9 \times (1 + \sin(A_{n\text{-}0,16} \times DS)) / 2 \qquad \text{(eq. 3.13)}$$

A Tabela 3.1 mostra os dezessete tipos de vegetação do Programa Internacional de Geosfera e Biosfera (CHANNAN et al., 2014) e suas respectivas constantes de inflamabilidade "$A_{n\text{-}0,16}$".

TABELA 3.1. Valores da constante de inflamabilidade "*A"* e tipos de vegetação.

Ordem	Vegetação	A
0	Porções de água *	-x-
1	Florestas Contato; Campinarana	2
2	Ombrófila densa; alagados	1,5
3	Florestas Decíduas; Campinarana	2
4	Florestas Decíduas e sazonais	1,72
5	Florestas Mistas	2
6	Caatinga fechada	2,4
7	Savana; Caatinga aberta	3
8	Savana arbórea	2,4
9	Savana	3
10	Pastagens Gramíneas	6
11	Alagados permanentes	1,5
12	Agricultura e diversos	4
13	Áreas urbanas e construídas *	-x-
14	Agricultura; vegetações naturais	4
15	Neve e gelo *	-x-
16	Solos expostos e mineração *	-x-

* valores indeterminados de *A*. Para estas classes, o RB é nulo.

A Figura 3.1 ilustra a variação do RB para os tipos de vegetação de mesma constante *A*. O princípio básico deste método está no cálculo dos "dias de secura", que indica tanto um período real de dias sem chuva, como também um período hipotético sem chuva calculado a partir da quantidade e distribuição temporal das chuvas ocorridas. Resumindo, para um mesmo número de dias sem chuva, uma pastagem terá o RB maior ao de uma floresta.

O RB tem valor máximo 0,9, e aumenta conforme uma curva senoidal ao longo do tempo. Atribuiu-se a função senoidal devido à semelhança da variação da intensidade e duração da luz solar ao longo do ano, adicionado a fenologia da vegetação que naturalmente tende a seguir o mesmo ritmo.

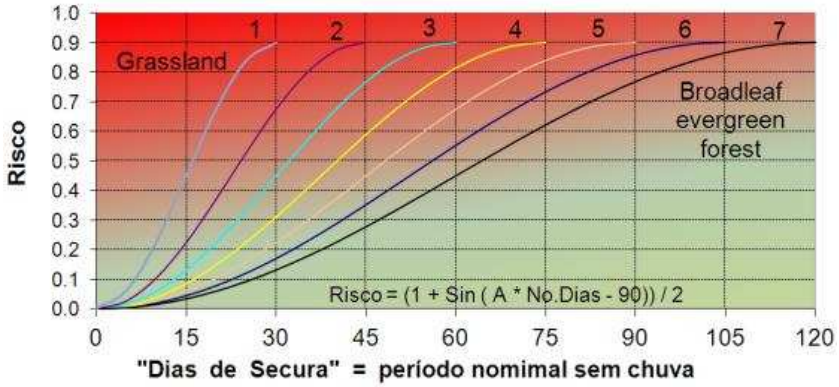

Figura 3.1. Variação senoidal do Risco Básico *RB* em função dos dias de secura *DS* para sete classes de vegetação. Neste caso, sem precipitação, todos os fatores de precipitação assumem valor 1,0.

5. Dois outros fatores são considerados para o cálculo do índice de risco de fogo potencial (PFI): a umidade relativa mínima (UR_{min}) e a temperatura máxima do ar (T_{max}), ambas observadas às 18h UTC. O risco aumenta (diminui) para UR_{min} abaixo (acima) de 40% e T_{max} acima (abaixo) de 30° C.

$$PFI = RB \times (a \times UR_{min} + b) \times (c \times T_{max} + d) \qquad \text{(eq. 3.14)}$$

onde, as constantes valem: a = -0,006; b = 1,3; c = 0,02 e d = 0,4. A Tabela 3.2 mostra as categorias para os níveis do PFI.

TABELA 3.2. Categorias do PFI.

Risco	*Mínimo*	*Baixo*	*Médio*	*Alto*	*Crítico*
PFI	< 0,15	0,15 < 0,4	0,4 < 0,7	0,7 < 0,95	≥ 0,95

Vale destacar que as parametrizações propostas pelo PFI não representam coerentemente a distribuição de risco de fogo potencial nas faixas extratropicais, devido às diferenças dos padrões de precipitação e temperatura entre a região equatorial e as demais latitudes (JUSTINO et al., 2013). Portanto, faz-se necessário a inserção de conceitos compatíveis aos padrões climáticos dos extratrópicos, que serão extraídos do Índice de Haines.

3.3 Índice de Risco Potencial de Fogo versão 2 (PFIv2)

O PFIv2 é uma busca de aprimoramento do PFI (JUSTINO et al., 2010). Sua base é mantida, porém acrescentam-se o Índice de Haines (HAINES, 1988) acoplado a função de crescimento logístico e um fator de correção da temperatura devido à variação da latitude, visando estimativas do risco de fogo coerentes às observadas em regiões extratropicais, cujos limiares de temperatura e umidade relativa do ar são totalmente distintas das faixas equatorial e tropical. Vale mencionar que o PFIv2 é de complexidade intermediária, pois preenche a lacuna entre os modelos mais simples e aqueles extremamente complexos.

Os modelos mais simples usam somente temperatura e umidade relativa para informar um índice relativo à condição inicial do fogo potencial (Índices de Angstron, Nesterov e Telicyn). Já os mais complexos, como aqueles desenvolvidos nos Estados Unidos e Canadá (*National Fire-Danger Rating System, NFRDS; Fire Weather Index, FWI; Fire Behavior Prediction System, FBP*) combinam medições de combustíveis, topografia, condições do tempo e risco de ignição devido à contribuição antropogênica ou natural.

O Índice de Haines (IH) segue uma linha que combina dois fatores atmosféricos importantes dentro de um modelo simplificado que razoavelmente indica as áreas mais susceptíveis ao fogo, sendo extensivamente utilizado por institutos de tempo e fogo nos Estados Unidos e Canadá. O IH estima a severidade do incêndio na superfície da floresta baseado nas taxas de

variações verticais da temperatura e umidade (WINKLER et al., 2005; POTTER, 2018). Seus cálculos dão-se pela combinação das três camadas da atmosfera (Baixa, Média e Alta), somando-se os termos de estabilidade e umidade do ar (Tabela 3.3).

TABELA 3.3. Cálculos dos termos A e B do Índice de Haines, conforme a elevação local.

Elevação (m)	**Componente de estabilidade (A)**		**Componente de umidade (B)**	
	Cálculos (hPa)	*Categorias*	*Cálculos (hPa)*	*Categorias*
Baixa (≥ 1500)	T950–T850	A=1 se < 4°C A=2 se 4-7°C A=3 se ≥ 8°C	T850–Td850	B=1 se < 6°C B=2 se 6-9°C B=3 se ≥ 10°C
Média (1500 a 3500)	T850–T700	A=1 se < 6°C A=2 se 6-10°C A=3 se ≥ 11°C	T850–Td850	B=1 se < 6°C B=2 se 6-12°C B=3 se ≥ 13°C
Alta (≥ 3500)	T700–T500	A=1 se < 18°C A=2 se 18-21°C A=3 se ≥ 22°C	T700–Td700	B=1 se < 15°C B=2 se 15-20°C B=3 se ≥ 21°C

Os componentes A e B são então somados, e o resultado do IH varia de 2 (risco muito baixo de crescimento de fogo) a 6 (risco alto). Contudo, tais limiares do IH serão redefinidos, em termos de temperatura do ar (JUSTINO et al., 2010). Contudo, a aplicação isolada do IH é incompleta, devido à ausência de uma base científica mais robustas (POTTER, 2018).

Por isso, em cada camada atmosférica do IH será aplicada a função de crescimento logístico nos termos de estabilidade e umidade do ar. Esta função considera um crescimento exponencial adicionado a uma capacidade limitante. Sua avaliação dá-se quanto às suas características matemáticas e quanto ao método de estimar seus parâmetros. A ideia da equação de crescimento logístico foi adaptada daquela inicialmente utilizada para a representação do crescimento animal e vegetal (SOUZA e FREITAS, 2014).

Sabe-se que as variáveis de umidade relativa mínima e de temperatura máxima são inversamente proporcionais e geram mutuamente uma contribuição exponencial para o crescimento da existência do fogo. Já a capacidade limitante, é o valor que representa o limite máximo do somatório

dos parâmetros de estabilidade (A) e umidade (B) para cada camada atmosférica do IH (Equação 3.15).

$$F_{i=0,05}^{i=1,05} = \left(\frac{K \times F_{i-0,05}}{F_{i-0,05} + (K - F_{i-0,05}) \times e^{-0,05r}} \right) \qquad \text{(eq. 3.15)}$$

onde:

F₀ é o valor mínimo do parâmetro de estabilidade (s) do IH;

r é a diferença entre o valor máximo do parâmetro de umidade (q) e o valor mínimo do parâmetro de estabilidade (s) do IH, em cada camada da atmosfera;

F é a conversão do IH em uma equação contínua (°C);

K é o fator limitante, que representa o valor máximo da soma de ambos os parâmetros do IH (umidade e estabilidade da atmosfera). Vale mencionar, que este cálculo também é para cada camada da atmosfera (Equação 3.16):

$$K = \begin{cases} 2 \times (s_{max} + q_{max}) = 36 \\ se: e \leq 1500\,m \\ 1,5 \times (s_{max} + q_{max}) = 36 \\ se: 1500\,m < e \leq 3500\,m \\ 1,0 \times (s_{max} + q_{max}) = 43 \\ se: e \geq 3500\,m \end{cases} \qquad \text{(eq. 3.16)}$$

Neste caso, o sistema combina os parâmetros A e B de cada camada do IH a um nível limitante, onde o crescimento da suscetibilidade ao fogo pela atmosfera é retido, devido à umidade e à estabilidade vertical da atmosfera.

Assim, o crescimento exponencial diminui e eventualmente se nivela a um estado de equilíbrio (Figura 3.2).

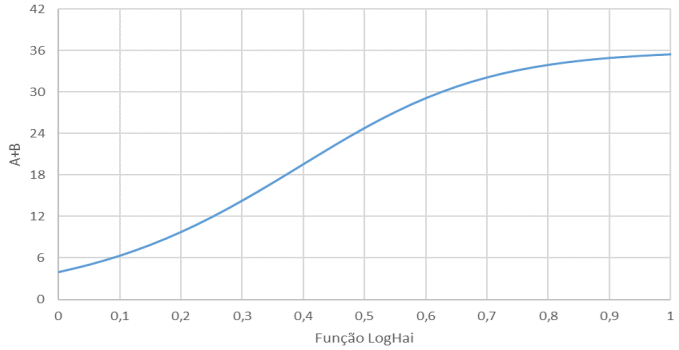

Figura 3.2. Função de crescimento logístico da variação total do IH. Apenas para a camada mais baixa do IH, altura inferior ou igual a 1.500 m.

Em termos analíticos, a função de crescimento logístico (FL) do IH é dada por:

$$FL = \begin{cases} 7\times10^{-5}\times W^3 - 0{,}0035\times W^2 + 0{,}072\times W - 0{,}26 \\ se: e \le 1500\,m \\ 1\times10^{-4}\times W^3 - 0{,}0056\times W^2 + 0{,}115\times W - 0{,}53 \\ se: 1500\,m < e \le 3500\,m \\ 9\times10^{-5}\times W^3 - 0{,}0067\times W^2 + 0{,}196\times W - 1{,}89 \\ se: e \ge 3500\,m \end{cases} \quad \text{(eq. 3.17)}$$

Em que, *W* é a soma dos parâmetros de estabilidade e umidade do IH (°C) e, o termo "*e*" é a elevação local (m).

Na sequência, um fator de correção da temperatura do ar, devido às variações da latitude também é incluído (Equação 3.18):

$$F_{orb} = (0{,}003 \times |Lat| + 1) \qquad \text{(eq. 3.18)}$$

O parâmetro |Lat| é o modulo da latitude. Finalmente, o PFIv2 é computado agregando-se todos os parâmetros, conforme a Equação 3.19.

$$PFIv2 = BR \times (a2 \times LF + b) \times (RT \times F_{orb}) \qquad \text{(eq. 3.19)}$$

Onde *b* = 1,3 e as variáveis BR e RT são as mesmas do PFI (JUSTINO et al., 2010; 2013), mas a constante *a2* = 0,006. O termo *(a2 x LF + b)* é o fator de impacto da função logística de Haines (Loghai). É importante mencionar que o PFIv2 mantém as mesmas categorias do PFI, com os valores variando de 0 a 1 (Tabela 3.2).

CAPÍTULO 4
COMPARAÇÕES ENTRE AS ESTIMATIVAS DO PFI E DO PFIV2

As avaliações do PFI e do PFIv2 foram realizadas globalmente, no período 2001-2016, para seis regiões da Organização Meteorológica Mundial (Figura 4.1): *(I)* África (45°S:36°N; 20°O:60°L); *(II)* Ásia (0:66°N; 60:180°L); *(III)* América do Sul (60°S:15°N; 90:30°O); *(IV)* Americas e Caribe (15:66°N; 180:50°O); *(V)* Pacífico Sudoestec (50°S:0; 90:180°L) e; *(VI)* Europa (36:66°N; 20°O:60°L).

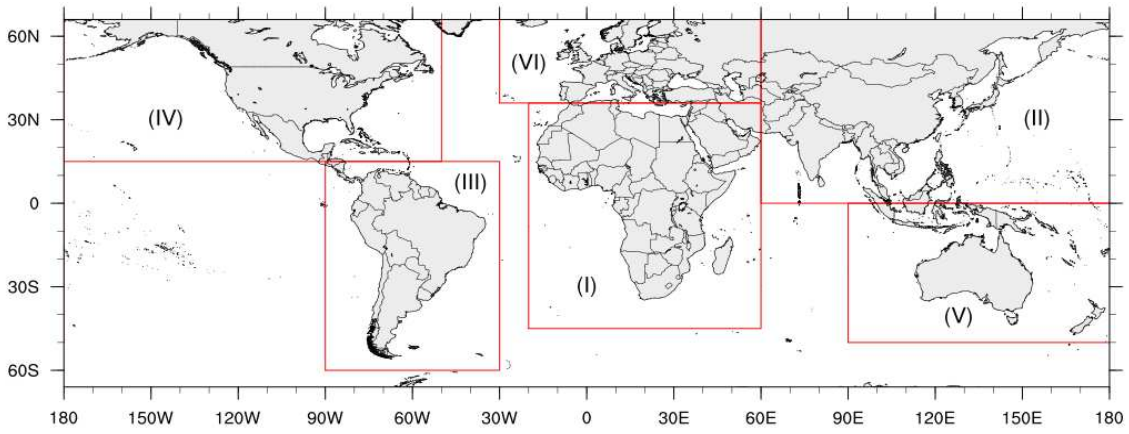

Figura 4.1. Áreas de estudo. Fonte: adaptado da OMM.

4.1 Ocorrências de queimadas no período 2001-2016

As ocorrências de queimadas detectadas pelo satélite Terra/MODIS foram computadas e reclassificadas sazonalmente durante o período 2001-2016 (Figura 4.2), para três diferentes intervalos: Novembro-Dezembro-Janeiro-Fevereiro (NDJF); Março-Abril-Maio-Junho (MAMJ) e; Julho-Agosto-Setembro-Outubro (JASO). Estes intervalos enfatizam as características periódicas das ocorrências de incêndios interanuais, nos níveis mínimo, intermediário e máximo.

Na Figura 4.2, pode-se observar que o período JASO apresenta as maiores incidências de queimadas, em escala global. As Figuras 4.2(a)-(c) mostram que as maiores ocorrências de queimadas são de julho a fevereiro na África, com ocorrências superando 1 milhão de registros, em anos específicos. Um período de transição é verificado no período MAMJ, com cerca de 300 mil queimadas por ano, caracterizando-se como uma estação de poucos incêndios. A alta atividade de queimadas na África (Figura 4.2c) é relacionada às práticas de conversão da vegetação natural em pastagem e outros propósitos agrícolas (SILVA et al., 2003).

As ocorrências de queimadas na Ásia são mostradas nas Figuras 4.2 (d)-(f). Durante o intervalo NDJF, os ventos no continente africano são predominantemente de sul e a precipitação se desloca para a Ásia, contribuindo com a redução e homogeneidade das queimadas (Figura 4.2d). Quando a intensidade de radiação solar se eleva na Ásia (Figura 4.2e), os ventos equatoriais tornam-se de norte e a monção asiática anula a atividade de

fogo. Adicionalmente, o sudoeste asiático é geralmente seco e quente, o que também contribui para o aumento de ocorrências de queimadas (WOLFSON, 2012). No verão boreal, há uma redução nas atividades de fogo (Figura 4.2f), devido à incidência dobrada na precipitação máxima, pelas áreas de monção (SERREZE & BARRY, 2010).

Em relação à distribuição dos focos de queimadas na América do Sul, as Figuras 4.2(g)-(h) mostram um padrão estável de novembro a junho, com valores médios, girando em torno de 180 mil. Durante o período JASO (Figura 4.2i), a região central do Brasil experimenta condições extremas de seca. Destaca-se também que os máximos valores de temperatura em superfície ocorrem nos meses de Setembro e Outubro e a incidência de focos de queimadas aumenta. A variabilidade interanual do fogo na América do Sul responde a fase positiva (negativa) da Oscilação do El Niño (ENOS) tais como em 2001, 2009 e 2014 (in 2005, 2007, 2008 e 2010). Estudos recentes associam o aumento da ocorrência de queimadas às mudanças antropogênicas da vegetação (SILVA et al., 2003; DAVIDSON et al., 2012; SPERA et al., 2016).

De acordo com as Figuras 4.2(j)-(l), a incidência de fogo na América do Norte e Caribe tende a ser estável de julho a fevereiro, quando as observações máximas se aproximam de 100 mil queimadas, no período 2001-2016. Recentemente, Van der Werf e colaboradores (2017) sugerem que as espécies vegetativas da América do Norte possuem níveis intensos de combustíveis, favorecendo as ocorrências de queimadas.

Na região do Pacífico Sudoeste (Figuras 4.2m-o), a baixa variação de atividade de fogo ocorre no intervalo MAMJ (Figura 4.2n). Por outro lado, variações interanuais são notórias nos períodos mais favoráveis ao fogo: NDJF (Figura 4.2m) e JASO (Figure 4.2o). Estas variações se intensificam, principalmente devido ao ciclo sazonal nas latitudes centrais da Austrália, que é defasada por aproximadamente um ou dois meses daquelas localizadas nas latitudes ao norte, cujos máximos ocorrem de novembro a janeiro, e os mínimos de abril a junho. Nas regiões ao sul da Austrália, o ciclo sazonal é atrasado em relação aos das latitudes centrais, com máximos geralmente de dezembro a fevereiro e, mínimos de junho a agosto. De fato, estas diferenças

são associadas com os incêndios em vegetação que são raros em alguns combustíveis, devido às características das plantas (CRUZ et al., 2018).

Embora as condições ambientais e dos atributos de vegetação sejam relativamente similares na Europa e América do Norte (WOOSTER & ZHANG, 2004), as ocorrências de queimadas não são padronizadas, como mostrado nas Figuras 4.2 (p)-(r). Destaca-se que apesar do aumento na ocorrência de fogo em outubro e novembro, uma tendência negativa é observada no intervalo JASO (Figura 4.2r).

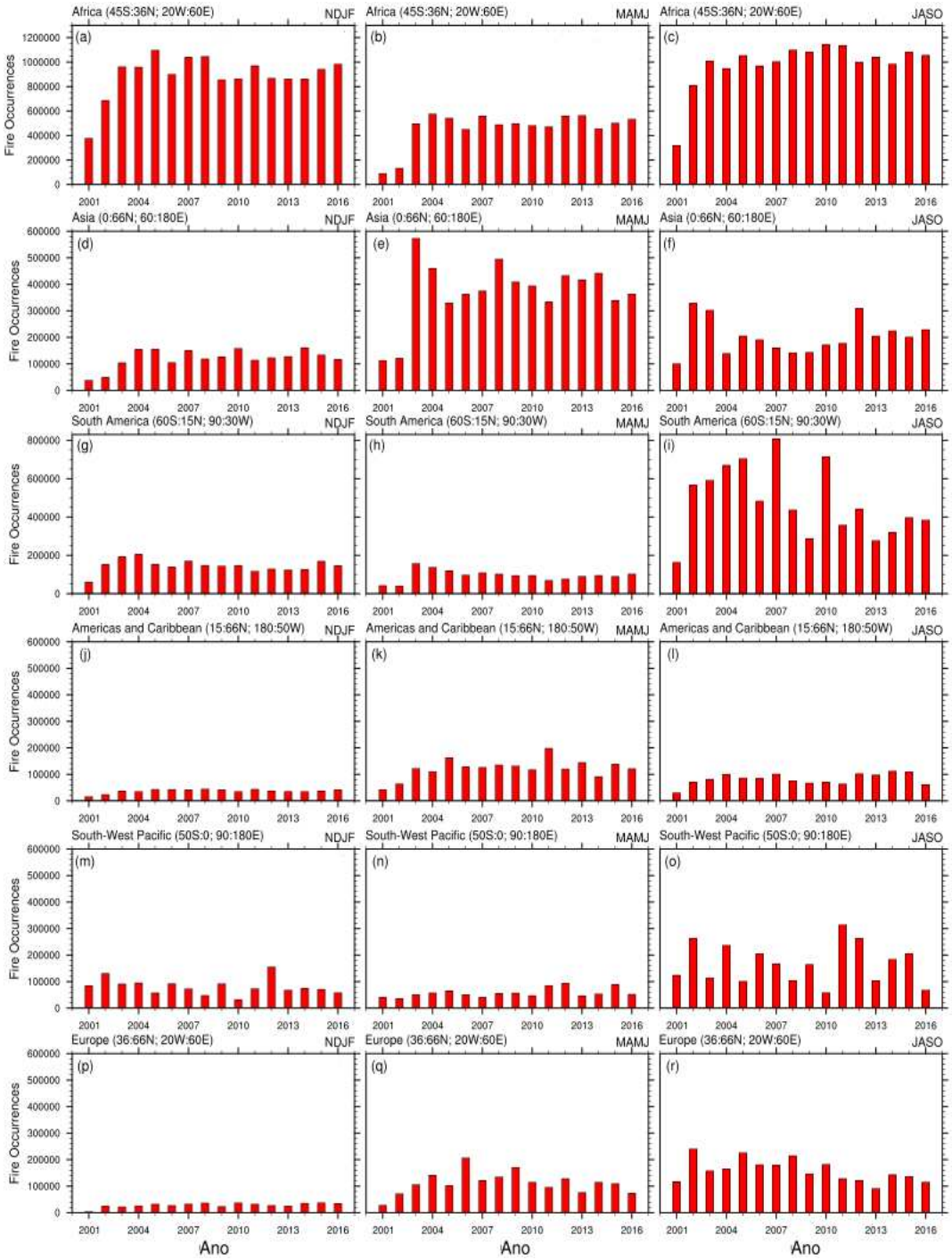

Figura 4.2. Sazonalidade das ocorrências de queimadas detectadas pelo satélite Terra/MODIS, de 2001 a 2016 para as seis áreas de estudo. Note: As escalas para a África *(a)-(c)* e América do Sul *(g)-(i)* são maiores.

4.2 Análises da variabilidade climática do PFI e do PFIv2

O PFI e o PFIv2 foram avaliados pela eficiência na detecção de ocorrências diárias de queimadas, nas classes máximas (entre 0,7 e 1) do risco

de fogo. As Figuras 4.3 a 4.8 apresentam, sequencialmente, as mesmas regiões e intervalos da Figura 4.2. Entretanto, uma avaliação anual para o período de 2001 a 2016 é adicionada.

Como visto anteriormente, a África é o continente com as maiores ocorrências de queimadas. As Figuras 4.3(a)-(c) mostram que ambos os índices detectam a variabilidade sazonal nas classes máximas (alto e crítico). No intervalo JASO (Figura 4.3a), a eficiência foi de 93,5% (93%) para o PFIv2 (PFI). A similaridade dos índices permaneceu, proporcionalmente ao número total de queimadas 88,7% (88,2%), no período NDJF (Figura 4.3b). Todavia, a Figura 4.3(c) mostra que no intervalo de menor atividade de fogo na África (MAMJ), a eficiência do PFIv2 superou em 0,7% a do PFI. Já na avaliação anual (Figura 4.3d), a porcentagem do número total de focos detectados nas classes máximas forai de 88,4% (87,9%) pelo PFIv2 (PFI).

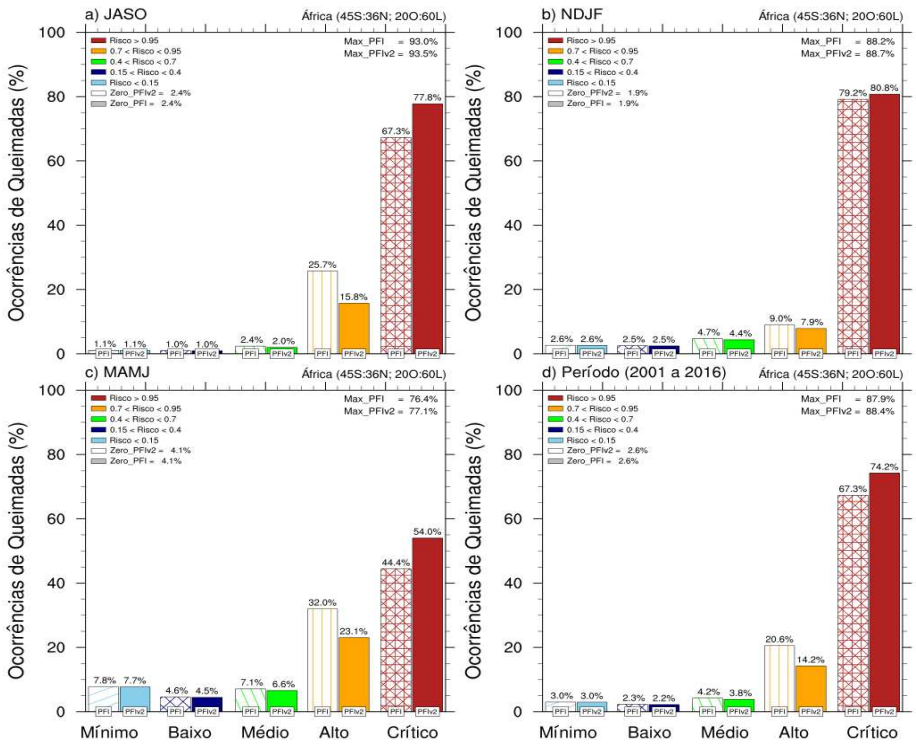

Figura 4.3. Porcentagem do fogo diário acumulado na África, em cada classe do PFI e do PFIv2, durante o período 2001-2016. Note: O fator ZERO representa a relação total de focos de queimadas que foram detectados próximos ao valor zero de cada índice.

Entre as regiões analisadas, a Ásia foi a que apresentou a menor variabilidade entre as classes dos índices. Isso ocorre porque a amplitude sazonal da ocorrência de queimadas é alta na Ásia, na qual as observações diferem-se em aproximadamente 400 mil observações entre os intervalos NDJF e MAMJ (Figuras 4.2d-e). Apesar disso, mais de 63% dos focos foram detectados sazonalmente pelas classes máximas do PFIv2 (Figuras 4.4a-c). No que tange à eficiência anual dos índices (Figura 4.4d), o PFI detectou 52,8% das atividades de fogo, enquanto que o PFIv2 cravou 63% nas classes máximas.

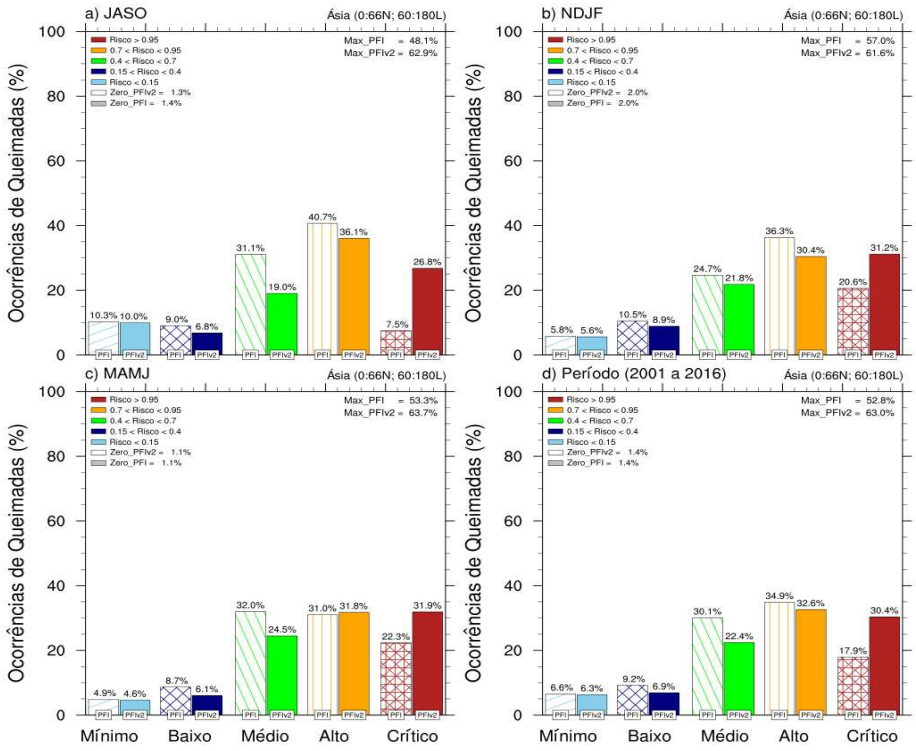

Figura 4.4. Porcentagem do fogo diário acumulado na Ásia, em cada classe do PFI e do PFIv2, durante o período 2001-2016. Note: O fator ZERO representa a relação total de focos de queimadas que foram detectados próximos ao valor zero de cada índice.

A América do Sul também é caracterizada com valores similares aos de detecção nas classes máximas dos índices (Figuras 4.5a-d). Porém a eficiência do PFIv2 é maior, em média 1%, do que a do PFI, como mostrado no intervalo JASO (Figura 4.5a).

É importante mencionar que a América do Sul é a região que apresentou a maior taxa de ocorrências de queimadas na classe mínima (Figura 4.5b). Isso se explica não somente pela variação sazonal, mas também pelo conjunto de dados de precipitação, que tem sido constantemente aprimorado para as latitudes tropicais e, pelo efeito antrópico nos avanços de fronteiras agrícolas. As eficiências no intervalo MAMJ e anuais (Figuras 4.5c-d) foram de 63,3% (61,9%) e 71,4% (70,4) para o PFIv2 (PFI).

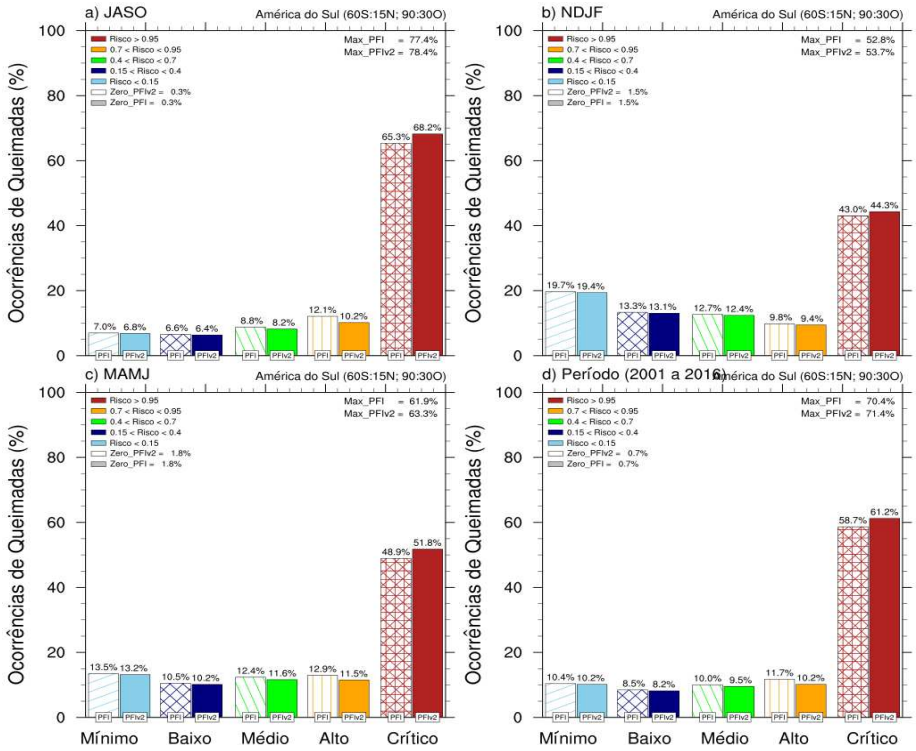

Figura 4.5. Porcentagem do fogo diário acumulado na América do Sul, em cada classe do PFI e do PFIv2, durante o período 2001-2016. Note: O fator ZERO representa a relação total de focos de queimadas que foram detectados próximos ao valor zero de cada índice.

As modificações nos parâmetros do PFIv2 para as latitudes extratropicais demonstram a eficiência do método em detectar as ocorrências de queimadas nas respectivas regiões. Na América do Norte e Caribe (Figuras 4.6a-d), as diferenças em relação ao PFI são de 5% e 3% nos intervalos JASO (Figura 4.6a) e MAMJ (Figura 4.6c), respectivamente.

Na eficiência anual, os valores são de 60,8% para o PFI e de 64,8% para o PFIv2. Estes resultados sugerem que o intervalo NDJF foi fundamental

para equilibrar as eficiências, ou seja: melhores ajustes ainda são necessários para os intervalos de baixas ocorrências de queimadas.

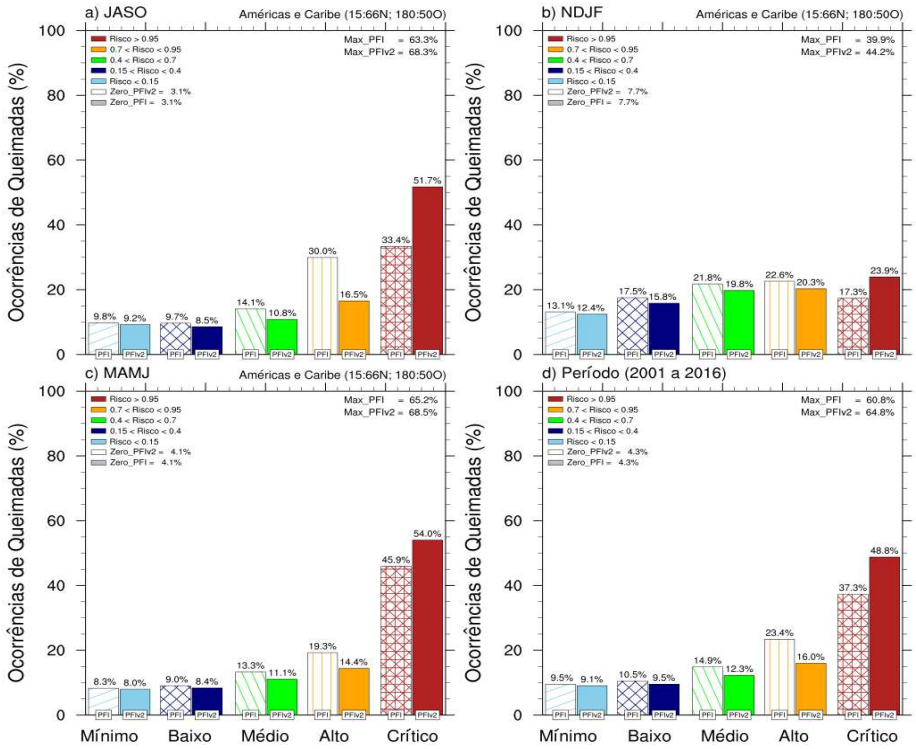

Figura 4.6. Porcentagem do fogo diário acumulado na América do Norte e Caribe, em cada classe do PFI e do PFIv2, durante o período 2001-2016. Note: O fator ZERO representa a relação total de focos de queimadas que foram detectados próximos ao valor zero de cada índice.

Em relação a região do Pacífico Sudoeste, que registra uma média de 150 mil ocorrências de queimadas no período 2001-2016 (Figures 4.2m-o), há uma eficiência superior a 74% nos intervalos JASO e NDJF, cujas atividades do fogo são máximas na região (Figuras 4.7a, b). As diferenças em relação ao PFI nestes intervalos são de 2,3% e 1,7%, respectivamente.

Entretanto, a maior diferença entre as eficiências dos índices pode ser observada no intervalo MAMJ (Figura 4.7c), cujo valor do PFIv2 (PFI) é 66,8% (60,8%). Na avaliação anual (Figura 4.7d), o PFIv2 mostra que o nível de acerto nas classes máximas é de 74,3%, enquanto que o PFI atinge 71,7%. Vale mencionar que a porcentagem dos focos que ocorrem nos níveis próximos a zero dos índices são iguais a 3,5%, o que pode ser considerado baixo, em se tratando de acumulados diários, para o período de 2001 a 2016.

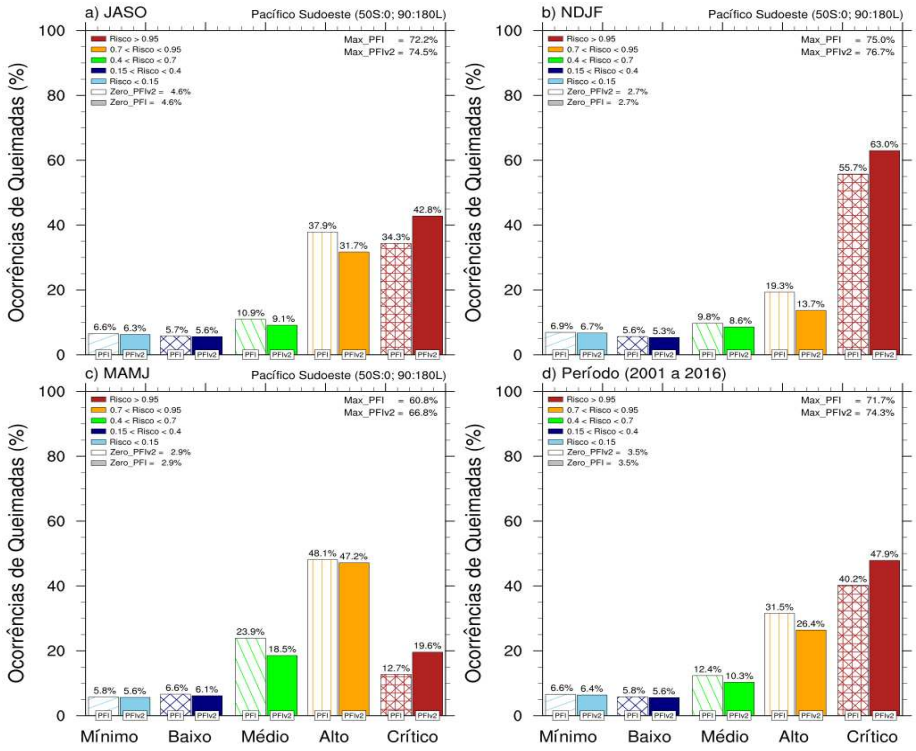

Figura 4.7. Porcentagem do fogo diário acumulado no Pacífico Sudoeste, em cada classe do PFI e do PFIv2, durante o período 2001-2016. Note: O fator ZERO representa a relação total de focos de queimadas que foram detectados próximos ao valor zero de cada índice.

As análises na Europa revelam os efeitos do aprimoramento do PFIv2, em todos os intervalos analisados. Pode-se observar que as diferenças nas eficiências máximas foram de 6% (Figura 4.8a) a incríveis 20,3% (Figura 4.8c). Contudo, um alerta é acionado: a necessidade de ajustes para os intervalos de ocorrências mínimas de fogo (Figura 4.8b). No intervalo NDJF, por exemplo, a razão dos focos detectados em áreas próximas a nulidade dos índices foi a máxima (39,3%) entre todas as 6 regiões.

Apesar dessa discrepância, a eficiência anual do PFIv2 na Europa está acima de 66,5%, representando uma diferença de 11,1%, em relação ao PFI. Esta identificação é de suma importância no entendimento de que ambos os índices indicam a suscetibilidade atmosférica ao fogo em vegetação, não separando sistematicamente as parcelas de contribuições antrópicas e naturais.

Assim, o próximo capítulo discutirá, o aprimoramento e a aplicação do PFIv2 nas análises climáticas e de estudos de casos na Europa. Este estudo visará a redução dos desafios encontrados pelos tomadores de decisões, na previsão da atividade de fogo em vegetação.

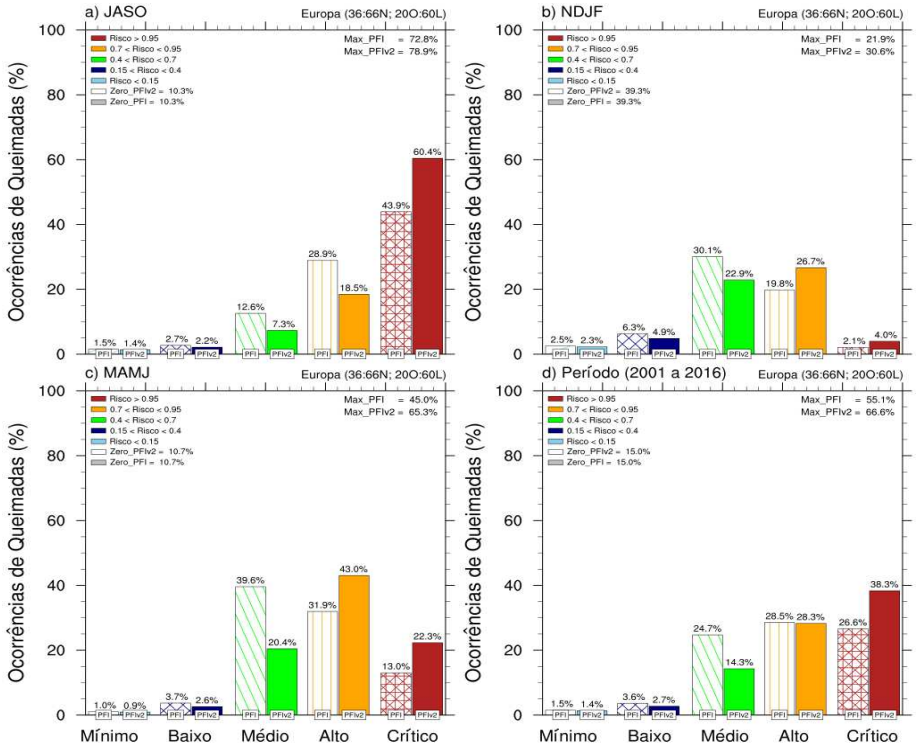

Figura 4.8. Porcentagem do fogo diário acumulado na Europa, em cada classe do PFI e do PFIv2, durante o período 2001-2016. Note: O fator ZERO representa a relação total de focos de queimadas que foram detectados próximos ao valor zero de cada índice.

REFERÊNCIAS

ARCHIBALD, S.; ROY, D. P.; VAN WILGEN, B. W.; and SCHOLES, R. J. What limits fire? An examination of drivers of burnt area in Southern Africa. **Global Change Biology**, v. 15, p. 613– 630, 2009.

ANDREWS, P. L.; and BRADSHAW, L. S. Use of meteorological information for fire management in the United States. In '**Workshop on Meteorological Information for Fire Management in the United States**', pp. 325-332, 1991.

BOND, W. J.; WOODWARD, F. I.; and MIDGLEY, G. F. The global distribution of ecosystems in a world without fire. **New Phytologist**, v. 165, p. 525-537, doi: 10.1111/j.1469-8137.2004.01252.x, 2005.

BRADSTOCK, R. A. A biogeographic model of fire regimes in Australia: current and future implications. **Global Ecology and Biogeography**, 19, 145-158. doi: 10.1111/j.1466-8238.2009.00512.x, 2010.

BUCHHOLZ, G.; and WEIDEMANN, D. The Use of Simple Fire Danger Rating Systems as a Tool for Early Warning in Forestry. Int. **Forest Fire News**, v. 23, p. 32–37. www.fire.unifreiburg.de/iffn/country/id/id_29.htm, 2000.

BURGAN, R. E. Revisions to the 1978 National Fire-Danger-Rating System. **USDA Forest Service**, Southeastern Forest Experiment Station Research Paper SE-273. (Asheville, NC), 1988.

CARROL, A.; VAN PELT, R.; and SILLET, S. C. Tree-Ring Indicators of Fire in Two Old-Growth Coast Redwood Forests. **Fire Ecology**, v. 14, p. 85-105, doi: 10.4996/fireecology.140185105, 2018.

CHANNAN, S.; COLLINS, K.; and EMANUEL, W. R. Global mosaics of the standard MODIS land cover type data. **University of Maryland and the Pacific Northwest National Laboratory**, College Park, Maryland, USA, 2014.

COLLINS, B. M.; and STEPHENS, S. L. Stand-replacing patches within a 'mixed severity' fire regime: quantitative characterization using recent fires in a long-established natural fire area. **Landscape Ecology**, v. 25, p. 927-939, doi: 10.1007/s10980-010-9470-5, 2010.

COSTA, M. H.; YANAGI, SILVIA, N. M.; SOUZA, P. J. O. P.; RIBEIRO, A.; ROCHA, E. J. P. Climate change in Amazonia caused by soybean cropland expansion, as compared to caused by pastureland expansion. **Geophysical Research Letters**, Vol. 34, p. L07706, 2007.

CRUZ, M. G.; GOULD, J. S.; HOLLIS, J. J.; and McCAW, W. L. A Hierarchical Classification of Wildland Fire Fuels for Australian Vegetation Types. *Fire*, 1, 13; doi:10.3390/fire1010013, 2018.

DAVIDSON, E. A.; de ARAÚJO, A. C.; ARTAXO, P.; BALC, J. K.; BROWN, I. F. e*t al*. The amazona basin in transition. **Nature**, v. 481, n. 7381, p. 321-328, 2012.

DEE, D. P.; UPPALA, S. M.; SIMMONS, A. J.; BERRISFORD, P.; POLI, P.; et al. The ERA-Interim reanalysis: Configuration and performance of the data assimilation system. **Quarterly Journal of the Royal Meteorological Society**, v. 137(656), p. 553-597, 2011.

DOBLAS-REYES, F. J.; GARCÍA-SERRANO, J.; LIENERT, F.; BIESCAS, A. P.; RODRIGUES, L. R. L. Seasonal climate predictability and forecasting: status and prospects. Wiley Interdisciplinary Rev.: **Climate Change**, Vol. 4, p. 245-268, 2013.

FAO. Fire management global assessment. A thematic study prepared in the framework of the Global Forest Resources Assesment. Food and Agriculture Organization of the United Nations, 2006.

FOSBERG, M.A.; STOCKS, B.J.; and LYNHAM, T.J. Risk analysis in strategic planning: fire and climate change in the boreal forest. Fire in Ecosystems of Boreal Eurasia. J.G. Goldammer and V.V. Furyaev, editors. **Kluwer Academic Publication**, Netherlands, p. 495-504, 1996.

GALANTER, M.; LEVY II, H.; and CARMICHAEL, G. R. Impacts of biomass burning on tropospheric CO, NOx and O3. **Journal of Geophysical Research**, Vol. 105, n. D5, p. 6633-6653, 2000.

GIGLIO, L.; RANDERSON, J. T.; and VAN DER WERF, G. R. Analysis of daily, monthly, and annual burned area using the fourth-generation global fire emissions database (GFED4). **Journal of Geophysical Research: Biogeosciences**, v. 118, p. 317-328, doi: 10.1002/jgrg.20042, 2013.

GIGLIO, L.; SCHROEDER, W.; JUSTICE, C. O. The collection 6 MODIS active fire detection algorithm and fire products. **Remote Sensing of Environment**, v. 178, p. 31-41, 2016.

HAINES, D. A. A lower atmospheric severity index for wildlands fires. **National Weather Digest**, v. 13, p. 23-27, 1988.

HARDY, C. C.; and HARDY, C. E. Fire danger rating in the United States of America: an evolution since 1916. **International Journal of Wildland Fire**, v. 16, p. 217-231, 2007.

HICKLER, T. et al. Implementing Plant Hydraulic Architecture within the LPJ Dynamic Global Vegetation Model. **Global Ecology and Biogeography**, v. 15, No. 6, pp. 567-577, 2006.

HOFFMANN, A. A.; PARRY, J.; CUAMBE, C.; KWESHA, D.; ZHAKATA, W. Climate change and wildland fires in Mozambique. In M. A. Cochrane (Ed.), Tropical Fire Ecology: Climate Change, Land Use, and Ecosystem Dynamics. **Springer/Praxis**, Heidelberg, Germany/Chichester, U.K., 2009.

JUSTINO, F.; de MELO, A. S.; SETZER, A.; SISMANOGLU, R.; SEDIYAMA, G. C.; RIBEIRO, G. A.; MACHADO, J. P.; STERL, A. Greenhouse gas induced changes in the fire risk in Brazil in ECHAM5/MPI-OM coupled climate model, **Climatic Changes**, Vol. 106, p. 285-302, 2010.

JUSTINO, F.; PELTIER, W. R.; BARBOSA, H. A. Atmospheric susceptibility to wildfire occurrence during the Last Glacial Maximum and mid-Holocene. **Palaeogeography, Palaeoclimatology, Palaeoecology**. Vol. 295, p. 76-88, 2010.

JUSTINO, F.; STORDAL, F.; CLEMENT, A.; COPPOLA, E.; SETZER, A.; and BRUMATTI, D. Modelling Weather and Climate Related Fire Risk in Africa. **American Journal of Climate Change**, v. 2, p. 209-224, 2013.

LATURNER, N.; SCHERER, H. W. As queimadas e os incêndios florestais em Mato Grosso. **Revista Geonotas**, Vol. 8, 2004.

LI, F.; BOND-LAMBERTY, B.; and LEVIS, S. Quantifying the role of fire in the Earth system – Part 2: Impact on the net carbon balance of global terrestrial ecosystems for the 20th century. **Bigeosciences**, **11**, 1345-1360, doi: 10.5194/bg-11-1345-2014, 2014.

LYNCH, A. H.; BERINGER, J.; KERSHAW, P.; MARSHALL, A.; MOONEY, S.; TAPPER, N.; TURNEY, C.; KARRS, S. V. D. Using the Paleorecord to Evaluate Climate and Fire Interactions in Australia, **Annual Review of Earth and Planetary Sciences**, Vol. 35: 215-239, 2007.

MANDEL, J et al. A wildland fire model with data assimilation. **Mathematics and Computers in Simulation**. Vol. 79, p. 584-606, 2008.

MANZANAS, R.; FRÍAS, M. D.; CONFIÑO, A. S.; GUTIÉRREZ, J. M. Validation of 40 year multimodel seasonal precipitation forecasts: the role of ENSO on the global skill. **Journal of Geophysical Research: Atmospheres,** v. 119, p. 1708-1719, 2014.

McRAE, R. H. D.; and SHARPLES, J. J. A process model for forecasting conditions conducive to blow-up fire events. Proceedings, **MODSIM Conference**, Adelaide, SA, 2013.

MEYN, A.; WHITE, P. S.; BUHK, C.; JENTSCH, A. Environmental drivers of large, infrequent wildfires: the emerging conceptual model. **Progress in Physical Geography**. Vol. 31, p. 287-312, 2007.

MOUILLOT, F.; and FIELD, C. B. Fire history and the global carbon budget: a 1° x 1° fire history reconstruction for the 20th century. **Global Change Biology**, 11**,** 398 – 420. doi: 10.1111/J.1365-2486.2005.00920.X, 2005.

POTTER, B. The Haines Index – it's time to revise it or replace it. **International Journal of Wildland Fire**, 27(7), p. 437-440 [https://doi.org/10.1071/WF18015], 2018.

PYNE, S. J.; ANDREWS, P. L.; and LAVEN, R.D. Introduction to Wildland Fire. **John Wiley & Sons**, Inc., New York, NY, 769 p., 1996.

SAN-MIGUEL-AYANZ, J.; MORENO, J. M.; and CAMIA, A. Analysis of large fires in European Mediterranean landscapes: Lessons learned and perspectives. **Forest Ecology and Management**, v. 294, p. 11-22, 2013.

SCHEITER, S.; and HIGGINS, S. I. Impacts of Climate Change on the Vegetation of Africa: An Adaptive Dynamic Vegetation Modeling Approach, **Global Change Biology**. Vol. 15, No. 9, p. 2224-2246, 2009.

SCOTT, J. H. Introduction to Wildfire Behavior Modeling. **National Interagency Fuels, Fire & Vegetation Technology Transfer**. Available: www.niftt.gov, 2012.

SERREZE, M. C.; and BARRY, R. G. Climate change. In: BARRY, R. G., CHORLEY, R. J. (Eds.), **Atmosphere. Weather and Climate**. Routledge, Oxon, 2010.

SETZER, A.; SISMANOGLU, R. A. Queimadas no Brasil. **Climanálise Boletim de Monitoramento e Análise Climática**, v. 7, n. 8, p. 40-53, 2002.

SILVA, J. M. N.; PEREIRA, J. M. C.; CABRAL, A. I.; VASCONCELOS, M. J. P.; MOTA, B.; and GREGOIRE, J. M. An Estimate of the Area Burned in Southern Africa during the 2000 Dry Season Using SPOT-VEGETATION Satellite Data. **Journal of Geophysical Research**, v. 108, No. D13, 2003.

SOUZA, L. A.; and FREITAS, C. E. C. Modelos populacionais de ecossistemas. **Revista Agrogeoambiental**. v. 6, No. 3, 2014.

SPERA, S. A.; GALFORD, G. L.; COE, M. T.; MACEDO, M. N.; and MUSTARD, J. F. Land-Use Change Affects Water Recycling in Brazil's Last Agricultural Frontier. **Global Change Biology**, doi:10.1111/gcb.13298, 2016.

STOCKS, B.J.; LAWSON, B.D.; ALEXANDER, M.E.; VAN WAGNER, C.E.; MCALPINE, R.S.; LYNHAM, T.J.; and DUBÉ, D.E. The Canadian Forest Fire Danger Rating System: an overview [reprinted from August 1989 issue, 65:258-265, with corrections and new pagination]. **Forestry Chronicle**, 65(6), p. 450-457, 1989.

STOCKS, B.J.; and LAWSON, B.D. El sistema Canadiense de evaluacion del grado de peligro de incendios forestales: Una vision general. p. 82-94 in J.A. Guillermo, Editor. Proc. Prognosis Y Gestion en Control de Incendios Forestales, **Actas del Taller Internacional**, November 8-10, 1995, Santiago de Chile. Proyecto FONDEF FI-13, Santiago de Chile, 1996.

THONICKE, K; SPESSA, A; PRENTICE, I. C.; HARRISON, S. P.; DONG, L.; and CARMONA-MORENO, C. The Influence of Vegetation, Fire Spread and Fire Behaviour on Biomass Burning and Trace Gas Emissions: Results from a Process-Based Model. **Biogeosciences Discussions**, V. 7, No. 1, pp. 697-743, 2010.

TOSCA, M. G.; RANDERSON, J. T.; and ZENDER, C. S. Global impact of smoke aerosols from landscape fires on climate and the Hadley circulation. **Atmospheric Chemistry and Physics**, v. 13, p. 5227-5241, doi: 10.5194/acp-13-5227-2013, 2013.

VAN DER WERF, G. R.; RANDERSON, J. T.; GIGLIO, L. *et al*. Global fire emissions estimates during 1997-2016. **Earth System Science Data**, v. 9, p. 697-720, https://doi.org/10.5194/essd-9-697-2017, 2017.

WEISSE, M.; and GOLDMAN, L. 2017 Was the Second-Worst Year on Record for Tropical Tree Cover Loss. **Global Forest Watch**. Online available at [https://blog.globalforestwatch.org/data-and-research/2017-foi-o-segundo-pior-ano-ja-registrado-de-perda-de-cobertura-florestal-tropical], 2018.

WINKLER, J. A et al. A climatology of the Haines Index for North America derived from NCEP/NCAR reanalysis fields. **Sixth Fire and Forest Meteorology Symposium**, American Meteorological Society, 2005.

WHITLOCK, C.; and BARTLEIN, P. J. Holocene fire activity as a record of past environmental change, in: Developments in Quaternary Science, edited by: Gillespie, A. R., Porter, S. C., and Atwater, B. F., **Elsevier**, Amsterdam, 2004.

WHITLOCK, C.; MORENO, P. I.; and BARTLEIN, P. Climatic controls of Holocene fire patterns in southern South America, **Quaternary Research**, v. 68, p. 28–36, 2006.

WOLFSON, R. Energy, Environment and Climate, second ed. WW Norton and Company Inc, New York, pp. 366-370, 2012.

WOOSTER, M. J.; and ZHANG, Y. H. Boreal forest fires burn less intensely in Russia than in North America. **Geophysical Research Letters**, v. 31, n. L20505, https://doi.org/10.1029/2004GL020805, 2004.

XIE, P.; CHEN, M.; and SHI, W. CPC unified gauge analysis of global daily precipitation. Preprints, **24th Conference on Hydrology**. Atlanta, Georgia. American Meteorological Society, 2.3A. [Avaiable online at https://ams.confex.com/ams/90annual/webprogram/Paper163676.html], 2010.

YORK, A.; BELL, T. L.; and WESTON, C. J. Fire regimes and soil-based ecological processes: implications for biodiversity. In Bradstock R. A et al (Eds) 'Flammable Australia, Fire regimes, biodiversity and ecosystems in a changing world' (**CSIRO Publishing: Collingwood, VIC**), p. 127-148, 2012.

CAPÍTULO 5
ARTIGO SUBMETIDO

IMPROVEMENT OF THE POTENTIAL WEATHER FIRE INDEX ON A GLOBAL PERSPECTIVE

A. Silva

Agricultural Engineering Department, Federal University of Vicosa, Brazil.

F. Justino

Agricultural Engineering Department, Federal University of Vicosa, Brazil.

A. Setzer

Fire Program of the National Institute of Space Research (INPE), Brazil.

A. Avila

Agricultural Engineering Department, Federal University of Vicosa, Brazil.

ABSTRACT

On a global perspective, fire activities have been significantly linked to multiple factors such as climate conditions, population density, agriculture, and substantial economic losses. Based on vegetation susceptibility to fire, this study presents the Potential Weather Fire Index version 2 (PFIv2). Here we use ERA-Interim Reanalysis and CPC Unified Precipitation as input data for the 2001-2016 period. It has to be noticed that the PFIv2 estimates the risk by considering local factors such as latitude, and topography profile. We demonstrate that PFIv2 has revealed an efficiency by up to 70% in presenting observed fires from Terra/MODIS satellite, over extratropical regions, mainly in North America, Europe, and Asia. To evaluate in further details the PFIv2 performance, two extreme fire occurrences in Europe are considered. The first event occurred in Portugal in 2003 (SC01), and the second in Greece in 2018 (SC02). In the SC01 event, the PFIv2 increases by up to 30%, over the highest fire concentration in Western Europe, between 40°N and 55°N, related to the direct influence of atmospheric instability, lower relative humidity, and precipitation deficit. During the SC02 event, there is an increase (decrease) variation of air temperature, over northern Europe (Balkan Peninsula), and dry conditions are dominant over most part of Europe. The PFIv2 reveals accuracy in reproducing the regions with fire activity in northern Central Europe, and southwestern Russia. Further analyzes indicate that there is no correlation between the North Atlantic Oscillation Index (NAO) and the PFIv2 with the highest fire occurrences in the SC01. Conversely, a positive correlation (statistically significant at 95%), between the NAO and the PFIv2 in the SC02 points that the atmospheric pattern linked to the NAO has the potential to increase the fire risk. These findings indicate that the PFIv2 is an useful tool for decision makers, in forecasting fire activity.

Keywords: Fire risk, vegetation, extratropical, atmospheric conditions, logarithmic function.

1. Introduction

Climate and wildfire interaction plays a dynamic role as disturbance agents affecting the structure and composition of flammable ecosystems (HOLLMANN et al., 2013). In recent decades, various sectors of society have expressed concern over the indiscriminate use of wildfire because vegetation wildfires are prominent in issues involving past and future climate change (e.g. HARRISON et al., 2007). Nevertheless, there is a lively debate on the importance of anthropogenic and climate forcing in contributing to the ignition of wildfires (HUANG et al., 2015).

Although the majority of vegetation wildfires has been observed in the tropics, the Arctic and the extra-tropics have experienced in recent decades an increased number of wildfires (VERAVERBEKE et al., 2017; MASRUR et al., 2018). These regions have been affected by increased temperature and have experienced distinct pattern of precipitation that can result in more vulnerable conditions for wildfire development (KRAUSE et al., 2014; VERAVERBEKE et al., 2017). In fact, there is a lack of studies on the interaction between climate changes and expansion or suppression of fire seasons on a global perspective. Thus, more investigation is necessary to disentangle the interchange between anthropogenic factors and the natural environmental changes.

Historical fire evidences suggest that the onset of industrialization and demand for land and timber, impose threat to forest cover in large parts of Europe, Central/South America, China and India (GFRA, 2015). Extreme erratic fires have been occurred leading to social disruptions and substantial economic losses. The National Iteragency Fire Center (NIFC, 2013) has shown that over the last decade, annual wildfire suppression costs on US federal lands exceeded $1.7 billion US dollars. While in Canada this values reached by up to $1 billion US dollars (GONZÁLEZ-CABÁN, 2013). Thus, the understanding and skill to predict wildfire occurrence and intensity is essential to designing and implementing necessary measures to mitigate these impacts.

In addition to the destructive power, burning in vegetation releases carbon dioxide (CO_2), carbon monoxide (CO), methane (CH_4), hydrocarbons and others, which return to the atmosphere in a matter of hours (GALANTER et al., 2000). Fires present a significant role in the global CO_2 balance, mainly over

an ecosystem restoring that suffered with fires. In this process, CO_2 is gradually removed from the atmosphere by photosynthesis and it is incorporated into the reconstructed vegetation (TOSCA et al., 2013; LI et al., 2014). Greenhouse gases originating from combustion in vegetation begin to intensify the global warming. According to the FAO report “Fire Management – Global Assessment 2006”, the amount of biomass burned annually from all sources is about 9.2 billion tons. Global fires in vegetation consume 5.13 billion tons, 42% only in Africa. Such fires release about 3.4 billion tons of CO_2 and other emissions.

Modelling the fire activity is vital. The state-of-art fire modelling uses several parameters that include complex methods to calculate the interaction among soil characteristics, carbon allocation, and the moisture content of soil litter (CATCHPOLE, 2002; ARCHIBALD et al., 2009; BRADSTOCK, 2010). However, these models may also present a considerable uncertainty level on parameterizing biomass fuel amount, which leads to a lack of accuracy between predicted and observed fires (HICKLER et al., 2006; WARMINK et al., 2010; FINNEY et al., 2012; SKINNER et al., 2014).

Van Wagner (1987) proposed the Fire Weather Index (FWI), which currently is a worldwide index. It combines three moisture indices: the Fine Fuel Moisture Code (FFMC) representing the moisture content in fine fuels. In addition, the Duff Moisture Code (DMC) shows loosely compacted organic material, while the Drought Code (DC) is a deep layer of compact organic material. The combination of these moisture parameters delivers the fire behavior indexes. Due to nonlinearity with respect to control effort, a power function for daily Severity Rating (DSR) is implemented to increase the weight of higher values of the FWI (VAN WAGNER 1970; WILLIAMS, 1959).

Similarly, the United States National Fire Danger Rating System (NFDRS) was revised with the addition of Keetch-Byram Drought Index (KBDI), to account for weather and climatic conditions in the eastern United States (BURGAN, 1988). There are eleven weather parameters that drive the various models of the NFDRS. In the NFDRS, 20 fuel models representing the vegetation and fuel types can be selected, ranging from annual grass and herbs to Alaskan tundra (ANDREWS and BRADSHAW, 1997). These fuel models are derived by using a combination of dead fuel moisture (1-hour, 10-hour, 100-hour, and 1000-hour) and live moisture (wood and grass) models (Burgan,

1988). The moisture content of live fuel and the four classes of dead fuel are calculated from weather data and moisture values (RICHARD and HEIM 2002). In summary, dead fuel is determined by the diameter of the wood or timelag. Currently, the lightning ignition efficiency algorithm is being used by the United States Wild Land Fire Assessment System (SOPKO et al., 2016).

Thus, the large number of degree of freedom arises criticism towards the need to include several parameters for simulating the link between fire and ecosystem dynamics (SCHEITER & HIGGINS, 2009). The Potential Weather Fire Index (PFI), presented by Justino et al (2010) to predict regions in Brazil more favorable to wildfires, formulated a simplified index based on four parameters to calculate the fire risk. The modification on the PFI proposed here replace the one level humidity factor by a logistic growth function, which inserts three atmospheric layers and the local altitude as addressed on Haines Index (1988). Afterwards, a correction factor of the air temperature due to latitudinal change is included.

The goal of this study is to introduce and validate a modified version of the Potential Weather Fire Index (JUSTINO et al., 2010), particularly on extratropical regions. Section 2 describes the vegetation and climate data utilized, the modelling formulation, and the validation methods. Section 3 discusses the capability of the PFIv2 in reproducing two cases of erratic fires in Portugal and Greece in 2003 and 2018, respectively. Concluding remarks and model limitation are described in Section 4.

2. Data and Methodology

2.1. Study area

The PFIv2, a modified version of the Potential Fire Index (PFI) proposed by Justino et al (2010) is applied globally (Figure 5.1a), over six subdivisions from World Meteorological Organization (WMO): *(I)* Africa (45°S:36°N; 20°W:60°E); *(II)* Asia (0:66°N; 60:180°E); *(III)* South America (60°S:15°N; 90:30°W); *(IV)* Americas and Caribbean (15:66°N; 180:50°W); *(V)* South-West Pacific (50°S:0; 90:180°E) and; *(VI)* Europe (36:66°N; 20°W:60°E). Information on the types of vegetation required for the computation of PFIv2 were obtained

from the classification of the International Geosphere-Biosphere Programme (IGBP), as shown in Figure 5.1(b).

2.2. Climate Data

The calculation of the second version of the Potential Weather Fire Index (PFIv2) is conducted based on the ERA-Interim Reanalysis (DEE at al., 2011), and on the CPC Unified Precipitation Project that is underway at NOAA Climate Prediction Center (Xie et al., 2010) for the 2001-2016 period. The spatial resolution of the ERA-Interim Reanalysis (ERAI) is the reduced Gaussian grid N128, which is symmetrical around the equator, with an approximately uniform spacing in the north-south direction, spinning around 0.703125° between the latitudes. There are 128 points aligned along the Greenwich Meridian, from the equator to the pole in both hemispheres. The number of points in the east-west direction varies with latitude, with uniform grid spacing of 0.703125° only in the regions of the tropics.

The CPC spatial resolution is 0.5° latitude and longitude grid over global land areas. This gauge-based analysis of daily precipitation uses reports from over 30,000 stations that are collected from multiple agencies. Historical records, independent information from measurements at nearby stations, radar and satellite observations, as well as numerical model forecasts are applied in the quality control of the data.

2.3. Potential Weather Fire Index version 2 (PFIv2)

The Potential Weather Fire Index version 2 (PFIv2) represents an improvement of an earlier version proposed by Justino et al (2010). The main assumption is maintained, but the PFIv2 includes a modified Haines Index (HAINES, 1988) embedded to a logistic growth function, and a temperature correction factor due to latitudinal variation to capture the wildfire risk estimates consistent with those observed in extratropical regions.

The PFIv2 is highly correlated with the duration of the dry periods, the type and natural cycle of defoliation of the vegetation, maximum temperature

and the humidity of the air. The reference of the calculations is the “Days of Dryness” (DD), which is a hypothetical number of days without precipitation during the last 120 days (JUSTINO et al., 2010), as described below:

1. Determine daily for a given geographic area, the value of precipitation, in millimeters (mm) accumulated for the 11 immediately preceding periods of 1, 2, 3, 4, 5, 6-10, 11-15, 16-30, 31-60, 61-90 and 91-120 days.
2. Calculate the “Precipitation Factors” (PF) with values ranging from 0 to 1 for each of the 11 periods (see Justino et al., 2010), using an empirical exponential function of the precipitation in millimeters for each period.

The equation 1 describes the days of droughts.

$$DD = 105 \times (PF_1 \times PF_2 \ldots \times PF_{61\text{-}90} \times PF_{91\text{-}120}) \qquad \text{(eq. 5.1)}$$

After computing the DD, the PFIv2 takes into account the vegetation type and their vulnerability to atmospheric conditions. This is important because savannas and grassland are, for instance, more susceptible to erratic wildfires as compared to evergreen forests. This is defined as the Basic Risk (BR; eq. 5.2):

$$BR = 0{,}9 \times (1 + \sin(A \times DD)) / 2 \qquad \text{(eq. 5.2)}$$

Figure 5.1(c) shows the variation of BR for the different types of vegetation. Based on Eq. 2, low values of *A* indicate that the vegetation needs a longer period without precipitation to reach the maximum BR. For instance, regions covered by non-forests would experience high BR under 45 days of dryness whereas areas covered by evergreen forests need 105 days of low precipitation to deliver similar BR. It should be noted that the “days without rain” axis, indicates both the real period of days without rain as well as the “days of drought (DD)”, which corresponds to a hypothetical period without rain calculated from the temporal quantity, and distribution of occurred rains. It is

assumed that the periods of “days without rain” or “days of drought” make up the basic principle of the PFIv2.

Other feature that must be included is the effect of the altitude upon the fire risk (TYMSTRA et al., 2010). The elevation and slope affect both the temperature and humidity of the air, and therefore, vegetation/fuels, and fire potential. Seasonally, some mountain tops and slopes can be still under snow and only the valley bottoms be dry enough to burn.

In this sense, a modified Haines Index “HI” (POTTER, 2018) is also included to compute the wildfire risk. The HI combines two important atmospheric factors within a simplified model that reasonably indicates the areas most susceptible to wildfire. The HI has been extensively used in the United States and Canada. It estimates the severity of the forest wildfire based on the rates of vertical variations of temperature and humidity (HAINES, 1988; WINKLER et al., 2007; POTTER, 2018). The HI is computed by the combination of the stability and humidity of the air at three atmospheric layers. However, the isolated application of the HI is incomplete, because it lacks a more robust scientific basis (POTTER, 2018). Therefore, at each atmospheric layer, we have modified the HI by applying a logistic growth function in terms of stability and humidity of the air according to Equation 5.3.

$$F_{i=0.05}^{i=1.05} = \left(\frac{K \times F_{i-0.05}}{F_{i-0.05} + (K - F_{i-0.05}) \times e^{-0.05r}} \right) \quad \text{(eq. 5.3)}$$

where:

F_0 is the minimum value of the stability parameter *(s)* from Haines index,

r is the difference between the maximum value of the humidity parameter *(q)* and the minimum value of the stability parameter *(s)* from Haines index at each atmosphere level,

F is the conversion of Haines Index to a continuous equation (°C),

K is the limiting factor, which means the maximum sum value of the both Haines’ parameters (humidity and stability of the atmosphere). It is calculated for each atmospheric level, as:

$$K = \begin{cases} 2 \times (s_{max} + q_{max}) = 36 \\ \quad for\ e \leq 1500m \\ 1.5 \times (s_{max} + q_{max}) = 36 \\ for\ 1500m < e \leq 3500m \\ (s_{max} + q_{max}) = 43 \\ \quad for\ e \geq 3500m \end{cases} \qquad \text{(eq. 5.4)}$$

Then, the logistic function of fire (LF) is analytically given by:

$$LF = \begin{cases} 7 \times 10^{-5} \times W^3 - 0.0035 \times W^2 + 0.072 \times W - 0.26 \\ \quad for\ e \leq 1500m \\ 1 \times 10^{-4} \times W^3 - 0.0056 \times W^2 + 0.115 \times W - 0.53 \\ \quad for\ 1500m < e \leq 3500m \\ 9 \times 10^{-5} \times W^3 - 0.0067 \times W^2 + 0.196 \times W - 1.89 \\ \quad for\ e \geq 3500m \end{cases} \qquad \text{(eq. 5.5)}$$

Where *W* is the sum of the stability and humidity parameters from the Haines Index (°C) and, *e* is the local elevation (m).

Due to PFI parametrization does not work properly on lower temperatures from extra-tropical climates (JUSTINO et al., 2013), a correction factor of the air temperature for latitudinal change is also included by F_{orb} = *(0,003 x |Lat| + 1)*, where |Lat| is the latitude module. Finally, the PFIv2 is computed taking into account all parameters as follow:

$$PFIv2 = BR \times (a2 \times LF + b) \times (RT \times F_{orb}) \qquad \text{(eq. 5.6)}$$

Where b = 1.3 and the variables BR and RT are the same as in the PFI (JUSTINO et al., 2010; 2013), but the constant a2 = 0.006. The term *(a2 x LF + b)* is the impact factor of the Haines logistic function (Loghai). The sequence of

PFIv2 calculations is shown in Figure 5.2. It is important to mention that the PFIv2 maintains the same PFI categories, with a scale ranging from 0 to 1 (Table 5.1).

2.4. Validation of the PFIv2 model

Active wildfire products from NASA's MODIS (2001-present) will be used to verify the capability of the PFIv2 for detecting the most susceptible region for erratic wildfires development. The wildfire products from the sixth collection of moderate-resolution spectral images of the Terra/MODIS includes algorithms for the elimination of false alarms, like those caused by the deforestation of small forests, precision in the detection of wildfires of reduced spatial scale, adjustment for the presence of cloudness and rejection expanded brightness of the sun. The products from Terra/MODIS are defined in a sine grid of the Earth to the spatial scales of 250-m, 500-m, or 1-km.

The validation of the PFIv2 versus satellite-derived wildfire can be carried out by checking the number of wildfires located in the high and critical wildfire risk grid. Evaluation of the wildfire risk based on PFIv2 may be validated with other satellite as well. For instance, GOES and NOAA products can be utilized. The limitation in satellite wildfires detection is that most of these products are not available prior 2000.

3. Results and Discussion

3.1. Temporal variability of global fires

Fires detected by Terra/MODIS satellite were computed and reclassified seasonally during 2001-2016 period (Figure 5.3), for three different intervals: November-December-January-February (NDJF); March-April-May-June (MAMJ) and; July-August-September-October (JASO). These intervals emphasize the periodic characteristics of minimum, intermediate and maximum occurrences of interannual fires.

Based on Figure 5.3, it is shown that the JASO period presents the highest incidence of fires on a global perspective. According to the figure, it can

be stated that the linear coefficient term is predominantly positive on the regions, except for all seasons in South America, for NDJF and JASO in South-West Pacific, and for JASO in Europe presenting a reduction on interannual incidence of fires.

Figures 5.3(a)-(c) show that the highest fire occurrences are from July to February in Africa with occurrences up to 1 million fires in specific years. A transitional period is verified in MAMJ with about 300 thousand fires/year characterizing the low fire season. The high fire activity in Africa (Figure 5.3c) is related to burning practices in order to convert natural vegetation into pasture and agricultural purposes (SILVA et al., 2003).

Annual fire occurrences in Asia are shown in Figures 5.3 (d)-(f). During the NDJF interval, the winds direction is predominantly northward and the rainfall moves to the Asia contributing to the reduction and homogeneity of fires (Figure 5.3d). When the solar insolation get higher in Asia (Figure 5.3e), southward cross equatorial wind and the Asian monsoon suppress the fire activity. In addition, the Southeast Asian is usually dry and warm which also contributes to the rising on occurrences (WOLFSON, 2012). In the Boreal summer, there is a reduction on fire occurrences (Figure 5.3f) due to most of double rainfall maximums received on monsoonal areas which can also affect regions that were not originally considered as monsoonal (SERREZE and BARRY, 2010).

Turning to the fire distribution in South America, Figures 5.3(g)-(h) show a steady pattern of occurrences from November to June, with mean values by about 180 thousand. During the JASO period (Figure 5.3i), the central part of Brazil experiences very dry conditions, without a complete lack of precipitation. It should also be highlighted that in September and October the highest values of surface temperature occurs and the incidence of fires reaches the highest magnitude. The interannual variability of fires responds to the positive (negative) El Nino-South Oscillation (ENSO) phase such as in 2001, 2009 and 2014 (in 2005, 2007, 2008 and 2010). Some recent studies have addressed the arising on fires to the anthropogenic vegetation changes (SILVA et al., 2003; DAVIDSON et al., 2012; MCTI, 2013; SPERA et al., 2016).

According to Figures 5.3(j)-(l) the incidence of fires in Central, North America and Caribbean regions trend to be stable from July to February when

the highest observation is close to 100 thousand fires in the 2001-2016 period. Similarly to the Asia region, there is an annual positive trend on fire occurrences with a which is intensified in MAMJ interval (Figure 5.3k). For the 1997-2016 period, Van der Werf et al (2017) suggest that the species in North America tended to promote fire in the emerging layer, with more intense levels of combustion in the entire canopy and mortality of trees.

In the South-West Pacific region (Figures 5.3m-o), the low yearly variation of fires occurs in the MAMJ interval (Figure 5.3n). In opposite, interannual changes and negative linear trends are coupled in the periods more favorable to wildfires: NDJF (Figure 5.3m) and JASO (Fiure 5.3o). These variations arise mainly due to the seasonal cycle in the central latitudes of Australia is delayed by about a month or two from that of the northern latitudes, with maxima occurring from about November to January and minima from April to June. In the southern parts of Australia the seasonal cycle is delayed from that of the central latitudes with maxima generally from December to February and minima from June to August. In fact, these differences are reasonably associated with wildland fires that are rare in some fuel types due to high fuel continuity and plant characteristics as shown in Cruz et al (2018).

Although environmental conditions and vegetation attributes are relatively similar in Europe and North America (WOOSTER and ZHANG, 2004), the burning occurrences are not standardized, as shown in Figures 5.3(p)-(r). It is intensify that the increase of fire occurrences in the November-October, a negative trend is observed in the JASO interval (Figure 5.3r).

According to Justino et al (2010), precipitation is vital on the Potential Weather Fire Index. It is included as a drought factor which is calculated using daily rainfall. Figure 5.4 shows anomalies in precipitation, and basic risk of fire (BR) for NDFJ (Figures 5.4a, b), MAMJ (Figures 5.4c, d), JASO (Figures 5.4e, f), and annual mean (Figures 5.4g, h), based on ERAI and ERAI – CPC differences for the 2001-2016 period. All intervals show maximum precipitation differences over the subtropical Africa, which are close to 7 mm/day. South America, and southern Asia also show positive values around 4 mm/day at 95% significance levels. Thus, ERAI dataset contributes to the reduction of the BR in these areas due to the large amount of precipitation with respect to CPC.

Opposite signals are shown in northeastern Brazil, eastern Asia, Australia, and east region of North America except in JASO interval (Figures 5.4e, f).

On a global perspective, JASO is a peculiar interval (Figures 5.4e, f). Because ERAI shows higher BR related to lower precipitation in North America, southeastern Africa, southern Brazil and Asia which are statistically significant at 95%. The overestimation of precipitation differences by ERAI (Figure 5.4e) leads to lower BR over the extratropical region, in particular in North America, eastern Europe, Asia, southeastern South America, and Australia (Figures 5.4e, f). Turning to the annual mean (Figures 5.4g, h), it is clear that the JASO interval is the most dominant period, and well correlated to the annual feature.

Figures 5.5(a)-(h) show the standard deviation of the BR (left side) and its anomalies (right side) based on ERAI and CPC data for NDJF, MAMJ, JASO, as well as the annual mean for 2001-2016 period. It is noticed that higher values are observed in Sub-Sahara Africa, South America and eastern North America in NDJF (Figure 5.5a). Turning to MAMJ is clear an increased variatity, and a migration northward of higher STD in South America and Africa. The highlighted feature, however, is the modification of STD over Eurasia and the Canadian Arctic in JASO (Figures 5.5e, f). By analyzing the difference between ERAI and CPC, it is demonstrated that ERAI understimates the fire risk over those regions mentioned previously. However, the annual variability is dominated by the highest variation of the BR in the JASO interval (Figures 5.5e-h).

In more details, the standandard deviation of the basic risk with CPC (Figure 5.5) highlights the western North America, southern Patagonia, central South America, subtropical Africa, Australia, parts of Europe and Asia, as areas prominent to burn. Conversely, the standard deviation of the BR with ERAI shows similar distribution but with smaller magnitudes, except over the regions less vulnerable to fire (Figure 5.5f). As shown previously, by using the CPC data the efficiency of the PFIv2 has been improved, thus from now on, the analyses performed here are based on CPC data for JASO interval in the 2001-2016 period.

Figure 5.6(a) shows the average Basic Risk (BR) in the JASO interval, for the 2001-2016 time period. Due to the importance of precipitation to the fire risk, the BR contributes of up to 0.85 to the final fire risk. As expected, analyses

for the Haines factor (Figure 5.6b) tend to highlight the regions dominated by dry conditions and susceptible to convection. This is shown by larger differences of the air and dewpoint temperatures according to the altitude of the grid point.

Turning to the temperature factor (Figure 5.6c), it is demonstrated that the most susceptible regions for fire occurrence are located in the tropics between 30°S and 30°N. In the Southern Hemisphere this might be expected because the Atlantic Subtropical High (ASH) extends toward the continent, which causes the subsidence of the air and consequently absence of clouds which induce higher temperature (REBOITA et al., 2010; FETTER et al., 2018).

The current effect of temperature to fire risk differs from the original PFI. The combination of these three factors (BR, Haines logistic factor, and temperature factor), applied individually to the global vegetation pattern (Figure 5.1b) is the formulation of the PFIv2.

The seasonality plays the dominant role for the cycle of fires (MARKGRAF et al., 2007; MARLON et al., 2008). A very important player, for instance, is the Intertropical Convergence Zone (ITCZ) which during the JASO period is predominantly located over the Northern Hemisphere. The PFIv2 reasonable reproduces the role of the climatic conditions implicit in the method. For example, the equatorial region (5°N – 15°N) is dominated by a high contribution of the temperature factor (Figure 5.6c), but low BR values. Thus, the PFIv2 delivers to minimum values (Figure 5.6d).

On the other hand, Figure 5.6(d) emphasizes that the susceptibility to fire risk due to atmospheric conditions is higher in latitudinal ranges between 0 – 25°S and 30°N – 35°N, in areas dominated by savannas, pastures, grasses, open and closed shrublands. According to the formulation of PFIv2, these biomes are associated with increased susceptibility of burning activity due to the vulnerability of dry combustion properties. Moreover, the temperature factor varies from moderate to high in consonance with low BR, and reduces precipitation (Figure 5.6a).

The situation in the east coast of North America useful serves to highlight the good performance of the PFIv2 to reproduce the primary versions of fire occurrence. In opposite, the Haines factor shows higher air humidity and low convective movement which hampers the fire vulnerability. Most important is the

temperature factor being relatively high (Figure 5.6c) in the southeast and northeastern coasts of the United States indicating very prone conditions to fire. In addition, there are deciduous and seasonal forests, whose litters are constituted of more dense layers.

The south part of Africa revealed that during JASO, the four PFIv2 parameters are in favor for fire occurrence, due to low precipitation, dry atmospheric conditions and susceptible vegetation pattern. Figure 5.6(a) shows that there are favorable conditions for the fire risk due to BR in the Scandinavian Peninsula, however, the contributions of the Haines logarithmic factor (Figure 5.6b) and the temperature factor corrected by the latitudinal effect reduce the PFIv2 to levels closest to zero (Figure 5.6d).

Figures 5.6(e)-(f) show the JASO annual trends and the standard deviation (STD) of the global PFIv2. It should be noted that the fire risk due to atmospheric conditions delivers an upward trend for the JASO period in the 2001-2016 interval. However, this pattern is not global positive trends near the northern boundary of sub-Saharan Africa (e.g. Mali, Nigeria, Sudan and Ethiopia), South Asia, the Far East Asia, southern Patagonia, southeast and northeast of the United States, and Central Europe (Figure 5.6e).

Although, with intermediate values the northern most part of the Northern Hemisphere exhibits a positive trend with potential implications to the Artict environment. Turning to the STD analyses (Figure 5.6f), it is revealed that JASO variability dominates the annual trend (Figure 5.6e). Accordingly, substantial changes are delivered over the Artic region and the east coast of North America (Figure 5.6f). Higher variability is also observed in the western part of India, central Africa, and southern Europe.

In order to validate the PFIv2 results, Figure 5.7 shows the capability of the PFIv2 model in locating the daily fires of the Terra/MODIS satellite, based on two global precipitation dataset (ERAI and CPC). This verification is done by comparing if the fire position is coincident with the highest PFIv2 levels (between 0.7 and 1). The ideal metrics would be that in which the PFIv2 shows all fire occurrences at the critical level (grater than 0.95). However, this prospect would implicitly bring about a false coherence, as a region could be fully susceptible to fire, without necessarily occurring fires. Thus, fire incidences in

the different classes of risk assures us that the model tends to discriminate the different amounts of daily outbreaks.

Africa is the continent with the highest fire occurrences on the globe. Figure 5.7(a) shows that the PFIv2 reasonable finds the annual variability that may be understood by the predominance fires in the highest classes (high and critical). The total number of fires detected on these classes are 77.9% and 88.4% by ERAI and CPC, respectively. Among the regions analysed, Asia was the subregion that presented the lowest variability among the risk classes. This is because the seasonal range of fire occurrences is high in Asia, whose observations differ in approximately 400 thousand observations between the NDJF and MAMJ intervals (Figures 5.3d-e). Despite this fact, more than half of the fire occurrences (52.9%) 63% reach the high and critical classes of the PFIv2 with (ERAI) CPC (Figure 5.7b).

South America is also characterized with wildfire to the occurrence in the high and critical classes of the PFIv2, with values by about (58.8%) 71.4% for (ERAI) CPC global precipitation dataset (Figure 5.7c). However, this is the region that presented the highest rate of fire occurrences in the minimum class. These results are explained not only by seasonal variation, but also by the precipitation data of the ERAI that has been constantly improved for tropical latitudes and by the anthropic effect in advancing agricultural boundaries.

The adjustment of PFIv2 to the extratropical latitudes demonstrates the efficiency of the method in detecting fire occurrences in the respective regions, mainly in America Central and North, and Europe (Figures 5.7d, f). More than 60% of detected fires by MODIS occurs in areas of PFIv2 between 0.7 and 1.

Regarding the Southwest Pacific region, which records an average of 150 thousand fire occurrences during 2001–2016 period (Figures 5.3m-o), there is an efficiency such as more than 74% were located in the high and critical PFIv2 classes (Figure 5.7e). However, the analyses for Europe (Figure 5.7f) shows that around 15% of the fire occurred in areas whose atmospheric conditions are not susceptible to the fire, PFIv2 very close to 0.1. In this sense, when considering the natural and anthropogenic sources based on climatic factors, PFIv2 indicates risk and vulnerability to erratic fires. Its identification is of fundamental importance, as they can cause substantial changes in plant communities, animal habitats and human health.

Thus, the following section discusses the application of the PFIv2 methodology in the analysis of extreme events of fire occurrences in Europe. This applicability aims at reducing the challenges encountered by politicians and decision makers.

3.2. Study of case analyses

After verifying the PFIv2 capability to locate the main regions of fire activity, it is applied to extreme fire occurrences in Europe. As shown in Figure 5.3, the JASO period concentrates the largest number of global fire. The first event analyzed is the erratic fires in Portugal in August 2003 (SC01). The second event (SC02) occurred in Greece in 2018 (TEDIM et al., 2014; WILDFIRETODAY, 2018).

To evaluate in further details the PFIv2 performance, analyses for the specific months of July and August were carried out in the 2001 – 2016 period, months which those events took place. Based on hundreds of thousands of satellite based detected fires, it is verified that more than 70% (ERAI) and 74% (CPC) of occurrences are in the critical class of the PFIv2 (i.e. high susceptibility; Figure 5.8).

If taking into account the high and critical classes, the efficiency of the PFIv2 exceeds 77% and 80% of accuracy levels with ERAI and CPC precipitation input dataset, respectively. Another factor to be highlighted is that the fire incident in areas which PFIv2 is in the lowest class is by about 2%. According to Camia et al (2017), July and August integrate the interval in which about 86% of the area is burned annually in Europe. Due to highest efficiency in PFIv2 (as showed previously), events SC01 and SC02 will be analysed with CPC precipitation global dataset.

3.2.1. July and August climatology in the 2001-2016 period

Figures 5.9(a)-(c) show the 2001-2016 climatologies of air temperature, relative humidity, and surface pressure from ERA-Interim reanalysis for July and August. Similarly, the individual climatologies of the precipitation, and basic risk

of fire (BR) from CPC are presented in Figures 5.9(d)-(e). The factors of the PFIv2, and the final modelling are shown in Figures 5.9(g)-(h).

During these months, maximum values of air temperature by around 34°C are noted in Portugal, Spain and Turkey (Figure 5.9a). Figure 5.9(b) shows that the temperature characteristics are accompanied by low relative humidity, between 20% and 30% resembling desert climatic conditions (CÁCERES et al., 2007). The contribution of both variables indicates extreme conditions to the fire risk. It has to be noticed that the PFIv2 with respect to the its previous version improves the risk estimates by considering local factors such as latitude, altitude and topography.

The surface pressure and precipitation (Figures 5.9c-d) show conditions in which the surface pressure is related to the cooler conditions and occurrence of precipitation. Generally speaking, the Southern part of Europe is dominated by low pressure system, whereas in the Northern part shows higher values. In the case of low humidity, low pressure system will favor fire development and increased risk related to enhanced vertical moviments.

It should be highlighted that most of Europe experiences very low values of precipitation during these months. Thus, high values of PFIv2 must be expected. In the individual climatologies of the PFIv2 factors, it is noted that the BR (Figure 5.9e) governs fire risk. It is worth mention that this factor considers the precipitation frequency of occurrence in the last 120 days before the due date in association with the type of vegetation.

Figure 5.9(f) displays that the Haines logarithmic factor contributes more effectively in Southern Europe, Russia and Turkey. This cleary reveals that regions such as the Iberian Peninsula, Italy, the Balkan Peninsula and Turkey have an atmosphere conducive to burning in July and August which can be enhanced due to anomalous conditions, such as heat waves and droughts. Figure 5.9g shows that the influence of temperature is most dominant over the Iberian Peninsula.

Figure 5.9h shows the climatological distribution of the PFIv2. It is clear that the BR dominates the continental distribution. Most part of Europe is very vulnerable for fire development related to dry conditions in particular over Italy, France, Iberian Peninsula, and Eastern Europe. In the following two case

studies are investigated in details, to verify the PFIv2 capability to reproduce these fire events.

4. Case Studies

4.1 August 1st to 15th, 2003 (SC01)

Figures 5.10(a)-(d) depict the climate anomalies during the SC01 event, in relation to the 2001-2016 climatology. The SC01 exhibits a remarkable warming over Europe, in particular over Portugal, Spain, France, northern Italy, Germany and the United Kingdom, where temperature differences were about 5°C higher, compared to climatological values. On the other hand, Eastern Europe experiences mid conditions with cooling of up to 3.5°C, over Ukraine and western part of Russia (Figure 5.10a).

As should be expected from the relationship between temperature and relative humidity, warmer conditions result in a drop of relative humidity by up to 22% over Western Europe (Figure 5.10b). In addition, the surface pressure increases (Figure 5.10c), which even favors drier conditions consequently reduzing precipitation (Figure 5.10d). Reduction of precipitation is more proeminent in central Europe, values much close to the climatology appear in the Iberian Peninsula and Turkey (Figure 5.10d).

It is worth noting that the first component to be considered in the PFIv2 is the BR, which depends on daily accumulated precipitation data. However, there are not proportional rates (in magnitude) of the anomalous precipitation regime (Figure 5.10d) and the BR distribution. The BR considers a period of up to 120 days before the beginning of the analysis. Therefore, it is evident that the increase in precipitation over Ukraine, Belarus, Lithuania and in western Russia was a specific occurrence from SC01. On the other hand, there is apredominance level closest to 0.6 in BR near the northeastern region of Spain, central France, Germany, Belgium and Netherlands (Figure 5.10e).

In relation to the Haines logarithmic factor (Figure 5.10f), it is observed a similar distribution to that demonstrated by the relative humidity (Figure 5.10b), in which most of Europe is favorable to fire development, considering the topographic factor and the specific thresholds of air and dew point temperatures

in the three tropospheric layers. Figure 5.10(g) presents the contribution of the temperature factor to the risk of fire in the SC01 interval. Similarly to temperature anomalies (Figure 5.10a), this parameter suggests that from the Iberian Peninsula to the central region of Poland, fire was susceptible to occur. However, the PFIv2 anomaly between the SC01 and the 2001-2016 period, over East Europe show condition of lower vulnerability, but as will be discussed below, fire incident was remarkable over there.

As shown in Figure 5.10(h), the PFIv2 increases by up to 0.3, in the regions that occurred the highest fire concentrations in Western Europe, between 40°N and 55°N. It is highlighted in Portugal, Spain, France, and the Balkan Peninsula. However, the western part of Eurasia experiences massive number of fires, related to direct influence of local elevation and atmospheric conditions such as much, lower relative humidity, and precipitation.

Figure 5.10(h) also points out that during the SC01 that PFIv2 maintained its conditions of high susceptibility to the fire occurrences, except in the southern region of Italy where the occurrence of anomalous precipitation (Figure 5.10d) weakened the atmospheric fire susceptibility.

4.2 July 21st to 31st 2018 (SC02)

Figures 5.11(a)-(h) show the difference of climate and PFIv2 components with respect to the 2001-2016 interval characteristics of the SC02 event. At the case of meteorological anomalies, Figure 5.11(a) presents a positive variation of air temperature at 2m, along the 48°N and 56°N latitudinal belt. Warmer conditions of up to 5°C are evident in northern France, United Kingdom, Germany, Belgium, Holland and the western part of Poland. Over East Europe, northeastern Turkey, Italy and the eastern part of the Iberian Peninsula, the anomalous warming during the SC02 period varies between 1°C and 4°C. However, negative anomalies are observed over the western Iberian Peninsula, on the Balkan Peninsula, and vicinities.

As expected, the spatial pattern of relative humidity (Figure 5.11b) is correlated to that of the air temperature at 2m. It is worth to mention that positive (negative) anomalies of relative humidity (air temperature at 2m) act in most of Eurasia to enhance the fire vulnerability. On the other hand, the low

pressure anomalous pattern over east Europe (Figure 5.11c) increases the atmospheric humidity.

Turning to precipitation (Figure 5.11d), it is clear that dry conditions are dominant over most part of Europe, but increase in precipitation during the July 21 to 31st is expressive over the eastward. Figure 5.11(e) shows the BR anomaly during the SC02, in relation to the 2001-2016 period. It is interesting to note that positive anomalies of BR are located in regions of different meteorological patterns. At first glance, it is observed that the north Europe shows positive anomalies close to 0.75, which reflects the drop in precipitation in Figure 5.11(d). On the other hand, positive anomalies of BR are verified in the United Kingdom, in disagreement to the monthly accumulated precipitation discussed previously. This may be explained by the fact that the anomalies are specific to the interval between 21st and 31st July 2018. The BR calculation takes into account the precipitation data that are accumulated in distinct intervals in the 120 days prior to the first day of the analysis. Therefore, in our approach the fire risk distribution is not dependent on the total precipitation but on how it is distributed.

As shown in Figures 5.11(f)-(g), the respective Haines logarithmic and temperature factors can efficiently reproduce regions which are prone to fire development. It is important to mention that the temperature factor (Figure 5.11g) is adjusted by latitudinal changes (eq. 5.6), which gives the threshold for each latitude in terms of fire risk. This differentiates the effect of temperature in the tropics and extratropics.

The anomaly of the PFIv2 reveals accuracy in the range of accumulated fires in northern Central Europe, southwest Russia and some localities in northern Turkey during the SC02 (Figure 5.11h), in agreement with the fire occurrence. The negative anomaly observed in the Balkans and Eastern Europe arise due to the anomalous characteristics of the SC02. Hundreds of accumulated fires in these areas does not match positive PFIv2 anomalies. It has to be mentioned that those regions climatologically exhibit high values of PFIv2 (see Figure 5.9h). Thus, the drop in the PFIv2 values, indicating lower fire risk during those days is not sufficient to suppress the fire activity, which was claimed to be one of the strongest event of forest fires of the 21st century (THE TELEGRAPH, 2018).

5. The North Atlantic Oscillation (NAO) and the fire activity

Over midlatitudes of the North Hemisphere (NH), the climate regime is mainly dictated by vacillation in the phase of the North Atlantic Oscillation (NAO; e.g., VISBECK et al. 2001; DURKEE et al. 2008; WARREN and BRADFORD, 2010). The NAO is associated with the differences in atmospheric pressure between the Arctic (polar low) and mid-Atlantic (subtropical high) regions. The strength of the low and high systems influences the wind magnitude which impacts on heat and moisture transport, surface temperature and the magnitude of precipitation (BACER et al. 2016).

In a positive NAO phase, when the Icelandic Low and Azores High are relatively stronger, the pressure difference is higher than average and its gradient produces surface westerlies stronger than average across the middle latitudes of the Atlantic towards to north-western Europe (HURREL et al. 2003). Although this is an important issue, no previous attempt has been made to systematically investigate the impact of the NAO on the fire risk.

Figures 5.12(a)-(b) show the correlation between the Basic Risk (BR) and the NAO for July and August climatologies, respectively. These analyses have also been made for the PFIv2 results (Figures 5.12c-d). Despite the strongest influence of the NAO occurs in winter (WARREN and BRADFORD, 2010), Figures 5.12(a)-(b) show that the precipitation induced by the NAO increases the BR (less precipitation amount) in northern Europe in July. On the other hand, Figures 5.12(c)-(d) display that the correlation between the PFIv2 and NAO is mostly intensified (reduced) in July (August) with respect to the BR.

The correlations among the daily NAO and PFIv2 factors for SC01 (Figures 5.13a-d) and SC02 (Figures 5.13e-h) show local aspects for each event. Indeed, the correlation between the NAO and the RB factors shows negative values over almost area on SC01 (Figure 5.13a), but a reduction in the significance of the SC02 event (Figure 5.13e). It is argued that the precipitation related to the NAO on the first case reduces the BR, while in the second analysis there are positive correlations on southern Balkan Peninsula, Irish isles, and French coast. The impact of the NAO on the Haines logarithmic function (LogHai) is higher over Central Europe (Balkan) with negative (positive)

correlation. It is important to highlight that the correlation between NAO and the LogHai is not statistically significant on Spain and Italian Peninsula.

Figures 5.13(c),(g) show that there are favorable conditions for a negative (positive) correlation between NAO and the temperature factor over central and western Europe on SC01 (SC02) event. It may be noticed that a dipole pattern is estabilished on Eurasia is so far as the relationship between the NAO and temperature is concerned.

Finally, on the analyses of the correlations between NAO and the PFIv2, it can be inferred that there is not a direct influence (not statistically significant), with the highest fire occurrences on the SC01 (Figure 5.13d). Conversely, the Figure 5.13(h) displays positive correlation on the SC02, that agrees with the high number of fires observed in the Attica region (southeastern Greece), between the July 23rd and 24th, 2018. This demonstrates the potential effect of the NAO, as a driven to increase the condition prone to fire development.

6. Concluding Remarks

Based on the second version of the Potential Weather Fire Index (PFIv2), this study evaluated the global susceptibility to the fire occurrences, according to current atmospheric patterns. It was demonstrated that the modification proposed in the PFIv2, could properly reproduces the regions with the highest incidence of fires in Asia, North America and Europe. The PFIv2 was also validated based on two study cases of atypical fire that occurred in August 2003 and July 2018.

Although the adjustment prioritizes the extratropic regions, the model was also efficient in the other areas of high susceptibility to the fire occurrences. The new correction factor of the air temperature, due to the latitudinal change and the Haines logarithmic function act as local parameters, such as: elevation of topography and latitude. This was verified, mainly in the Africa continent, with accuracy level in the maximum classes of PFIv2 with CPC (ERAI) precipitation dataset close to 88.4% (78%). The efficiency of the PFIv2 in reproducing regions with fire susceptibility was also demonstrated in Asia, where 400 thousand fires have been observed. Only the high and critical classes of the model accounted for more than half of the incident fires (53% and 63%) based

on ERAI and CPC, respectively. The efficiency of the PFIv2 is shown because the majority of the observed fire is located in fire risk classes of model larger than 0.75 (high and critical).

The most important limitation of PFIv2 is the high dependence of the days of dryness, which is computed from the precipitation data. For precipitation is still an uncertain parameter in the forecasts of the present climate and also presents divergences among the atmospheric models. However, it was demonstrated that the CPC analysis is more reasonable than the ERAI dataset, which tends to overestimate the daily precipitation. Future perspectives to improve even more the parameterization of PFIv2 are variations in the litter, the inclusion of lightining, density population function, for instance. Although the results presented in this article are based solely on atmospheric vulnerability, it is known that regardless of the source of ignition, climatic factors are primordial for the fire occurrences.

7. Acknowledgements

To the people management of the Federal University of West Para (Ordinance N ° 594, of March 4th, 2015). To the Graduate Program in Applied Meteorology of the Federal University of Vicosa (www.posmet.ufv.br) and to the Fire Program of the National Institute of Space Research (INPE) – Brazil (http://www.inpe.br/queimadas/portal).

REFERENCES

Andrews, P. L., and Bradshaw, I. S. (1997). Fires: Fire Information Retrieval and Evaluation System – A program for fire danger rating analysis. **General Technical Report (GTR)**. INT-GTR-367. Ogden, UT, U. S. Department of Agriculture, Forest Service, Intermountain Research Station, 64p.

Archibald, S., Roy, D. P., Van Wilgen, B. W., and Scholes, R. J. (2009). What limits fire? An examination of drivers of burnt area in Southern Africa. **Global Change Biology**, 15, 613– 630.

Bacer, S., Christoudias, T., and Pozzer, A. (2016). Projection of North Atlantic Oscillation and its effect on tracer transport. **Atmospheric Chemistry and Physics**, 16, 15581-15592, doi:10.5194/acp-16-15581.

Bradstock, R. A. (2010). A biogeographic model of fire regimes in Australia: current and future implications. **Global Ecology and Biogeography**, 19, 145-158. doi: 10.1111/j.1466-8238.2009.00512.x.

Burgan, R. E. (1988). Revisions to the 1978 National Fire Danger Rating System. Res. Paper SE-273. **U. S. Department of Agriculture, Forest Service,** Southeastern Forest Experiment Station, Asheville, NC.

Cáceres, I., Gómez-silva, B., Garró, X., Rodriguez, V., Monardes, V., and Mckay, C. P. (2007). Relative humidity patterns and fog water precipitation in the Atacama Desert and biological implications. **Journal of Geophysical Research**, VOL. 112, doi:10.1029/2006JG000344.

Camia, A., Libertá, G., and San-miguel-ayanz, J. (2017). Modeling the impacts of climate change on forest fire danger in Europe. Sectorial results of the PESETA II Project. **Joint Research Centre**, doi: 10.2760/768481.

Catchpole, W. (2002). Fire properties and burn patterns in heterogeneous landscapes. Flammable Australia: the fire regimes and biodiversity of a continent (ed. by R.A. Bradstock, J.E. Williams and A.M. Gill), pp. 50 – 75. **Cambridge University Press**, Cambridge.

Cruz, M. G., Gould, J. S., Hollis, J. J. and Mccaw, W. L. (2018). A Hierarchical Classification of Wildland Fire Fuels for Australian Vegetation Types. *Fire*, 1, 13; doi:10.3390/fire1010013.

Davidson, E. A., de Araújo, A. C., Artaxo, P., Balcj, J. K., Brown, I. F. e*t al*. (2012). The amazona basin in transition. **Nature**, v. 481, n. 7381, p. 321-328.

Dee, D. P., Uppala, S. M., Simmons, A. J., Berrisford, P., Poli, P. *et al*. (2011). The ERA-Interim reanalysis: Configuration and performance of the data assimilation system. **Quarterly Journal of the Royal Meteorological Society**, v. 137(656), p. 553-597.

Durkee, J. D., Frye, J. D., Fuhrmann, C. M., Lacke, C. M., Jeong, H. G., and Mote, T. L. (2008). Effects of the North Atlantic Oscillation on precipitation-type frequency and distribution in the eastern United States. **Theoretical and Applied Climatology**, 94, 51-65.

FAO. (2006). Fire management global assessment. A thematic study prepared in the framework of the Global Forest Resources Assesment. Food and Agriculture Organization of the United Nations.

Fetter, R., Carlos, H., and Steinke, E. (2018). Um Índice para Avaliação da Variabilidade Espaço-Temporal das Chuvas no Brasil. **Revista Brasileira de Meteorologia**, n. 2, p. 225-237.

Finney, M. A., Cohen, J. D., Mcallister, S. S., and Jolly, W. M. (2012). On the need for a theory of wildland fire spread. **International Journal of Wildland Fire**, 22(1), 25–36.

Galanter, M., Levy, H., and Carmichael, G. R. (2000). Impacts of biomass burning on tropospheric CO, NO_x, and O_3. **Journal Geophys. Res.-Atmos.**, 105, 6633-6653.

González-Cabán, A. (2013). Vegetation Fires and Global Change: Challenges for Concerted International Action. **Global Fire Monitoring Center** (GFMC).

Global Forest Resources Assessment (GFRA). (2015). **Food and Agriculture Organization of the United Nations / FAO.** ISBN 978-92-5-108826-5.

Haines, D. A. (1988). A lower atmosphere severity index for wildland fires. **National Weather Digest**, 13, 23-27.

Harrison, S. P., Power, M., and Bond, W. (2007). Paleofires and the Earth system. **iLEAPS Newsletter**, v. 3, p. 18-20.

Hickler, T. e*t al*. (2006). Implementing Plant Hydraulic Architecture within the LPJ Dynamic Global Vegetation Model. **Global Ecology and Biogeography**, V. 15, No. 6, pp. 567-577.

Hollmann, R., Merchant, C., Saunders, R., Downy, C. et al. (2013). The ESA climate change initiative: satellite data records for essential climate variables. **Bulletin of the American Meteorological Society**, 94, p. 1541-1552.

Huang, X., Rein, G., and Chein, H. (2015). Computational smoldering combustion: Predicting the roles of moisture and inert contents in peat wildfires. **Proceedings of the Combustion Institute**, v. 35, p. 2673-2681.

Hurrel, J. W., Kushnir, Y., Ottersen, G., and Visbeck, M. (2003). An overview of the North Atlantic Oscillation, in: The North Atlantic Oscillation: Climate Significance and Environmental Impact, edited by: HURRELL, J. W.; KUSHNIR, Y.; OTTERSEN, G. and VISBECK, M. **Geophysical Monograph Series**, 134, American Geophysical Union, Washington DC, 1-35.

Justino, F., Melo, A. S., Setzer, A., Sismanoglu, R., Sediyama, G. C., Ribeiro, G. A., Machado, J. P., and SterL, A. (2010). Greenhouse gas induced changes in the Fire Risk in Brazil in ECHAM5/MPI-OM Coupled Climate Model. **Climatic Changes**, vol. 106, n. 2, p. 285-302.

Justino, F., Stordal, F., Clement, A., Coppola, E., Setzer, A., and Brumatti, D. (2013). Modelling Weather and Climate Related Fire Risk in Africa. **American Journal of Climate Change**, 2, p. 209 – 224.

Krause, A., Kloster, S., Wilkenskjeld, S., and Paeth, H. (2014). The sensitivity of global wildfires to simulated past, present, and future lightning frequency.

Journal of Geophysical Research: Biogeosciences, doi: 10.1002/2013JG002502.

Li, F., Bond-Lamberty, B., and Levis, S. (2014). Quantifying the role of fire in the Earth system – Part 2: Impact on the net carbon balance of global terrestrial ecosystems for the 20th century. **Bigeosciences**, **11**, 1345-1360, doi: 10.5194/bg-11-1345-2014.

Markgraf, V., Whitlock, C., and Haberle, S. (2007). Vegetation and Fire History during the Last 18,000 calyr B. P. in Southern Patagonia: Mallin Pollux, Coyhaique, Province Aisen (45° 41' 30"S, 71° 50' 30" W, 640 m Elevation). **Palaeogeography, Palaeoclimatology, Palaeoecology**.

Marlon, J. R. et al. (2008). Climate and Human Influences on Global Biomass Burning over the Past Two Millennia. **Nature Geoscience**, v. 1, n. 10, pp. 697-702.

Masrur, A., Petrov, S. N., and Degroote, J. (2018). Circumpolar spatio-temporal patterns and contributing climatic factors of wildfire activity in the Arctic tundra from 2001-2015. **Environmental Research Letters**, v. 13, 014019. [https://doi.org/10.1088/1748-9326/aa9a76.

Ministério da Ciência, Tecnologia e Inovação (MCTI). (2013). Estimativas Anuais de Emissões de Gases de Efeito Estufa no Brasil. **MCTI**, Brasilia. Available on http://www.mct.gov.br/upd_blob/0226/226591.pdf.

National Interagency Fire Center (NIFC). (2013). Federal firefighting costs **https://www.nifc.gov/fireInfo/fireInfo_documents/SuppCosts.pdf** (suppression only).

Potter, B. (2018). The Haines Index – it's time to revise it or replace it. **International Journal of Wildland Fire**, 27(7), p. 437-440 [https://doi.org/10.1071/WF18015].

Reboita, M. S. et al. (2010). Regimes de precipitação na América do Sul: uma revisão bibliográfica. **Revista Brasileira de Meteorologia**, v. 25, n. 2, p. 185-204.

Richard, R., and Heim, J. R. (2002). A review of twentieth-century drought indices used in the United States. **American Meteorological Society**, [https:/doi.org/10.1175/1520-0477-83.8.1149], p. 1149-1165.

Scheiter, S., and Higgins, S. I. (2009). Impacts of Climate Change on the Vegetation of Africa: An Adaptive Dynamic Vegetation Modelling Approach. **Global Change Biology**, V. 15, No. 9, pp. 2224-2246.

Serreze, M. C., and Barry, R. G. (2010). Climate change. In: BARRY, R. G., CHORLEY, R. J. (Eds.), Atmosphere. Weather and Climate. Routledge, Oxon.

Silva, J. M. N., Pereira, J. M. C., Cabral, A. I., Vasconcelos, M. J. P., Mota, B., and Gregoire, J. M. (2003). An Estimate of the Area Burned in Southern Africa during the 2000 Dry Season Using SPOT-VEGETATION Satellite Data. **JournalofGeophysicalResearch**, v. 108, No. D13.

Skinner, D. J., Rocks, S. A., and Pollard, S. J. (2014). A review of uncertainty in environmental risk: characterising potential natures, locations and levels. **Journal of Risk Research**, 17(2), 195–219.

Sopko, P., Bradshaw, I., and Jolly, M. (2016). Spatial products available for identifying areas of likely wildfire ignitions using lightning location data-Wildland Spera, S. A., Galford, G. L., Coe, M. T., Macedo, M. N., Mustard, J. F. (2016). Land-Use Change Affects Water Recycling in Brazil's Last Agricultural Frontier. **Global Change Biology**, doi: 10.1111/gcb.13298.

Spera, S.A., Galford, G. L., Coe, M. T., Macedo, M. N., Mustard, J. F. (2016). Land-Use Change Affects Water Recycling in Brazil's Last Agricultural Frontier. **Global Change Biology**, doi:10.1111/gcb.13298.

Tedim, F., Remelgado, R., Martins, J., and Carvalho, S. (2014). The largest forest fires in Portugal: the constraints of burned area size on the comprehension of fire severity. **Journal of Environmental Biology**. ISSN: 2394-0379.

The telegraph. (2018). Greece wildfires: 'At least 60' killed near Athens as residents and tourists forced to flee into the sea". **The Telegraph**. Retrieved 24 July 2018.

Tosca, M. G., Randerson, J. T., and Zender, C. S. (2013). Global impact of smoke aerosols from landscape fires on climate and the Hadley circulation. **Atmospheric Chemistry and Physics**, 13, 5227-5241, doi: 10.5194/acp-13-5227-2013.

Tymstra, C., Bryce, R. W., Wotton, B. M., Taylor, S. W., and Armitage, O. B. (2010). Development and structure of Prometheus: the Canadian Wildland Fire Growth Simulation Model. **Natural Resources Canada**, Information Report NOR-X-417. Canadian Forest Service, Northern Forestry Centre.

Van der Werf, G. R., Randerson, J. T., Giglio, L. *et al*. (2017). Global fire emissions estimates during 1997-2016. **Earth System Science Data**, v. 9, p. 697-720, https://doi.org/10.5194/essd-9-697-2017.

Van Wagner, C. E. (1970). Conversion of William's Severity Rating for use with the Fire Weather Index, Information Report PS-X-21, **Canadian Forestry Service**, Ontariom Canada.

Van Wagner, C. E. Development and structure of the Canadian forest fire weather index system. (1987). **Forest Technology Report**, v. 35 (Canadian Forestry Service: Ottawa).

Veraverbeke, S., Borges, B. M., Goulden, M. L. et al. (2017). Lightning as a major driver of recent large fire years in North American boreal forests. **Natural Climate Change**, v. 7, p. 529-534, doi: 10.1038/nclimate3329.

Visbeck, M. H., Hurrel, J. W., Polvani, I., and Cullen, H. M. (2001). The North Atlantic Oscillation: Past, present, and future. **Procedings of the National Academy of Sciences**, v. 98, pp. 12876-12877, doi: 10.1073/pnas.231291598.

Warmink, J., Janssen, J., Booij, M. J., and Krol, M. S. (2010). Identification and classification of uncertainties in the application of environmental models. **Environmental Modelling & Software**, 25(12), 1518–1527.

Warren II, R. J., and Bradford, M. A. (2010). Seasonal Climate Trends, the North Atlantic Oscillation, and Salamander Abundance in the Southern Appalachian Mountain Region. **Journal of Applied Meteorology and Climatology**, v. 49, doi: 10.1175/2010JAMC2511.1.

Wildfiretoday. (2018). Report issued on one of the devastating fires near Athens, Greece / July 2018 Attica (Central Greece) wildfires. **Scientific Report (Version 1.1)**. [https://wildfiretoday.com/2018/08/02/report-issued-on-the-devastating-fire-near-athens-greece/] (Accessed in 2018).

Williams, D. E. (1959). Fire season severity rating. **Department of Northern Affairs and National Resources,** Forest Research Division. Technical Note, no. 73, pp. 13.

Winkler, J. A., Potter, B. E., Wilhelm, D., Shadbolt, R. P., Piromsopa, K., and Bian, X. (2007). Climatological and statistical characteristics of the Haines Index for North America. **International Journal of Wildland Fire**, 16, 139-152, doi: 10.1071/WF06086.

Wolfson, R. (2012). Energy, Environment and Climate, second ed. WW Norton and Company Inc, New York, pp. 366-370.

Wooster, M. J., and Zhang, Y. H. (2004). Boreal forest fires burn less intensely in Russia than in North America. **Geophysical Research Letters**, v. 31, n. L20505, https://doi.org/10.1029/2004GL020805.

Xie, P., Chen, M., and Shi, W. (2010). CPC unified gauge analysis of global daily precipitation. Preprints, **24th Conference on Hydrology**. Atlanta, Georgia. American Meteorological Society, 2.3A. [Avaiable online at https://ams.confex.com/ams/90annual/webprogram/Paper163676.html].

Tables

TABLE 5.1. Fire risk (PFIv2) levels.

Levels	*PFI (0 to 1)*
Minimum	< 0.15
Low	0.15 to 0.40
Medium	0.40 to 0.70
High	0.70 to 0.95
Critical	≥ 0.95

Figures

Fig. 5.1 *(a)* Study areas according to the WMO classification. *(b)* Vegetation distribution by IGBP (adapted from FRIEDL et al., 2010). *(c)* Temporal evolution of basic risk as function of the days of drought and vegetation.

Fig. 5.2 Flowchart presenting the sequence of calculation for the PFIv2.

Fig. 5.3 Seasonality of fire occurrences detected by satellite Terra/MODIS from 2001 to 2016 for all six study areas.The trend equations are shown in the top right of each annual fire distribution. Note: The range values for Africa *(a)-(c)* and South America *(g)-(i)* are bigger than for another regions.

Fig. 5.4 Anomalies in Precipitation (left side), and Basic Risk of fire (right side) for NDJF *(a)-(b)*, MAMJ *(c)-(d)*, JASO *(e)-(f)*, and 2001-2016 period *(g)-(h)* by ERAInterim averages with respect to CPC averages for the period of 2001-2016. Black dots show statistically significant differences at 95%.

Fig. 5.5 Standard deviation of the Basic Risk by CPC data (left side), and anomalies between ERA-Interim and CPC averages (right side) for NDJF *(a)-(b)*, MAMJ *(c)-(d)*, JASO *(e)-(f)*, and for all 2001-2016 period *(g)-(h)*.

Fig. 5.6 Present day (2001-2016) PFIv2 factors *(a)-(c)* for July-August-September-October (JASO), *(d)* is the PFIv2 based on ERAInterim climate data and on IGBP vegetation classes. Figures *(e)* and *(f)* are the standard deviation and the annual trend, respectively.Note. Figures *(b)* and *(f)* were multiplied by a hundred.

Fig. 5.7 Percentage of accumulated daily fire at each PFIv2 level based on ERAInterim, and CPC precipitation data for the 2001-2016 period. *(a)* Africa, *(b)* Asia, *(c)* South America, *(d)* Americas and Caribbean, *(e)* South-West Pacific and *(f)* Europe. ZERO indices are the percentage of fire events that were observed in a level closest to zero by PFIv2 (displayed in the top left corner of each panel).

Fig. 5.8 Percentage of accumulated daily fire at each PFIv2 level in Europe for July *(a)* and; August *(b)* during the 2001-2016 period. ZERO indices are the percentage of fire events that were observed in a level closest to zero by PFIv2 (displayed in the top left corner of each panel).

Fig. 5.9 July and August climatology in the 2001-2016 period. Maximum temperature at 2 m (*(a)*, °C), relative humidity *(b)*, surface pressure (*(c)*, hPa), precipitation (*(d)*, mm/day), PFIv2 factors *(e)-(g)* and, *(h)* PFIv2 over the accumulated fire event from 2003 (dots).

Fig. 5.10 Anomalies in *(a)* maximum temperature at 2 m (°C), *(b)* relative humidity (%), *(c)* surface pressure (hPa), *(d)* precipitation (mm/day), *(e)-(g)* PFIv2 factors, and *(h)* PFIv2 distribution for August 1st to 15th 2003 with respect to August averages for the period 2001-2016. Black dots on *(h)* denote local fires.

Fig. 5.11 Anomalies in *(a)* maximum temperature at 2 m (°C), *(b)* relative humidity (%), *(c)* surface pressure (hPa), *(d)* precipitation (mm/day), *(e)-(g)* PFIv2 factors, and *(h)* PFIv2 distribution for July 21st to 31st 2018 with respect to July averages for the period 2001-2016. Black dots on *(h)* denote local fires.

Fig. 5.12 Correlation between Basic Risk and NAO for July *(a)* and August *(b)* in the 2001 – 2016 period. Correlation between PFIv2 and NAO for both months *(c)-(d)* at same period. Gridpoints that do not show statistically significant differences are shown in grey.

Fig. 5.13 Correlation of individual and combined PFIv2 factors with NAO for SC01 *(a)-(d)* and SC02 *(e)-(h)*. Gridpoints that do not show statistically significant differences are shown in grey.

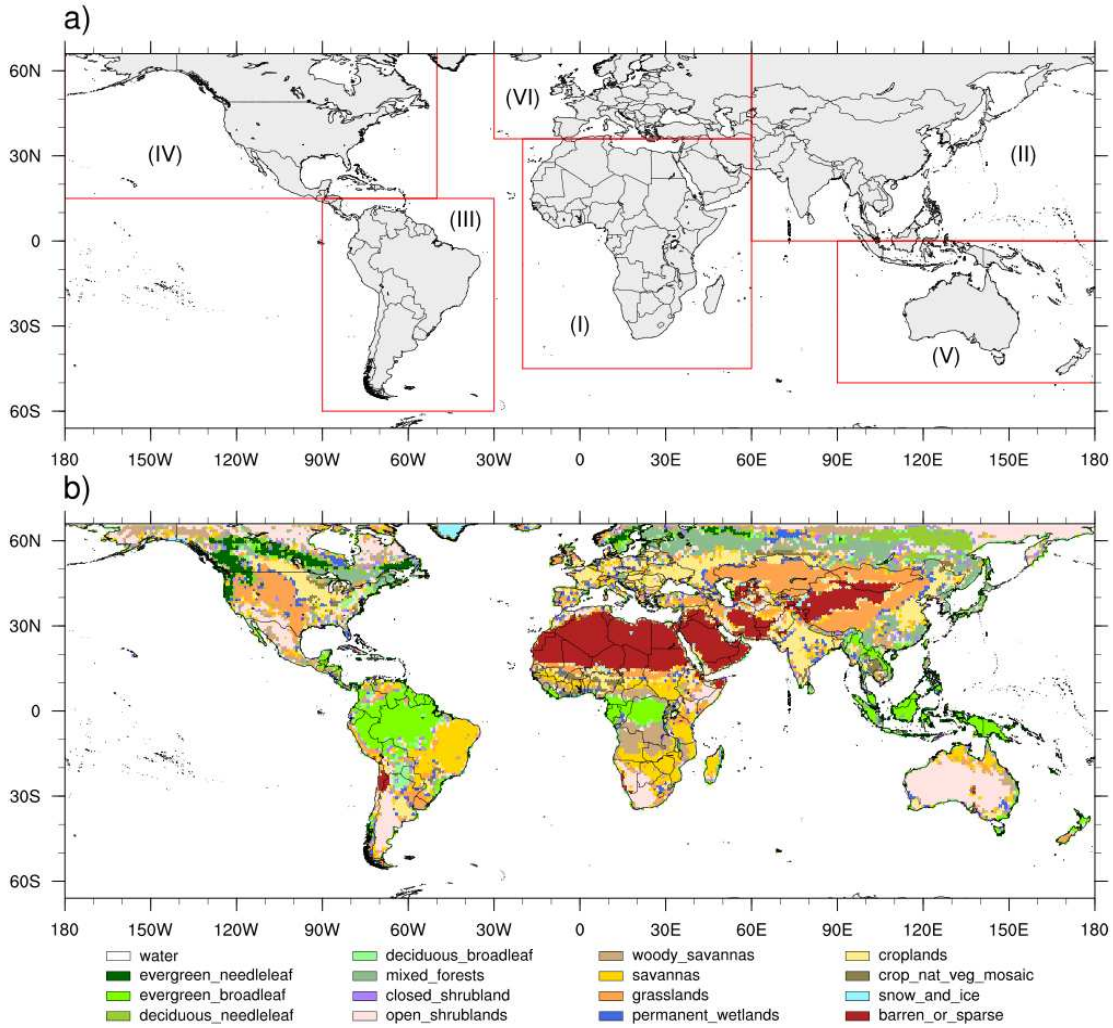

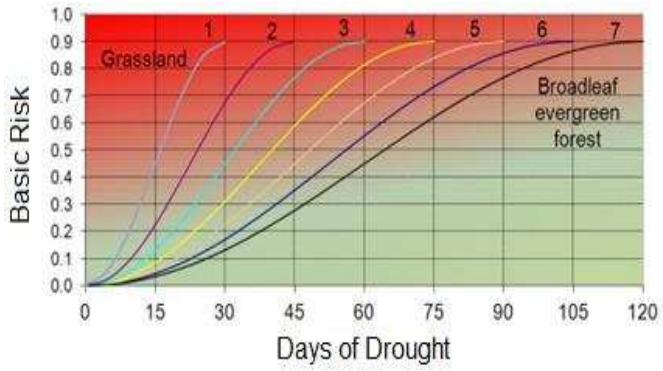

Figure 5.1. *(a)* Study areas according to the WMO classification. *(b)* Vegetation distribution by IGBP (adapted from FRIEDL et al., 2010). *(c)* Temporal evolution of basic risk as function of the days of drought and vegetation.

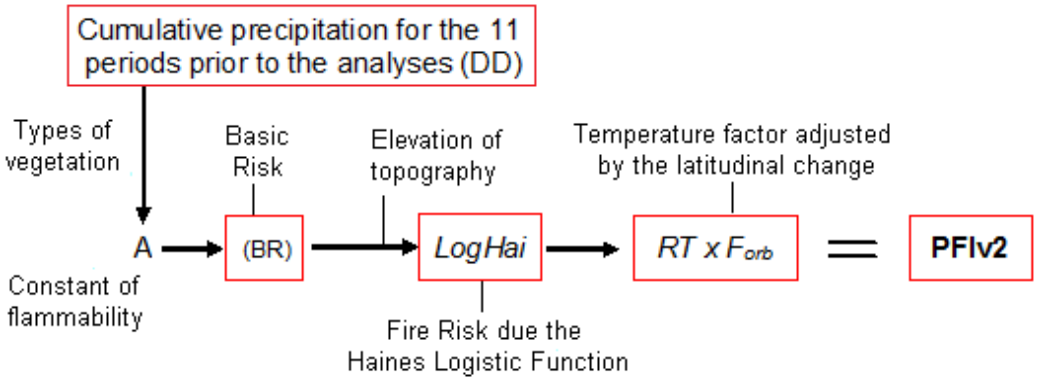

Figure 5.2. Flowchart presenting the sequence of calculation for the PFIv2.

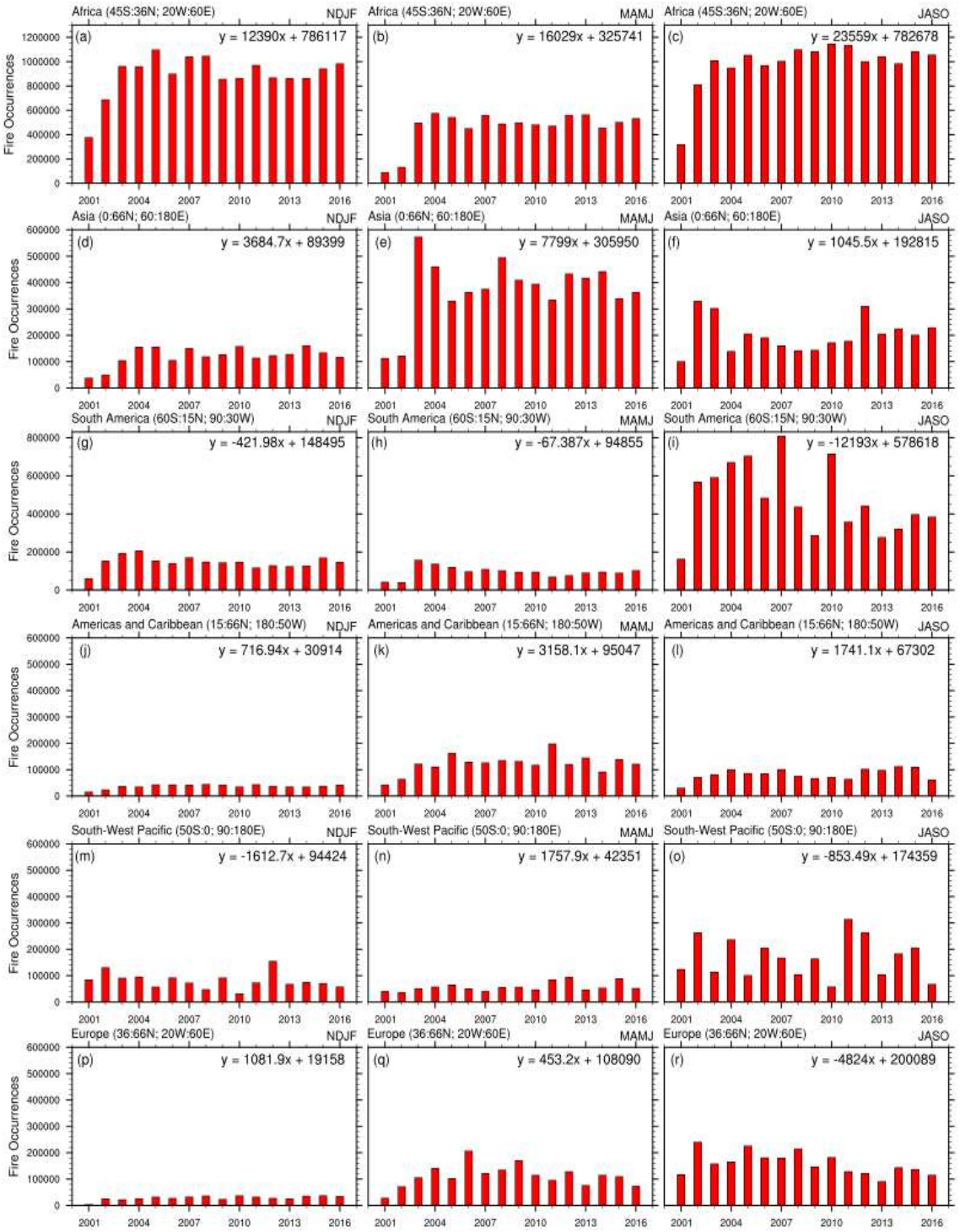

Figure 5.3. Seasonality of fire occurrences detected by satellite Terra/MODIS from 2001 to 2016 for all six study areas.The trend equations are shown in the top right of each annual fire distribution. Note: The range values for Africa *(a)-(c)* and South America *(g)-(i)* are bigger than for another regions.

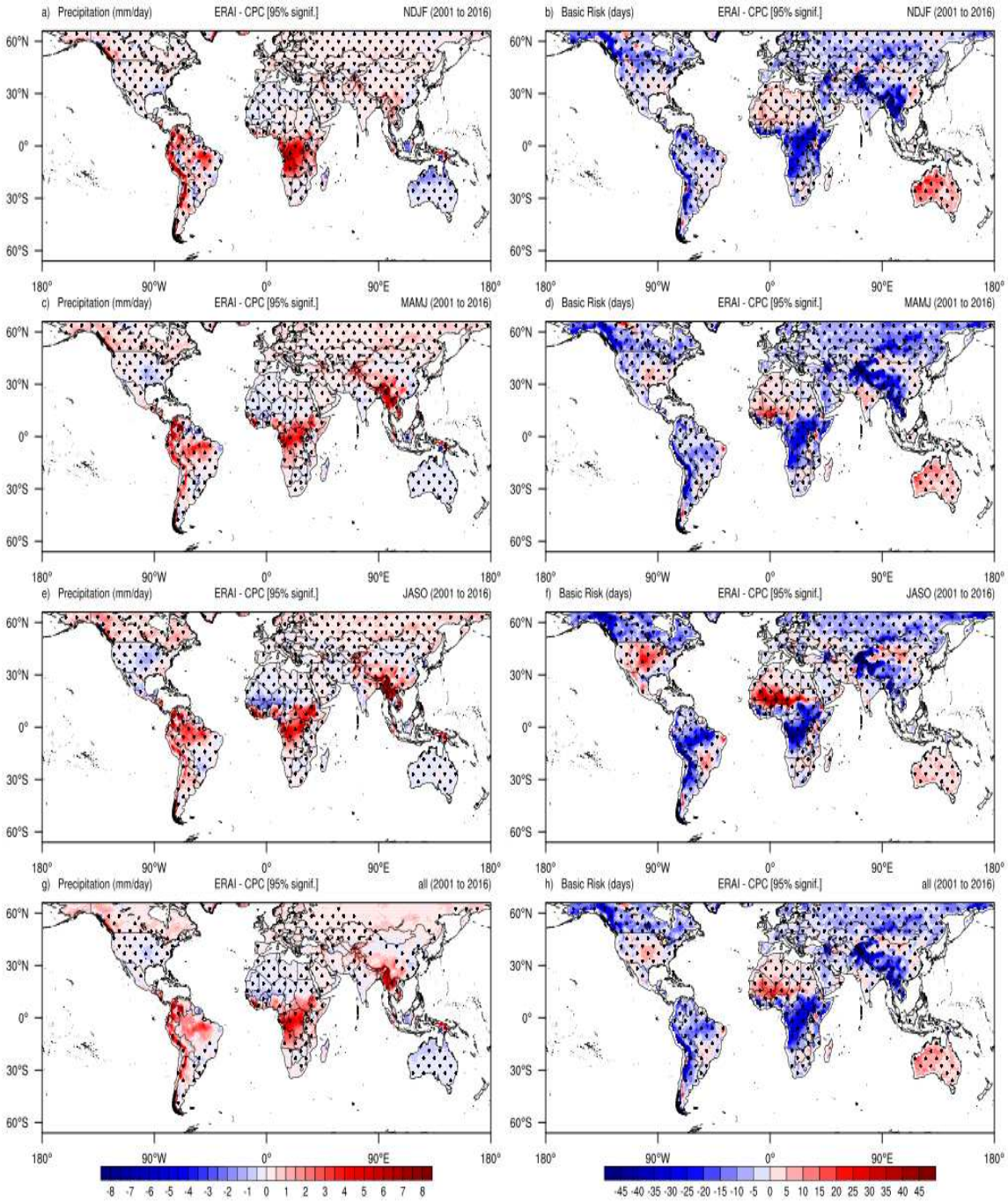

Figure 5.4. Anomalies in Precipitation (left side), and Basic Risk of fire (right side) for NDJF *(a)-(b)*, MAMJ *(c)-(d)*, JASO *(e)-(f)*, and 2001-2016 period *(g)-(h)* by ERAInterim averages with respect to CPC averages for the period of 2001-2016. Black dots show statistically significant differences at 95%.

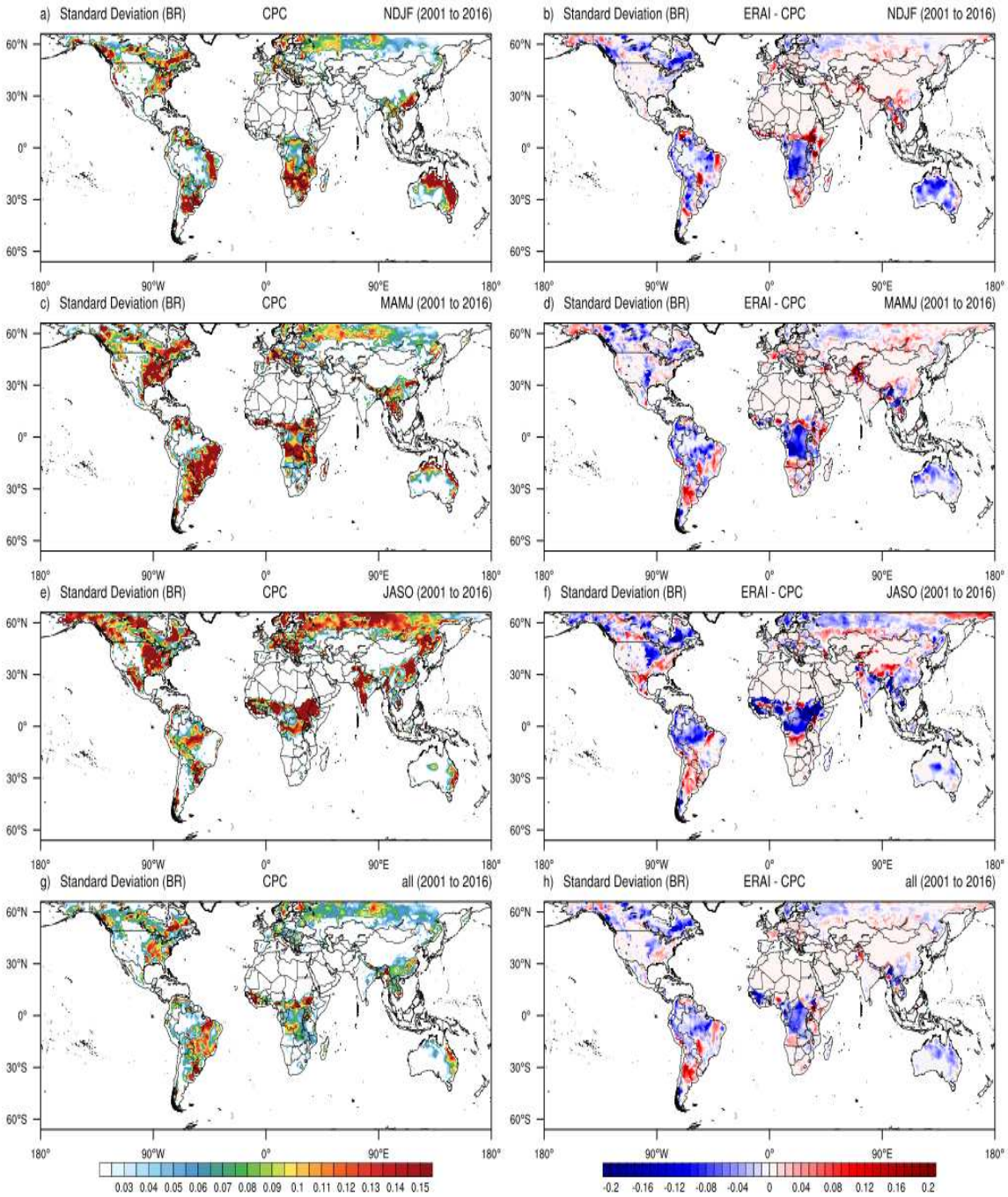

Figure 5.5. Standard deviation of the Basic Risk by CPC data (left side), and anomalies between ERA-Interim and CPC averages (right side) for NDJF *(a)-(b)*, MAMJ *(c)-(d)*, JASO *(e)-(f)*, and for all 2001-2016 period *(g)-(h)*.

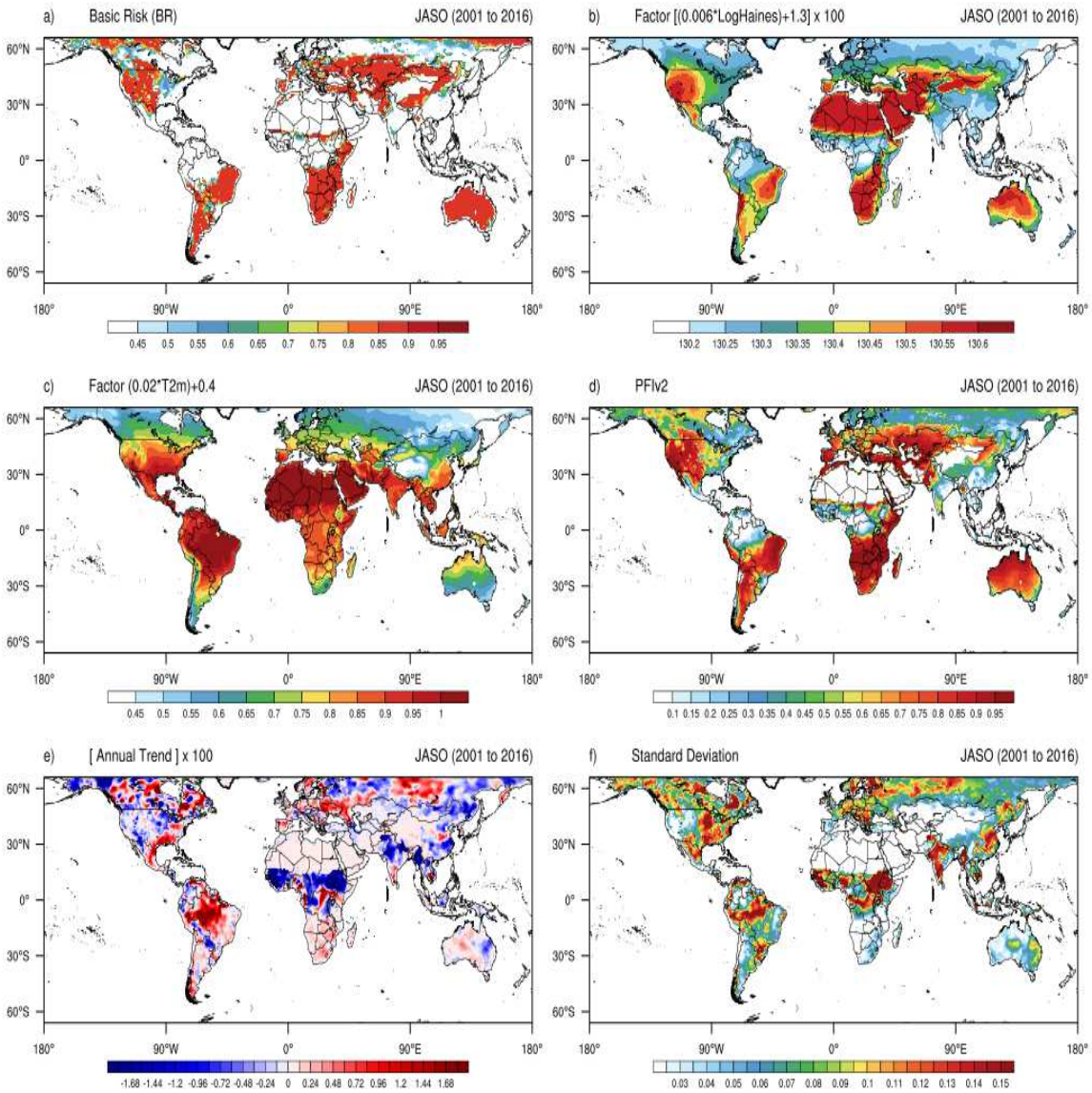

Figure 5.6. Present day (2001-2016) PFIv2 factors *(a)-(c)* for July-August-September-October (JASO), *(d)* is the PFIv2 based on ERAInterim climate data, on CPC global Precipitation, and on IGBP vegetation classes. Figures *(e)* and *(f)* are the annual trend and the standard deviation, respectively. Note. Figures *(b)* and *(e)* were multiplied by a hundred.

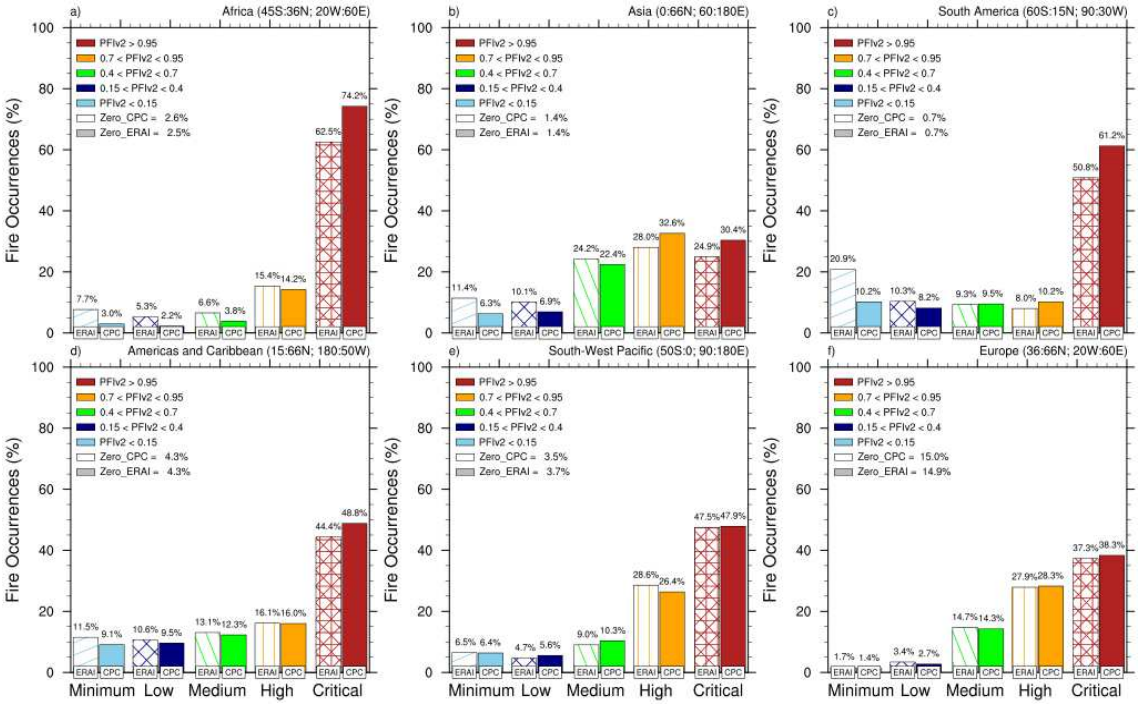

Figure 5.7. Percentage of accumulated daily fire at each PFIv2 level based on ERAInterim, and CPC precipitation data for the 2001-2016 period. *(a)* Africa, *(b)* Asia, *(c)* South America, *(d)* Americas and Caribbean, *(e)* South-West Pacific and *(f)* Europe. ZERO indices are the percentage of fire events that were observed in a level closest to zero by PFIv2 (displayed in the top left corner of each panel).

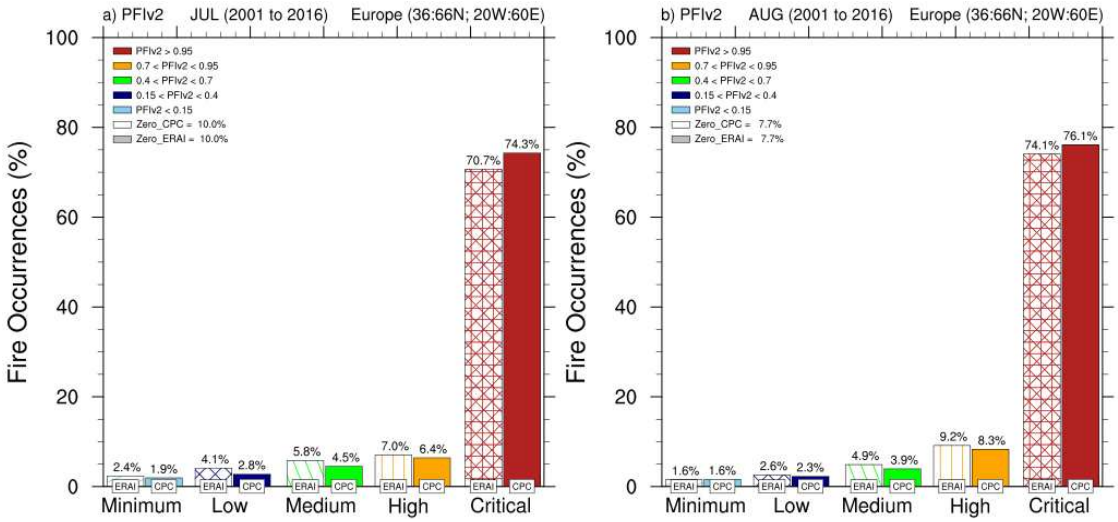

Figure 5.8. Percentage of accumulated daily fire at each PFIv2 level in Europe for July *(a)* and; August *(b)* during the 2001-2016 period. ZERO indices are the percentage of fire events that were observed in a level closest to zero by PFIv2 (displayed in the top left corner of each panel).

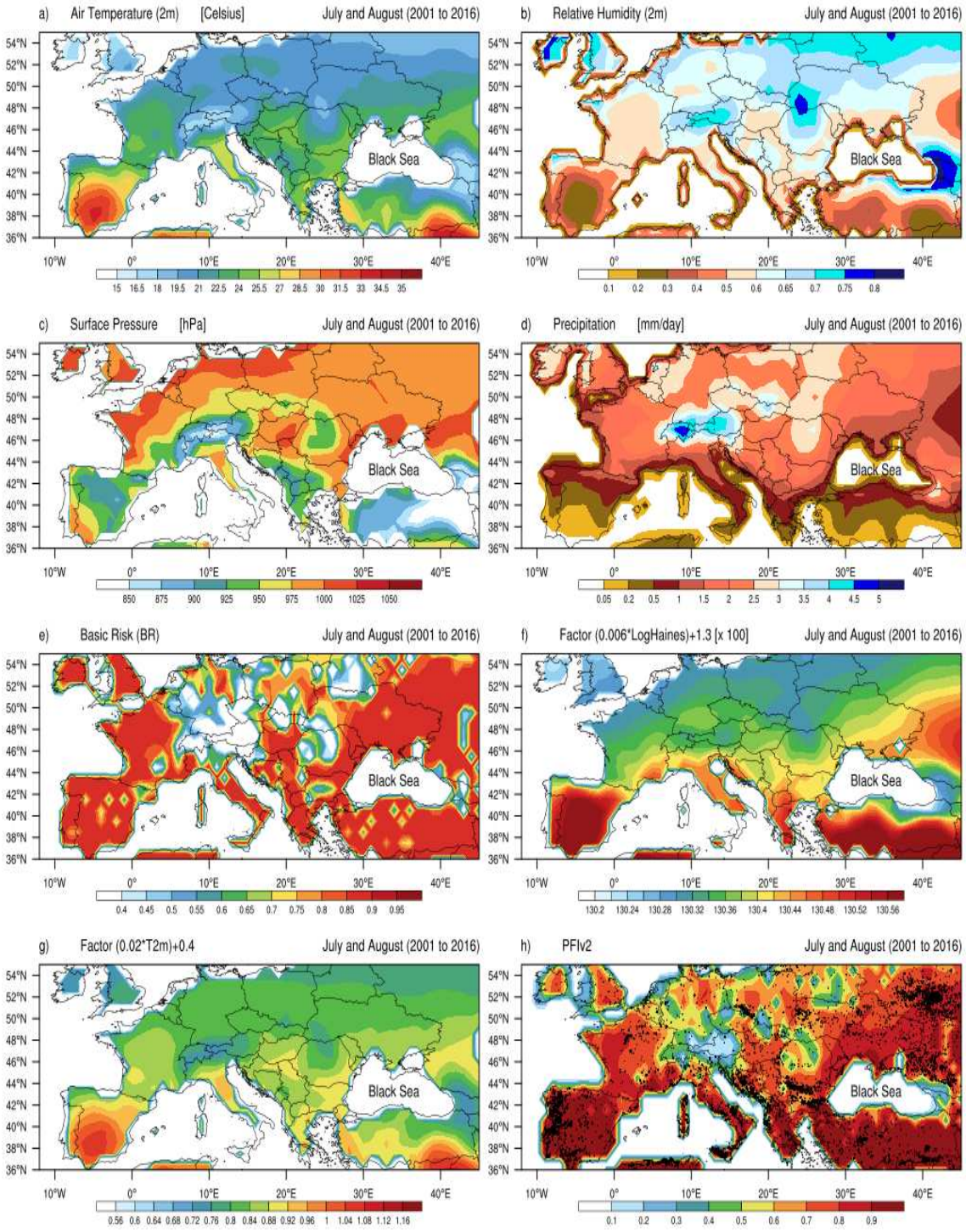

Figure 5.9. July and August climatology in the 2001-2016 period. Maximum temperature at 2 m (*(a)*, °C), relative humidity *(b)*, surface pressure (*(c)*, hPa), precipitation (*(d)*, mm/day), PFIv2 factors *(e)-(g)* and, *(h)* PFIv2 over the accumulated fire event from 2003 (dots).

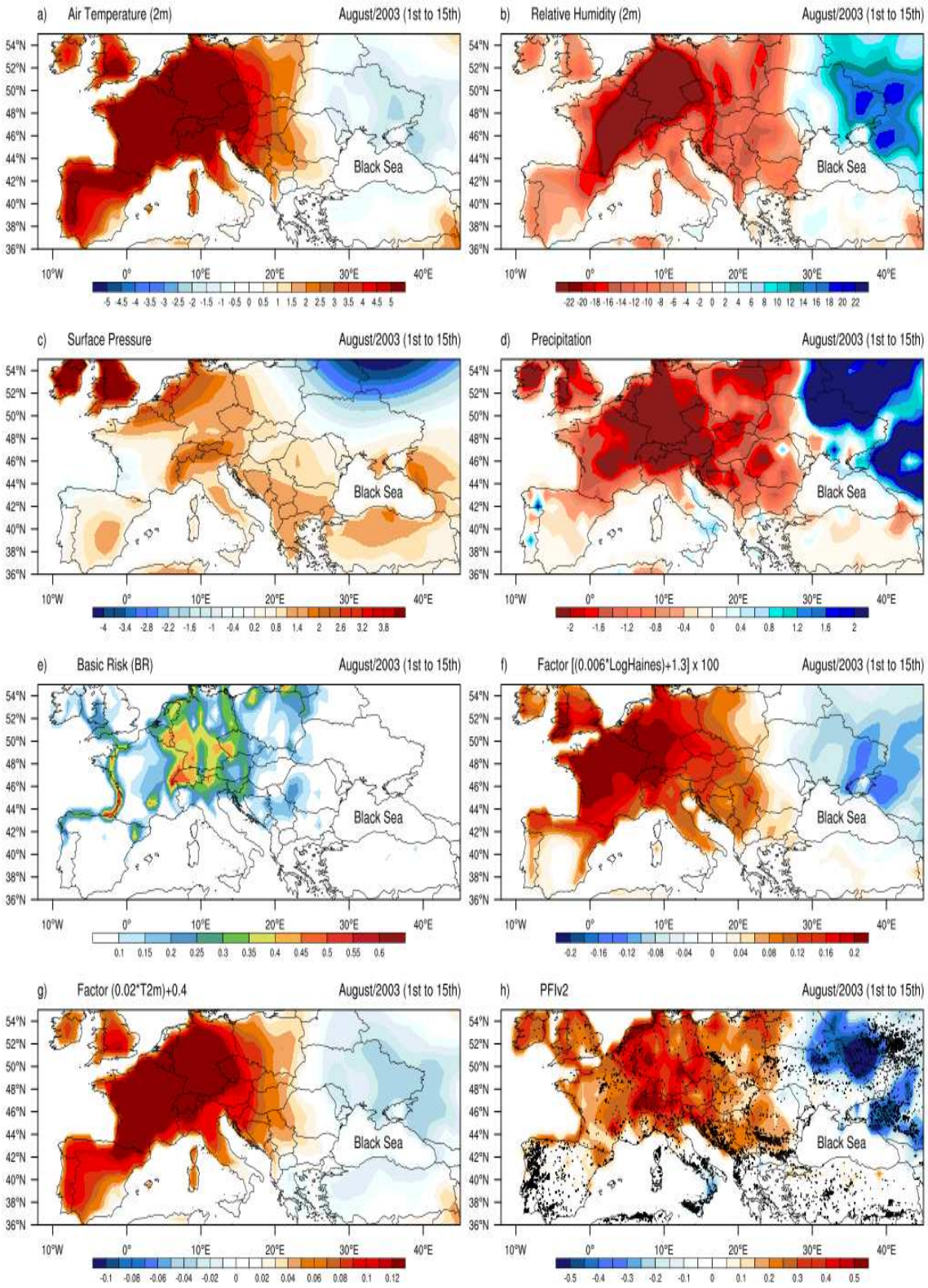

Figure 5.10. Anomalies in *(a)* maximum temperature at 2 m (°C), *(b)* relative humidity (%), *(c)* surface pressure (hPa), *(d)* precipitation (mm/day), *(e)-(g)* PFIv2 factors, and *(h)* PFIv2 distribution for August 1st to 15th 2003 with respect to August averages for the period 2001-2016. Black dots on *(h)* denote local fires.

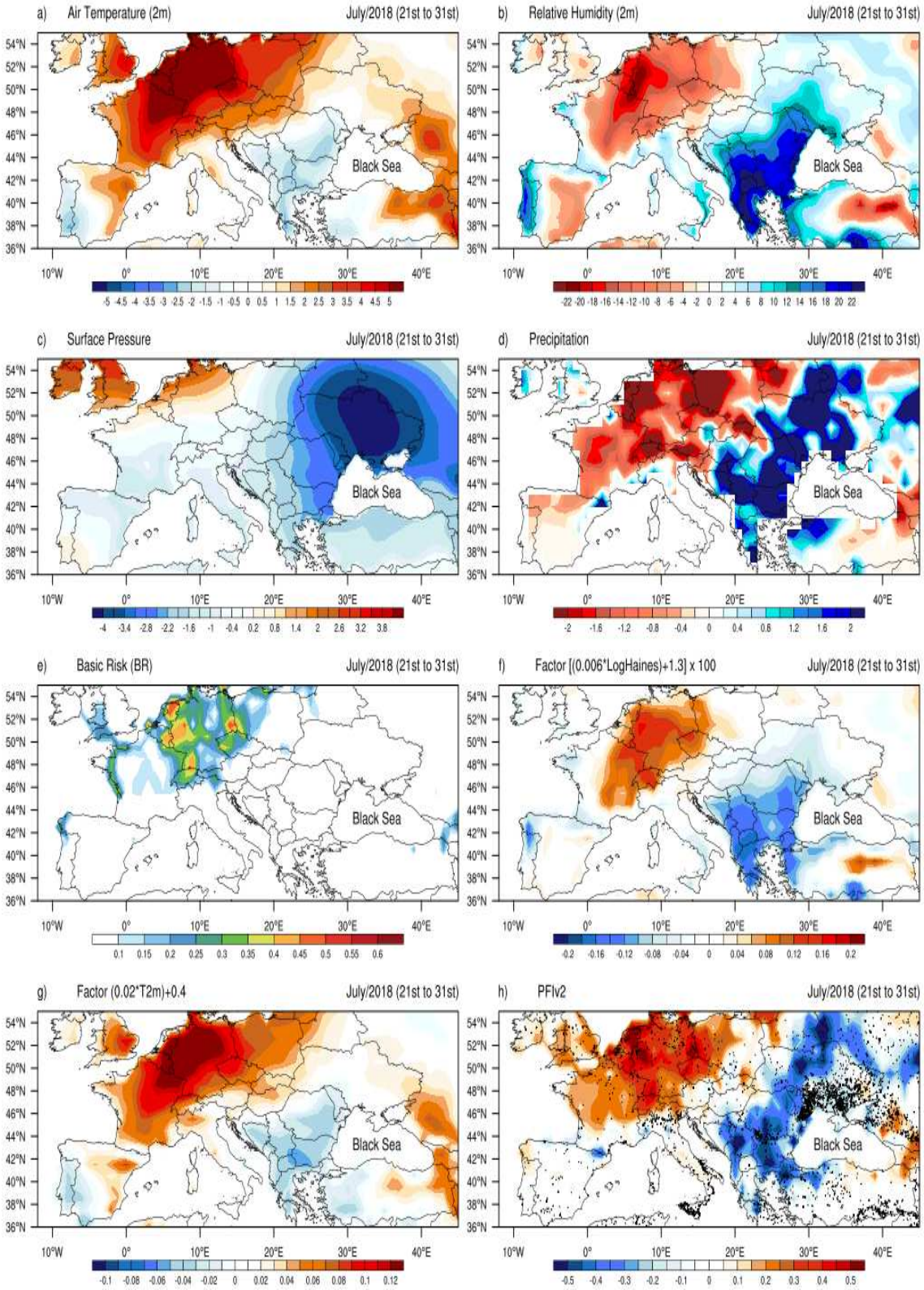

Figure 5.11. Anomalies in *(a)* maximum temperature at 2 m (°C), *(b)* relative humidity (%), *(c)* surface pressure (hPa), *(d)* precipitation (mm/day), *(e)-(g)* PFIv2 factors, and *(h)* PFIv2 distribution for July 21st to 31st 2018 with respect to July averages for the period 2001-2016. Black dots on *(h)* denote local fires.

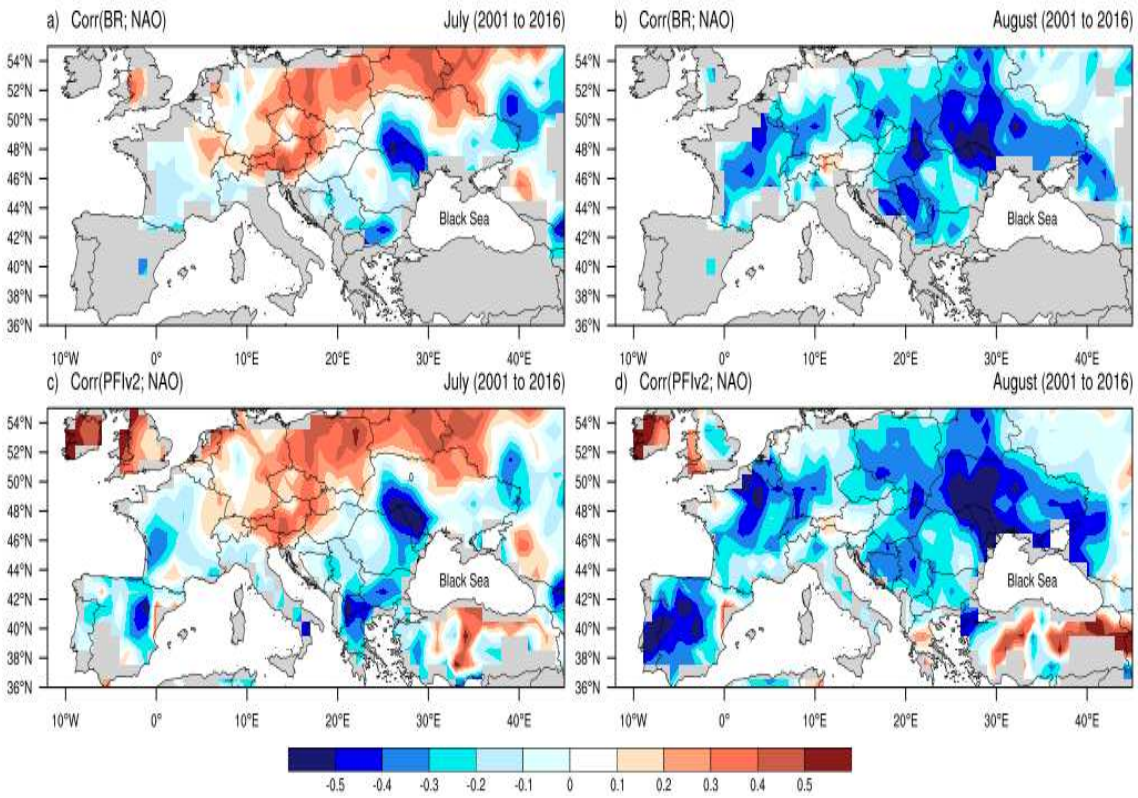

Figure 5.12. Correlation between Basic Risk and NAO for July *(a)* and August *(b)* in the 2001–2016 period. Correlation between PFIv2 and NAO for both months *(c)-(d)* at same period. Gridpoints that do not show statistically significant differences are shown in grey.

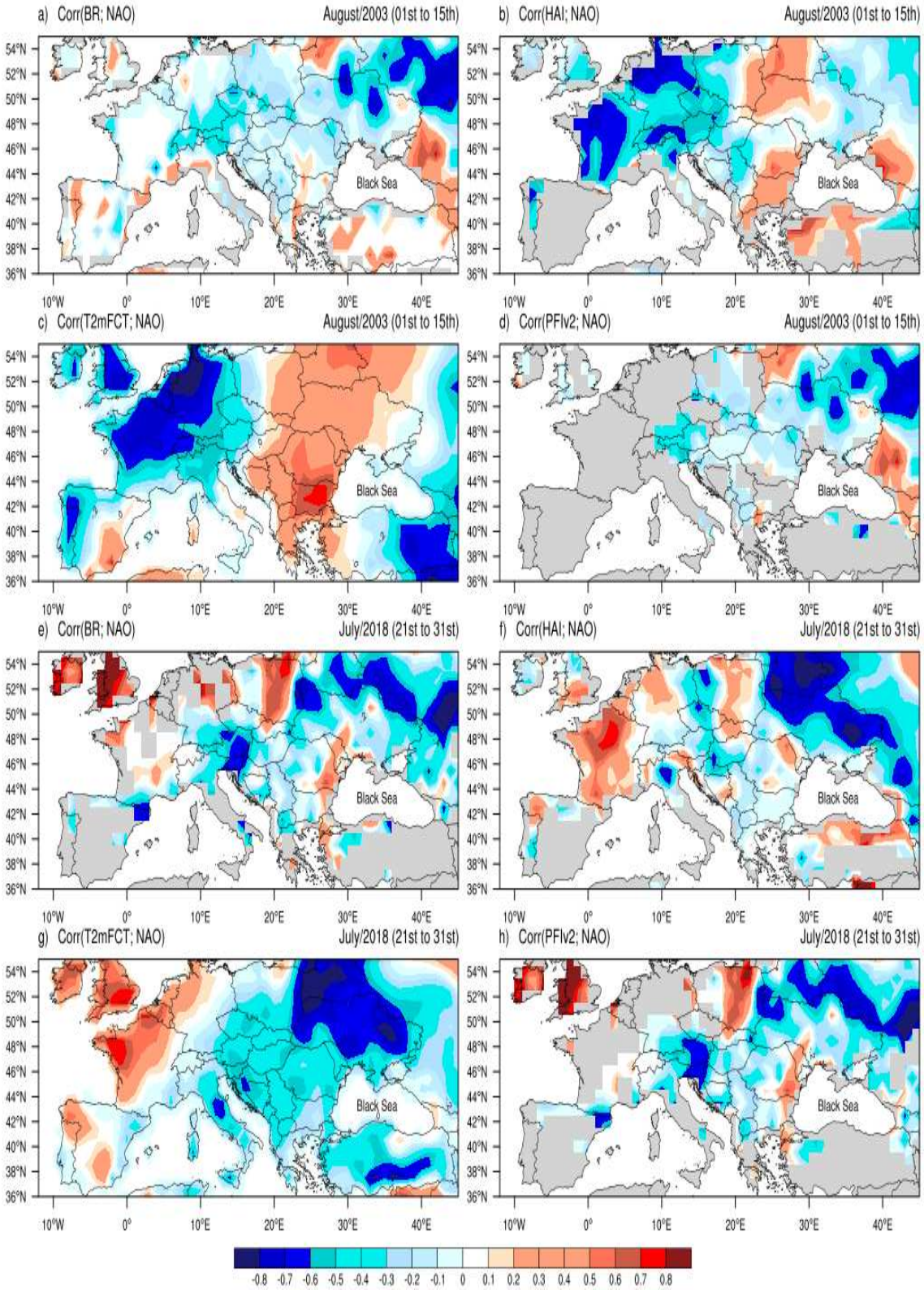

Figure 5.13. Correlation of individual and combined PFIv2 factors with NAO for SC01 *(a)-(d)* and SC02 *(e)-(h)*. Gridpoints that do not show statistically significant differences are shown in grey.

CAPÍTULO 6
ARTIGO PROPOSTO

TROPICAL WILDFIRE RISK PERFORMED BY THE POTENTIAL FIRE INDEX VERSION 2

A. Silva

Agricultural Engineering Department, Federal University of Vicosa, Brazil.

F. Justino

Agricultural Engineering Department, Federal University of Vicosa, Brazil.

A. Setzer

Fire Program of the National Institute of Space Research (INPE), Brazil.

ABSTRACT

Fire activities over tropical regions have been induced several impacts on civilizations and ecosystems. These events are probably the main contributors in the ensuing agricultural and economic disturbances. Based on atmospheric susceptibility to fire, this study discusses the climatological El Nino Southern Oscillation (ENSO) aspects associated with the Potential Weather Fire Index version 2 (PFIv2). The response of fires to the ENSO is complex and has not been evaluated systematically across different continents. Here we use ERA-Interim Reanalysis and CPC Unified Precipitation as input data for the 1998-2018 period. It has to be noticed that the PFIv2 estimates the risk by considering local factors such as latitude, and topography profile. We demonstrate that PFIv2 has revealed an efficiency by up to 70% in presenting observed fires from Terra/MODIS satellite, over tropical regions, mainly in South America, and Africa. To evaluate in further details the PFIv2 performance, two extreme ENSO occurrences are considered. The first event is a La Nina occurred in 2011 (CS01), and the second is an El Nino in 2015 (CS02). In the CS01 event, the PFIv2 increases by up to 10%, over the highest fire concentration in South America, between 40°S and 15°N, related to the direct influence of atmospheric instability, lower relative humidity, and precipitation deficit. During the CS02 event, there is an increase (decrease) variation of air temperature, over northern Australia (southern Africa), and dry conditions are dominant over most part of South America. The PFIv2 reveals accuracy in reproducing the regions with fire activity in northern South America, and southeastern Africa. Further analyzes indicate that there is no correlation between the ENSO and the PFIv2 with the highest fire occurrences when all period is considered. On the other, in the CS01 (CS02) negative (positive) correlations between the ENSO and the PFIv2 (statistically significant at 95%) were found. This study indicates that the PFIv2 is able to be applied on a variety of meteorological and time scales.

Keywords: Fire, El Nino, La Nina, tropical, atmospheric conditions, basic risk.

1. Introduction

Wildland fire is vital in shaping the earth system properties and have widespread impacts on climate cycle and human health (BOWMAN et al., 2009; JOHNSTON et al., 2012; HOLLMANN et al., 2013). Fires affect global climate through changes in greenhouse gases, vegetation and soil carbon stocks (BODEN et al., 2017).

The occurrence of fire in vegetation can be described as any fire activity on the landscape that consumes natural resources, regardless of the source of ignition (YORK et al., 2012). It has the ability to cause significant damage to an ecosystem or it can help keep it, make it more resilient. However, managed forest fire is largely determined by the conditions under which fire exists and the expected or desired results of management efforts. Fire hazard classification systems allow land managers to assess the environmental conditions that contribute to the fire (or potential) hazard and fire distribution (STOCKS et al., 1996; JUSTINO et al., 2013).

Sectors of society have expressed concern over the indiscriminate use of wildfire because vegetation wildfires are prominent in issues involving past and future climate change (e.g. HARRISON et al., 2007). The amount of biomass burned annually from all sources is about 9.2 billion tons of which 5.13 billion tons are consumed by global fires in vegetation (FAO 2006). Over 80% of the global area burned occurs in grasslands and savannas, primarily in Africa and Australia but also in South America (CHEN et al., 2017).

According to Costa et al (2007), the burning of biomass in ecosystems due to the expansion of the agricultural frontier, the conversion of vegetation in pastures, and the renewal of agricultural crops, are some of the most important factors that cause impacts on climate and biodiversity. The fires still cause the impoverishment of the soil, the destruction of the vegetation, erosion problems and they are linked to alterations in the chemical composition of the atmosphere (YORK et al., 2012).

In fact, the distribution and ecological properties of many biomes in the world are significantly affected by fire regimes (BOND et al., 2005). Weisse and Goldman (2018) showed that the annual losses of green forests reached levels of 29.7 million hectares in 2016, however deforestation showed trends of

reduction for the period between August 2016 and July 2017, due to environmental preservation and ecological planning areas.

The main cause of natural fire proceeds from lightning activities. Globally, however, human activity is the most burnt cause (WHITLOCK, 2004). Nevertheless, there is a lively debate on the importance of anthropogenic and climate forcing in contributing to the ignition of wildfires (HUANG et al., 2015).

Recent advances in atmospheric-ocean coupled circulation modeling have led to the development of numerical models (global climatic models, GCMs) that produce dynamic forecasts on the seasonal scale (DOBLAS-REYES et al., 2013). The potential of such forecasting systems to inform decision-makers in different economic sectors is enormous due to the provision of a large number of physically consistent variables, on a broad temporal scale (MANZANAS et al., 2014). Although large improvements have been achieved in the estimation of fire risk (MOUILLOT et al., 2005; GIGLIO et al., 2016), it is still challenging to accurately estimate it using the conventional models. In recent decades, several computer-based studies have been arguing for fire role as a dynamical factor influencing large-scale variations in woody vegetation cover in the tropics (MURPHY and BOWMAN, 2012; DANTAS et al., 2015).

Under current condition, Kloster et al (2010) found the best agreement between simulation and observations for the fire by explicitly considering human caused ignition and fire suppression as a function of population density. Pechony and Shindell (2010) have also found it, however, they added temperature, precipitation, relative humidity, lightning activity and land cover datasets. They argued that future climate conditions will play the major role in driving global fire trends, overcoming the human effect on fire ignition. It has also been demonstrated that increased surface soil moisture conditions limit the extent of burned area (LEHSTEN et al., 2010).

Whitlock et al. (2006) have attributed the variations of the fire regime in the Andes to interannual increase in climate variability and the intensification of the El Nino South Oscillation (ENSO). According to CHEN et al (2017), ENSO is a periodic variation in the coupled ocean-atmospheric system with unusually warm (El Nino) and cold (La Nina) sea surface temperature (SST) in the tropical eastern Pacific, affecting the atmospheric conditions over the continents. In most of the tropics, fires are usually limited to the dry season or periods of

unusual drought associated with ENSO events (HOFFMANN et al., 2009). The response of fires to the ENSO is complex and has not been evaluated systematically across different continents. Here, we consider a threshold of +/- 0.5 °C for the Oceanic Nino Index (ONI), which uses a 3 month running mean of SST anomalies in the Nino 3.4 region (5°S – 5°N; 120° - 170° W) (TRENBERTH et al., 2019).

With the lack of available observational data of sufficient length, models which account for interactions among multiple fire drivers may be used to provide information about how fires respond tropically to variations in climate across timescales. Dynamic models have been used to simulate the interactions between climate variability and fire occurrences (WARD et al., 2016). However, the large number of degree of freedom arises criticism towards the need to include several parameters for simulating it (BRADSTOCK, 2010; SOPKO et al., 2016).

This study aims to investigate how changes in climate by ENSO events impact the fire risk in the tropical region (atmospheric susceptibility to fire initiation) during the 1998-2018 period. The method proposed here is built on the Potential Weather Fire Risk version 2 (PFIv2), presented by Silva et al (2019). This is a simplified index based on four factors to calculate the risk of fire. It uses a logistic growth function, which inserts three atmospheric layers, the local altitude as addressed on Haines Index (1988), and a correction factor of the air temperature due to latitudinal change. The incidence of seasonal fires on high and critical classes of the PFIv2 highlight the efficiency to show the atmospheric conditions linked to fire occurrences. The student's T-test is applied to the anomalies in precipitation, and linear correlations among ENSO and all PFIv2 factors are also performed on study of cases. It must be noted that the ignition of fires is not taken into account, so that the risk is only potential in this respect.

The paper is organized as follows: descriptions of the vegetation, climate data, modelling formulation, and the validation methods in section 2. Section 3 is dedicated to results and discussion. Section 4 provides the capability of the PFIv2 in reproducing two cases of erratic fires in La Nina (2011) and El Nino (2015), respectively. The conclusions are described in Section 5.

2. Experimental design and model description

The PFIv2, proposed by Silva et al (2019) is applied on tropical region (Figure 6.1a), over three subdivisions: *(I)* South America (40°S:15°N; 90°W:30°W); *(II)* Africa (40°S:15°N; 20W:60°E); and *(III)* Australia (40°S:15°N; 65°E:180°E). Information on the types of vegetation required for the computation of PFIv2 were obtained from the classification of the International Geosphere-Biosphere Programme (IGBP), as shown in Figure 6.1b.

The calculation of the Potential Weather Fire Index version 2 (PFIv2) is conducted based on the ERA-Interim Reanalysis (DEE at al., 2011), and on the CPC Unified Precipitation Project (Xie et al., 2010) that is underway at National Oceanographic and Atmospheric Administration Climate Prediction Center (NOAA / CPC) for the 1998-2018 period. The spatial resolution of the ERA-Interim Reanalysis (ERAI) is 1° latitude and longitude grid in the regions of the tropics.

The CPC spatial resolution is 0.5° latitude and longitude grid over tropical land areas. This gauge-based analysis of daily precipitation uses reports from over thousands of stations that are collected from multiple agencies. Historical records, independent information from measurements at nearby stations, radar and satellite observations, as well as numerical model forecasts are applied in the quality control of the data.

It has been used the daily Optimum Interpolation Sea Surface temperature (OISST) in the Nino3.4 region (5°S:5°N; 120°:170°W) from the NOAA (TRENBERTH et al., 2019) to build a climatology of El Nino and La Nina years over a 21-year period from 1998 to 2018. The Nino3.4 SST anomaly index was calculated using Oceanic Nino Index (ONI). It is based on a threshold of +/- 0.5°C on 3 month running mean anomalies in the Nino3.4 region.

2.1. Potential Weather Fire Index version 2 (PFIv2)

The Potential Weather Fire Index version 2 (PFIv2) proposed by Silva et al (2019) includes a modified Haines Index (HAINES, 1988) embedded to a logistic growth function, and a temperature correction factor due to latitudinal

variation to capture the wildfire risk estimates consistent with those observed in tropical regions. Its final formulation combines three parameters (Equation 6.1).

$$PFIv2 = BR \times (a2 \times LF + b) \times (RT \times F_{orb}) \qquad \text{(eq. 6.1)}$$

Where b = 1.3 and the variables Basic Risk (BR) and Run Temperature (RT) are the same as in the original index (JUSTINO et al., 2010; 2013), but the constant a2 = 0.006. The term $(a2 \times LF + b)$ is the impact factor of the Haines logistic function (Loghai), and the variable $F_{orb} = (0{,}003 \times |Lat| + 1)$ is a correction factor of the air temperature for latitudinal change. The sequence of PFIv2 calculations is shown in Figure 6.2. It is important to mention that the PFIv2 categories range from 0 to 1 (Table 6.1).

Active wildfire products from NASA's MODIS (2001 to 2018) will be used to verify the capability of the PFIv2 for detecting the most susceptible region for erratic wildfires development. The wildfire products from the sixth collection of moderate-resolution spectral images of the Terra/MODIS includes algorithms for the elimination of false alarms, like those caused by the deforestation of small forests, precision in the detection of wildfires of reduced spatial scale, adjustment for the presence of cloudness and rejection expanded brightness of the sun. The products from Terra/MODIS are defined in a sine grid of the Earth to the spatial scales of 250-m, 500-m, or 1-km.

Fires detected by Terra/MODIS satellite were computed and reclassified seasonally during the 2001-2018 period. The time scale was selected according to the negative and positive phases of the El Nino Southern Oscillation (ENSO), as proposed by Trenberth et al (2019). Figure 6.3 shows the specific years with sea surface temperature higher than 0.5°C (El Nino) and that ones lower than -0.5°C (La Nina).

The validation of the PFIv2 versus satellite-derived wildfire can be carried out by checking the number of wildfires located in the high and critical wildfire risk grid. Evaluation of the wildfire risk based on PFIv2 may be validated with other satellite as well. For instance, GOES and NOAA products can be utilized. The limitation in satellite wildfires detection is that most of these products are not available prior 2000.

3. Results and Discussion

3.1. Sea surface temperature and precipitation variabilities

Figure 6.4(a) shows the climatology of the sea surface temperature (SST) in the 1998-2018 period. The Nino 3.4 region which is highlighted over tropical eastern Pacific, is linked to atmospheric conditions over the continents. According to McPhaden et al (2006), this climate variability has a pronounced influence on year-to-year variations in climate. The selected data presenting positive and negative phases of the ENSO from ONI methodology show well-defined La Nina (Figure 6.4b) and El Nino (Figure 6.4c) events. Although the differences in SSTs between El Nino and La Nina were largest during June-April, strong positive and negative anomalies were found beyond the end of the El Nino and La Nina SST anomalies.

Recently, Chen et al (2017) showed that ENSO leads changes in the precipitation regimes over the tropical region. In fact, the timing and magnitude of the modified pattern of precipitation alters the landscape fire activity, with larger interannual variability in fires. According to Justino et al (2010), precipitation plays a key role on the Potential Weather Fire Index. For inserting a drought factor which is calculated by daily rainfall. The interannual variability of fires responds to the positive (negative) El Nino-South Oscillation (ENSO) phase such as in 2001, 2009 and 2014 (in 2005, 2007, 2008 and 2010). ENSO events cause changes on the regional Hadley and Walker cells that influence negative anomalies of precipitation in northeastern South America.

Figures 6.5 show the anomalies in precipitation for El Nino and La Nina events, based on CPC data in the 1998-2018 period. During the El Nino events, reductions around 1.5 mm/day are verified in the precipitation over central and northern regions of the South America, in subtropical Africa, and Australia (Figure 6.5a). Thus, the ENSO positive phase contributes to the intensification of the BR in these areas due the short amount of precipitation with respect to present climatology. Although, opposite signals closest to 1.5 mm/day at 95% significance levels are shown in southern Brazil, Patagonia, and Madagascar. These findings are similar from the results found by Curtis and Adler (2003). On the other hand, the overestimation of precipitation differences during La Nina

events has potential to weak the conditions of fire activity over the tropical region, in particular in northern Brazil and Australia (Figure 6.5b). These differences present opposing responses to ENSO, and this limited the degree of predictability at a continental scale.

3.2. Climatology in the 1998-2018 period

Figures 6.6(a)-(c) show the 1998-2018 climatologies of air temperature, relative humidity, and surface pressure from ERA-Interim reanalysis for the tropical region. Similarly, the individual climatologies of the precipitation, and basic risk of fire (BR) from CPC are presented in Figures 6.6(d)-(e). The factors of the PFIv2, and the final modelling are shown in Figures 6.6(g)-(h).

In the tropical troposphere, the temperature gradients are weaker than in extratropical regions, so the term of horizontal advection is minimal and the temperatures in some specific localities vary slightly from one day to the next (Figure 6.6a). On the other hand, Figures 6.6 (b)-(c) show that the rates of diabatic warming in the tropical convection regions are higher than those typically observed in the medium and high latittudes. In Figure 6.6(d) is observed that the values closest to 8 mm/day are consistent with the upward movement concentrated in precipitation belts, such as the Intertropical Convergence Zone (ITCZ), where heating due to latent heat released by condensation is practically compensated by the cooling induced by vertical velocity.

In the tropical region, in addition to the southern circulation resulting from the activity of Hadley cells, there is a large-scale zonal circulation due to Walker's cells (PHILANDER, 1990). This circulation is attributed basically to the differential warming that occurs between the continents and oceans, having been better understood in the southern hemisphere, due to the greater distribution of continental areas in the northern hemisphere.

In the individual climatologies of the PFIv2 factors, it is noted that the BR (Figure 6.6e) governs fire risk. It is worth mention that this factor considers the precipitation frequency of occurrence in the last 120 days before the due date in association with the type of vegetation. This is consistent with some recent studies which have addressed the arising on fires to the anthropogenic

vegetation changes (SILVA et al., 2003; DAVIDSON et al., 2012; SPERA et al., 2016).

Figure 6.6(f) displays that the Haines logistic factor contributes more effectively in Chile, southern Africa, central and western Australia. Figure 6.6(g) shows that the influence of temperature is most dominant over the South America, mainly in Brazil. This cleary reveals that regions such as northern South America, subtropical Africa and northern Australia have an atmosphere conducive to burning seasonally which can be enhanced due to anomalous conditions, such as heat waves and droughts.

Figure 6.6(h) shows the climatological distribution of the PFIv2. It is clear that the BR dominates the continental distribution. Most part of South America and southern Africa are very vulnerable for fire development related to dry conditions in particular between July and September. In the following the changes on this parameters by ENSO events are investigated in details, to verify the PFIv2 capability to reproduce extreme events in fire activity.

3.3. The El Nino Southern Oscillation (ENSO) and the fire activity

Over tropical latitudes, the climate regime is mainly dictated by vacillation in the phase of the ENSO. This natural phenomenon shows interannual sea surface temperature and air pressure anomalies in the Tropical Pacific (DESER et al., 2010). When it comes to SST variability related to ENSO, variations induce to precipitation changes in the Tropical Pacific Ocean. This local variability is crucial on global climate changes (ZHOU et al., 2014). Extreme changes in SST over the tropical Pacific characterize the influence of the inter-tropical Atlantic SST gradients as being significant in modulating the influence of ENSO by intensifying the Southern Atlantic Convergence Zone (SACZ) and Intertropical Convergence Zone (ITCZ).

The oceanic and atmospheric conditions in the Tropical Pacific Ocean have been changed irregularity between warm (El Nino) and cold (La Nina) phases. During El Nino periods, the air surface pressure get high up to typical patterns from Australia, South America, and Africa, inducing dry periods. These conditions also act in northeastern Brazil and southern Africa. On the other hand, low pressure are developed in the central and east regions of Pacific,

across western South America coast. In winter, heavy precipitation and flooding are commonly observed near Uruguay. Similarly, dry regions during El Nino tend to be characterized by elevated humidity on La Nina occurrences.

Figure 6.7(a) shows the average Basic Risk (BR) for El Nino events in the 1998-2018 time period. Due to the importance of precipitation to the fire risk, the BR contributes of up to 0.85 to the final fire risk. As expected, analyses for the Haines factor (Figure 6.7b) tend to highlight the regions dominated by dry conditions and susceptible to convection. This is shown by larger differences of the stability and humidity parameters according to the altitude of the grid point.

When it comes to temperature factor (Figure 6.7c), it is demonstrated that the most susceptible regions for fire occurrence are located in South America. This might be expected because the Atlantic Subtropical High extends toward the continent, which causes the subsidence of the air and dry wheater conditions (FETTER et al., 2018). It is important to mention that the PFIv2 reasonable reproduces the role of the climatic conditions implicit in the method. For example, the central region of Brazil is dominated by a high contribution of the temperature factor (Figure 6.7c), but low to medium BR values. Thus, the PFIv2 delivers to minimum values. Under northeastern Brazil these factors are proportional and the response is direct (Figure 6.7d).

The south part of Africa revealed that the four PFIv2 parameters are in favor for fire occurrence, due to low precipitation, dry atmospheric conditions and susceptible vegetation pattern. Figure 6.7(d) also shows that there are favorable conditions for the fire risk due to BR in Australia, however, the contributions of the Haines logistic factor (Figure 6.7b) and the temperature factor corrected by the latitudinal effect reduce the PFIv2 to levels (Figure 6.7d).

Figure 6.7(e) shows the standard deviation (STD) of the tropical PFIv2. It is observed that a latitudinal gradient is constructed in sub-Saharan Africa and northern South America. In addition, higher variability is also observed in the central part of Brazil, and subtropical Africa.

In the same way, Figures 6.7(f)-(j) show the differences between the El Nino and La Nina events. This highlights that under El Nino conditions there are higher contribution to the intensification of fire risk than in La Nina. Furthermore, it is clear that the BR (Figure 6.7f) has the main contribution to elevate the final

index. It can be noted that the Haines and temperature factors play specifically over the most susceptible areas (Figures 6.7g-h).

Turning to the PFIv2 anomaly (Figure 6.7i), it is emphasized that the reduction in precipitation during the El Nino characterizes the highest prominent regions, mainly in northern South America, southern Africa and Australia. In consequence, these areas also have the most risk fire variations, as showed by the STD (Figure 6.7j).

In order to validate the PFIv2 results, Figure 6.8 shows the capability of the PFIv2 model in locating the daily fires of the Terra/MODIS satellite, based on both ENSO phases. This verification is done by comparing if the fire position is coincident with the highest PFIv2 levels (between 0.7 and 1). The ideal metrics would be that in which the PFIv2 shows all fire occurrences at the critical level (grater than 0.95). Figure 6.8(a) shows that the PFIv2 reasonable finds the annual variability that may be understood by the predominance fires in the highest classes (high and critical). The total number of fires detected on these classes are 66.5% and 58.4% in La Nina and El Nino, respectively. This soft unexpected difference is explained by the higher frequencies of La Nina in the period, and also by the precipitation dataset that has been constantly improved for tropical latitudes and by the anthropic effect in advancing agricultural boundaries.

It is important to mention that Africa which is the continent with the highest fire occurrences presents the highest levels in fire detection (Figure 6.8b). Among the regions analysed, Australia (Figure 6.8c) was the subregion that presented the lowest variability among the risk classes. This is because the seasonal range of fire occurrences is high in Australia, whose observations differ approximately 100 thousand observations between the March and October interval.

To identify the main teleconnection patterns between the ENSO and PFIv2, the Pearson correlation (WILKS, 2006) is used (Figures 6.9). It is a dimensionless index with values raging from -1.0 (inverse proportional) to 1.0 (directly proportional) which reflects the intensity of a linear relation between two dataset. As previously mentioned, differences on timing and magnitude scales of the events highlighted the regions favorable to burn, but also brings challenges to future scientific studies. Figure 6.9(a) displays the strong positive

influence of the ENSO on the PFIv2 over northern South America, southern Africa, and northern Australia. Under La Nina conditions (Figure 6.9b), the mainly contribution occurs in central part of Brazil, which usually experiences high levels of fire between July and September interval. Similarity, the high susceptibility of fire is located over subtropical Africa. In summary, the correlation are presenting reasonable the dipoles between both events, this can be noted over southern Africa, northern and southern Brazil.

Thus, the following section discusses the application of the PFIv2 methodology in the analysis of extreme events of fire occurrences in La Nina and El Nino events. This applicability aims at reducing the challenges encountered by decision makers, in fire activity forecasting.

4. Case Studies

After verifying the PFIv2 capability to locate the main regions of fire activity, it is applied to extreme fire occurrences in La Nina and El Nino occurrences. The first event analyzed is the erratic fires in tropical region during La Nina 2011 (CS01). The second event (CS02) is under an El Nino event in 2015 (CHEN et al., 2017).

Figures 6.10 show the distribution of the SST on the following analyses: climatology for the 1998 to 2018 period (Figure 6.10a); anomalies in the La Nina (Figure 6.10b); and in the El Nino (Figure 6.10c). The cold (warm) conditions of the central Pacific in CS01 (CS02) exhibits a remarkable magnitude to change all individual and combined PFIv2 factors.

4.1. Tropical fire risk and the La Nina 2011 (CS01)

Figures 6.11(a)-(d) depict the climate anomalies during the CS01 event, in relation to the 1998-2018 climatology. The CS01 exhibits a remarkable cooling over northeastern Brazil, southeastern Africa, and northern Australia (Figure 6.11a). These atmospheric conditions are proportional to the relative humidity and precipitation (Figures 6.11b,d), except for the central and northwestern parts of Brazil where temperature differences were about 1.5°C higher, compared to climatological values.

As should be expected from the relationship between temperature and relative humidity, warmer conditions result in a drop of relative humidity by up to 8% over southern Africa and Australia (Figure 6.11b). In addition, the surface pressure decreases (Figure 6.11c), which even favors wet conditions consequently intensifying precipitation (Figure 6.11d). Reduction of precipitation is more proeminent in southern South America, central part of Africa, values much close to the climatology appear in the southeastern Brazil (Figure 6.11d).

It is worth noting that the first component to be considered in the PFIv2 is the BR, which depends on daily accumulated precipitation data. However, there are not proportional rates (in magnitude) of the anomalous precipitation regime (Figure 6.11d) and the BR distribution. The BR considers a period of up to 120 days before the beginning of the analysis. Therefore, it is evident that the increase in precipitation over northeastern South America, southeast region of Africa, and Australia were specific occurrences from CS01. On the other hand, there is a predominance level closest to 0.6 in BR near the southern region of Patagonia (Figure 6.11e).

In relation to the Haines logistic factor (Figure 6.11f), it is observed a similar distribution to that demonstrated by the relative humidity (Figure 6.11b), in which most of tropical region is neutral or favorable to fire development, except in Australia. Figure 6.11(g) presents the contribution of the temperature factor to the risk of fire in the CS01 interval. Similarly to temperature anomalies (Figure 6.11a), this parameter suggests that from the central part of Brazil to northwestern South America fire was susceptible to occur. However, the PFIv2 anomaly between the CS01 and the 1998-2018 period, over eastern Brazil, southern Africa, and northern South America show condition of lower vulnerability, but as will be discussed below, fire incident was remarkable over there.

As shown in Figure 6.11(h), the PFIv2 decreases by up to 0.15, in Australia, and southern Africa between 40°S and 20°S. However, the southern South America experiences massive number of fires, related to direct influence of local elevation and atmospheric conditions such as much, lower relative humidity, and precipitation.

4.2. Tropical fire risk and the El Nino 2015 (CS02)

Figures 6.12(a)-(h) show the difference of climate and PFIv2 components with respect to the 1998-2018 interval characteristics of the CS02 event. At the case of meteorological anomalies, Figure 6.12(a) presents a positive variation of air temperature at 2m, along the 40°S and 15°N latitudinal belt. Warmer conditions of up to 1.5°C are evident in South America, subtropical Africa, and western Australia.

As expected, the spatial pattern of relative humidity (Figure 6.12b) is correlated to that of the air temperature at 2m. It is worth to mention that positive (negative) anomalies of relative humidity (air temperature at 2m) act in most of tropical region to enhance the fire vulnerability. The lowest pressure anomalous patterns are over Patagonia and southeastern part of South America (Figure 6.12c) increases the atmospheric humidity.

Turning to precipitation (Figure 6.12d), there is a clear relationship among low pressure regions as previously observed in South America (Figures 6.12c,d). Conversely, dry conditions are dominant over most part of Brazil and Australia. Figure 6.12(e) shows the BR anomaly during the CS02, in relation to the 1998-2018 period. It is interesting to note that positive anomalies of BR are located in regions of different meteorological patterns, such as in southern Brazil. It is also observed that the northeastern Brazil shows positive anomalies close to 0.3, which reflects the drop in precipitation in Figure 6.12(d). The absence of proportional links between the precipitation (Figure 6.12d) and the BR (Figure 6.12e) over the central region of Africa may be explained by the fact that the anomalies are specific to the El Nino event. The distribution of the precipitation is an important parameter in the PFIv2, for the BR calculation takes into account the precipitation data that are accumulated in distinct intervals in the 120 days prior to the first day of the analysis.

As shown in Figures 6.12(f)-(g), the respective Haines logistic and temperature factors can efficiently reproduce regions which are prone to fire development. Both functions tend to concentrate the higher atmospheric vulnerability to burn. Figure 6.12(f) highlights prominent regions of Brazil and the southern Africa. In addition, Figure 6.12(g) shows that the temperature

factor also plays an important role in detecting the contribution by the latitudinal changes.

The anomaly of the PFIv2 reveals accuracy in the range of accumulated fires in northern South America, southwest Africa and some localities in northern Australia during the CS02 (Figure 6.12h), in agreement with the fire occurrence. The negative anomaly observed from the southern to western South America coast, and in central part of Africa arise due to the anomalous characteristics of precipitation and humidity in the CS02. Hundreds of accumulated fires in these areas does not match positive PFIv2 anomalies.

4.3. Accumulated daily fire in the CS01 and CS02

Finally, to validate the PFIv2 results in the CS01 and CS02, Figures 6.13 show the capability of the PFIv2 model in locating the daily fires of the Terra/MODIS satellite, based on both ENSO phases. Due the quality on satellite information, this verification is restricted for the 2001-2018 period, by comparing if the fire position is coincident with the highest PFIv2 levels (between 0.7 and 1).

Figure 6.13(a) confirms that our previously climate analyses were consistent, showing a higher fire detection in South America during an El Nino event. The difference between the efficiency of El Nino and La Nina reached values around 15%. In Africa, the efficiency of the PFIv2 was reasonable demonstrated with 71.6% and 72.3% of the total accumulated daily data over the critical class in the CS01 and CS02, respectively.

As discussed on Figures 6.8, among all regions analyzed, Australia has the highest sazonal variability in fire occurrences. It is important to mention that values near to 11% detected in the minimum class may be associated with previous environmental conditions. Despite this characteristic, the PFIv2 detected up to 64.8% of the fire occurrences only in the critical class in the CS02 (El Nino) event.

5. Conclusions

Based on the Potential Weather Fire Index version 2 (PFIv2), this study evaluated the tropical susceptibility to the fire occurrences, according to current atmospheric patterns. It was demonstrated that the PFIv2 could reasonable reproduce the annual variability of the fire occurrences in South America, Africa, and Australia. Two case studies were investigated in order to validate the PFIv2: *(i)* In the La Nina occurred in 2011 and; *(ii)* in the El Nino from 2015.

The findings elucidate that the modifications proposed on the PFIv2 to improve the prediction of fire risk over the extratropical regions also contributed to the current quality of the original version in detecting regions favorable to fire occurrences in tropical regions. This was verified, mainly in the Africa continent, with accuracy level in the maximum classes up to 73% and 75% under La Nina and El Nino events, respectively.

The most important limitation of PFIv2 is the high dependence of the days of dryness, which is computed from the precipitation data. For precipitation is still an uncertain parameter in the forecasts of the present climate and also presents divergences among the atmospheric models. However, it was demonstrated that the CPC dataset is reasonable to detect the climate variabilities.

It is known that the majority of present day fires have an anthropogenic origin. However, the results presented in this paper are entirely independent of human action and are based only upon the atmospheric vulnerability to the occurrence of fire. Nonetheless, increased fire weather in a changing climate will be one of many ingredients that will continue to shape changes in fire activity. Despite different manners to start and maintain fire, climatic conditions need to be favorable to the fire occurrences.

6. Acknowledgements

To the people management of the Federal University of West Para (Ordinance N ° 594, of March 4th, 2015). To the Graduate Program in Applied Meteorology of the Federal University of Vicosa (www.posmet.ufv.br) and to the

Fire Program of the National Institute of Space Research (INPE) – Brazil (http://www.inpe.br/queimadas/portal).

REFERENCES

BOND, W. J., WOODWARD, F. I., and MIDGLEY, G. F. The global distribution of ecosystems in a world without fire. **New Phytologist**, v. 165, p. 525-537, doi: 10.1111/j.1469-8137.2004.01252.x, 2005.

BODEN, T. A., MARLAND, G., and ANDRES, R. J. Global, Regional, and National Fossil-Fuel CO2 Emissions. **Carbon Dioxide Information Analysis Center**, Oak Ridge National Laboratory, U.S. Department of Energy, Oak Ridge, Tenn., U.S.A., https://doi.org/10.3334/CDIAC/00001_V2017, 2017.

BOWMAN, D. M. J. S. et al. Fire in the Earth system. ***Science***, v. 324, p. 481-484, 2009.

BRADSTOCK, R. A. A biogeographic model of fire regimes in Australia: current and future implications. **Global Ecology and Biogeography**, 19, 145-158. doi: 10.1111/j.1466-8238.2009.00512.x, 2010.

CHEN, Y. et al. A pan-tropical cascade of fire driven by El Niño/Southern Oscillation. **Nature Climate Change**, v. 7, p. 906-911, doi:10.1038/s41558-017-0014-8, 2017.

COSTA, M. H., YANAGI, SILVIA, N. M., SOUZA, P. J. O. P., RIBEIRO, A., ROCHA, E. J. P. Climate change in Amazonia caused by soybean cropland expansion, as compared to caused by pastureland expansion. **Geophysical Research Letters**, Vol. 34, p. L07706, 2007.

CURTIS, S., and ADLER, R. F. Evolution of El Niño-precipitation relationships from satellites and gauges. **J. Geophys. Res.**, 108, 4153, 2003.

DANTAS, V. L., HIROTA, M., OLIVEIRA, R. S., and PAUSAS, J. G. Disturbance maintains alternative biome states. **Ecology Letters**, v. 19, p. 12-19, 2015.

DAVIDSON, E. A., de ARAÚJO, A. C., ARTAXO, P., BALC, J. K., BROWN, I. F. e*t al*. The amazona basin in transition. **Nature**, v. 481, n. 7381, p. 321-328, 2012.

DEE, D. P., UPPALA, S. M., SIMMONS, A. J., BERRISFORD, P., POLI, P. *et al*. The ERA-Interim reanalysis: Configuration and performance of the data assimilation system. **Quarterly Journal of the Royal Meteorological Society**, v. 137(656), p. 553-597, 2011.

DESER, C., XIE, S-P., ALEXANDER, M. A., and PHILLIPS, A. S. Sea surface temperature variability: patterns and mechanisms. **Annual Review of**

Marine Science, v. 2, p. 115-143, doi: 10.1146/annurev-marine-120408-151453, 2010.

DOBLAS-REYES, F. J., GARCÍA-SERRANO, J., LIENERT, F., BIESCAS, A. P., and RODRIGUES, L. R. L. Seasonal climate predictability and forecasting: status and prospects. Wiley Interdisciplinary Rev.: **Climate Change**, Vol. 4, p. 245-268, 2013.

FAO. Fire management global assessment. A thematic study prepared in the framework of the Global Forest Resources Assesment. Food and Agriculture Organization of the United Nations, 2006.

FETTER, R., CARLOS, H., and STEINKE E. Um Índice para Avaliação da Variabilidade Espaço-Temporal das Chuvas no Brasil. **Revista Brasileira de Meteorologia**, n. 2, p. 225-237, 2018.

GIGLIO, L., SCHROEDER, W., and JUSTICE, C. O. The collection 6 MODIS active fire detection algorithm and fire products. **Remote Sensing of Environment**, v. 178, p. 31-41, 2016.

HARRISON, S. P., POWER, M., and BOND, W. Paleofires and the Earth system. **iLEAPS Newsletter**, v. 3, p. 18-20, 2007.

HOFFMANN, A. A., PARRY, J., CUAMBE, C., KWESHA, D., and ZHAKATA, W. Climate change and wildland fires in Mozambique. In M. A. Cochrane (Ed.), Tropical Fire Ecology: Climate Change, Land Use, and Ecosystem Dynamics. **Springer/Praxis**, Heidelberg, Germany/Chichester, U.K., 2009.

HOLLMANN, R., MERCHANT, C., SAUNDERS, R., DOWNY, C. et al. The ESA climate change initiative: satellite data records for essential climate variables. **Bulletin of the American Meteorological Society**, 94, p. 1541-1552, 2013.

HUANG, X., REIN, G., and CHEIN, H. Computational smoldering combustion: Predicting the roles of moisture and inert contents in peat wildfires. **Proceedings of the Combustion Institute**, v. 35, p. 2673-2681, 2015.

JOHNSTON, F. H. et al. Estimated Global Mortality Attributable to Smoke from Landscape Fires, **Environmental Health Perspectives**, v. 120, p. 695–701, https://doi.org/10.1289/ehp.1104422, 2012.

JUSTINO, F., STORDAL, F., CLEMENT, A., COPPOLA, E., SETZER, A., and BRUMATTI, D. Modelling Weather and Climate Related Fire Risk in Africa. **American Journal of Climate Change**, 2, p. 209 – 224, 2013.

KLOSTER, K et al. Fire Dynamics During the 20th Century Simulated by the Community Land Model, **Biodigeosciences**, Vol. 7, No. 6, p. 1877-1902, 2010.

LEHSTEN, P., HARMAND, P., PALUMBO, I., and ARNETH, A. Modelling Burned Area in Africa, **Biogeosciences**, Vol. 7, p. 3199-3214, 2010.

MANZANAS, R., FRÍAS, M. D., CONFIÑO, A. S., and GUTIÉRREZ, J. M. Validation of 40 year multimodel seasonal precipitation forecasts: the role of ENSO on the global skill. **Journal of Geophysical Research: Atmospheres,** v. 119, p. 1708-1719, 2014.

MCPHADEN, M. J., ZEBIAK, S. E., and GLANTZ, M. H. ENSO as an integrating concept in Earth science. **Science**, v. 314, p. 1740-1745, 2006.

MOUILLOT, F., and FIELD, C. B. Fire history and the global carbon budget: a 1° x 1° fire history reconstruction for the 20th century. **Global Change Biology**, 11**,** 398 – 420. doi: 10.1111/J.1365-2486.2005.00920.X, 2005.

MURPHY, B. P., and BOWMAN, D. M. What controls the distribution of tropical forest and savanna? **Ecology Letters**, v. 15, p. 748-758, 2012.

PECHONY, O., and SCHINDELL, D. T. Driving Forces of Global Wildfires over the Past Millennium and the Forthcoming Century, **Proceedings of the National Academy of Sciences**, 2010.

PHILANDER, S. G. El Niño, La Niña, and the Southern Oscillation. **Academic San Diego**, 1990.

SOPKO, P., BRADSHAW, I., and JOLLY, M. Spatial products available for identifying areas of likely wildfire ignitions using lightning location data-Wildland Spera, S. A., Galford, G. L., Coe, M. T., Macedo, M. N., Mustard, J. F. (2016). Land-Use Change Affects Water Recycling in Brazil's Last Agricultural Frontier. **Global Change Biology**, doi: 10.1111/gcb.13298, 2016.

SPERA, S. A., GALFORD, G. L., COE, M. T., MACEDO, M. N., and MUSTARD, J. F. Land-Use Change Affects Water Recycling in Brazil's Last Agricultural Frontier. **Global Change Biology**, doi:10.1111/gcb.13298, 2016.

STOCKS, B.J., and LAWSON, B.D. El sistema Canadiense de evaluacion del grado de peligro de incendios forestales: Una vision general. p. 82-94 in J.A. Guillermo, Editor. Proc. Prognosis Y Gestion en Control de Incendios Forestales, **Actas del Taller Internacional**, November 8-10, 1995, Santiago de Chile. Proyecto FONDEF FI-13, Santiago de Chile, 1996.

TRENBERTH, K., and National Center for Atmospheric Research Staff (Eds). The Climate Data Guide: Nino SST Indices (Nino 1+2, 3, 3.4, 4; ONI and TNI). Retrieved from **https://climatedataguide.ucar.edu/climate-data/nino-sst-indices-nino-12-3-34-4-oni-and-tni**. Last modified 11 Jan 2019.

YORK, A., BELL, T. L., and WESTON, C. J. Fire regimes and soil-based ecological processes: implications for biodiversity. In Bradstock R. A et al (Eds) 'Flammable Australia, Fire regimes, biodiversity and ecosystems in a changing world' (**CSIRO Publishing: Collingwood, VIC**), p. 127-148, 2012.

WARD, D. S., SHEVLIAKOVA, E., MALYSHEV, S., LAMARQUE, J-F., and WITTEMBERG, A. T. Variability of fire emissions on interannual to multi-decadal timescales in two Earth System models. **Environmental Research Letters**, v. 11, doi:10.1088/1748-9327/11/12/125008, 2016.

WEISSE, M., and GOLDMAN, L. 2017 Was the Second-Worst Year on Record for Tropical Tree Cover Loss. **Global Forest Watch**. Online available at [https://blog.globalforestwatch.org/data-and-research/2017-foi-o-segundo-pior-ano-ja-registrado-de-perda-de-cobertura-florestal-tropical], 2018.

WHITLOCK, C., and BARTLEIN, P. J. Holocene fire activity as a record of past environmental change, in: Developments in Quaternary Science, edited by: Gillespie, A. R., Porter, S. C., and Atwater, B. F., **Elsevier**, Amsterdam, 2004.

WHITLOCK, C., MORENO, P. I., and BARTLEIN, P. Climatic controls of Holocene fire patterns in southern South America, **Quaternary Research**, v. 68, p. 28–36, 2006.

WILKS, D. S. **Statistical Methods in the Atmosphere Sciences**, 2006.

ZHOU, Z. -Q., XIE, S. -P., ZHENG, X. -T., LIU, Q., and WANG, H. Global warming-induced changes in El Niño teleconnections over the North Pacific and North America. **Journal of Climate**, v. 27, p. 9050-9064, doi: https://doi.org/10.1175/JCLI-D-14-00254.1, 2014.

Tables

TABLE 6.1. Fire risk (PFIv2) levels.

Levels	*PFI (0 to 1)*
Minimum	< 0.15
Low	0.15 to 0.40
Medium	0.40 to 0.70
High	0.70 to 0.95
Critical	≥ 0.95

Figures

Fig. 6.1 *(a)* Study areas. *(b)* Vegetation distribution by IGBP (adapted from FRIEDL et al., 2010).

Fig. 6.2 Flowchart presenting the sequence of calculation for the PFIv2.

Fig. 6.3 Annual series of the ONI from 1998 to 2018. Blue and red lines are the limit values for La Nina and El Nino, respectively. Souce: OSST/NOAA.

Fig. 6.4 Sea Surface Temperature (SST) climatology in the 1998-2018 period *(a)*. *(b)* SST anomaly on La Nina events and; *(c)* SST anomaly on El Nino events.

Fig. 6.5 Anomalies in CPC precipitation for El Nino *(a)*; and La Nina *(b)* events in the 1998-2018 period. Black dots show statistically significant differences at 95%.

Fig. 6.6 Present day (1998-2018) climatology. Maximum temperature at 2 m (*(a)*, °C), relative humidity *(b)*, surface pressure (*(c)*, hPa), precipitation (*(d)*, mm/day), PFIv2 factors *(e)-(g)* and, *(h)* PFIv2.

Fig. 6.7 PFIv2 factors on El Nino events during the 1998-2018 period *(a)-(d)*. Figure *(e)* is the standard deviation. The same sequence is shown from *(f)-(j)*, but for the difference between El Nino and La Nina events.

Fig. 6.8 Percentage of accumulated daily fire at each PFIv2 for El Nino and La Nina events in *(a)* South America, *(b)* Africa, and *(c)* Australia in the 2001-2018 period. ZERO indices are the percentage of fire events that were observed in a level closest to zero by PFIv2 (displayed in the top left corner of each panel).

Fig. 6.9 Correlation between the PFIv2 and ENSO for El Nino *(a),* and La Nina *(b)* events in the 1998-2018 period. Gridpoints that do not show statistically significant differences are shown in grey.

Fig. 6.10 Sea Surface Temperature (SST) climatology in the 1998-2018 period *(a)*. *(b)* SST anomaly on a La Nina event (2011) and; *(c)* SST anomaly on a El Nino event (2015).

Fig. 6.11 Anomalies in *(a)* maximum temperature at 2 m (°C), *(b)* relative humidity (%), *(c)* surface pressure (hPa), *(d)* precipitation (mm/day), *(e)-(g)* PFIv2 factors, and *(h)* PFIv2 distribution for 2011 (La Nina event) with respect to climatology from 1998 to 2018.

Fig. 6.12 Anomalies in *(a)* maximum temperature at 2 m (°C), *(b)* relative humidity (%), *(c)* surface pressure (hPa), *(d)* precipitation (mm/day), *(e)-(g)* PFIv2 factors, and *(h)* PFIv2 distribution for 2015 (El Nino event) with respect to climatology from 1998 to 2018.

Fig. 6.13 Percentage of accumulated daily fire at each PFIv2 level in *(a)* South America; *(b)* Africa; and *(c)* Australia on La Nina (2011) and El Nino (2015) events. ZERO indices are the percentage of fire events that were observed in a level closest to zero by PFIv2 (displayed in the top left corner of each panel).

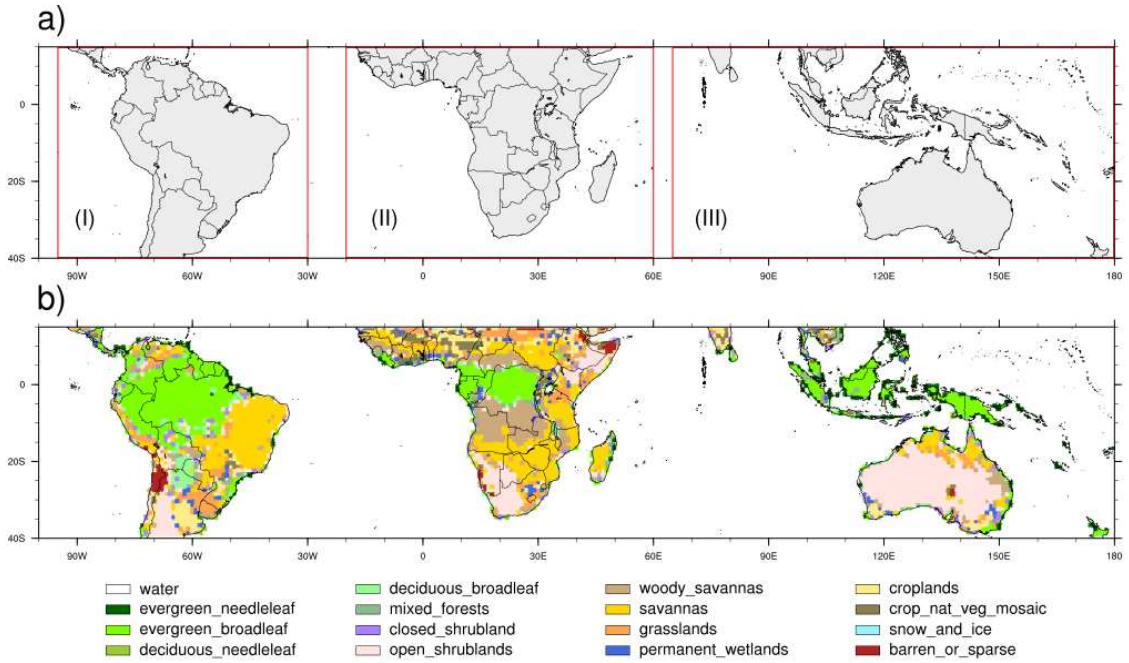

Figure 6.1. *(a)* Study areas. *(b)* Vegetation distribution by IGBP (adapted from FRIEDL et al., 2010).

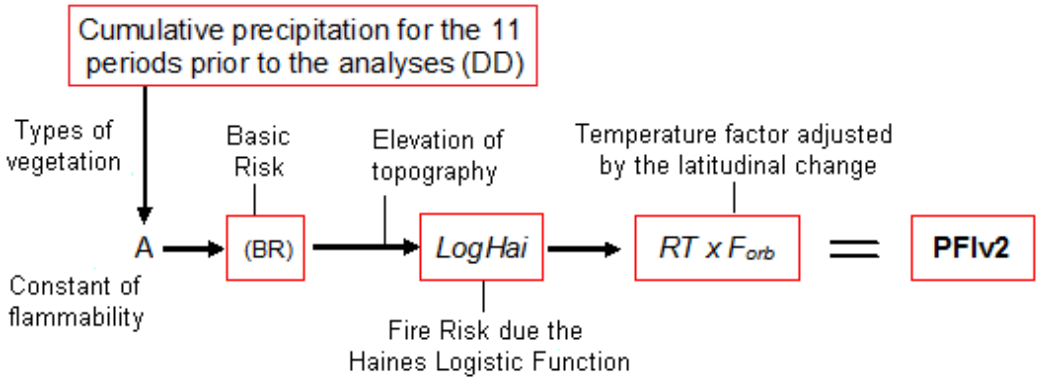

Figure 6.2. Flowchart presenting the sequence of calculation for the PFIv2.

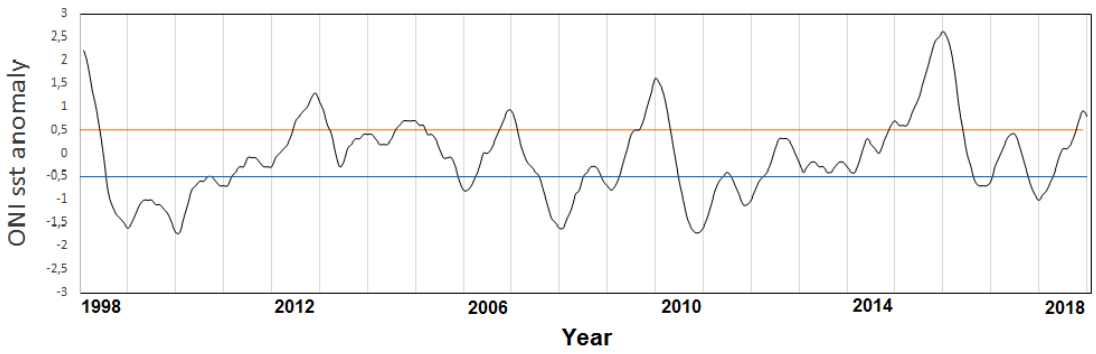

Figure 6.3. Annual series of the ONI from 1998 to 2018. Blue and red lines are the limit values for La Nina and El Nino respectively. Source: OISST/NOAA.

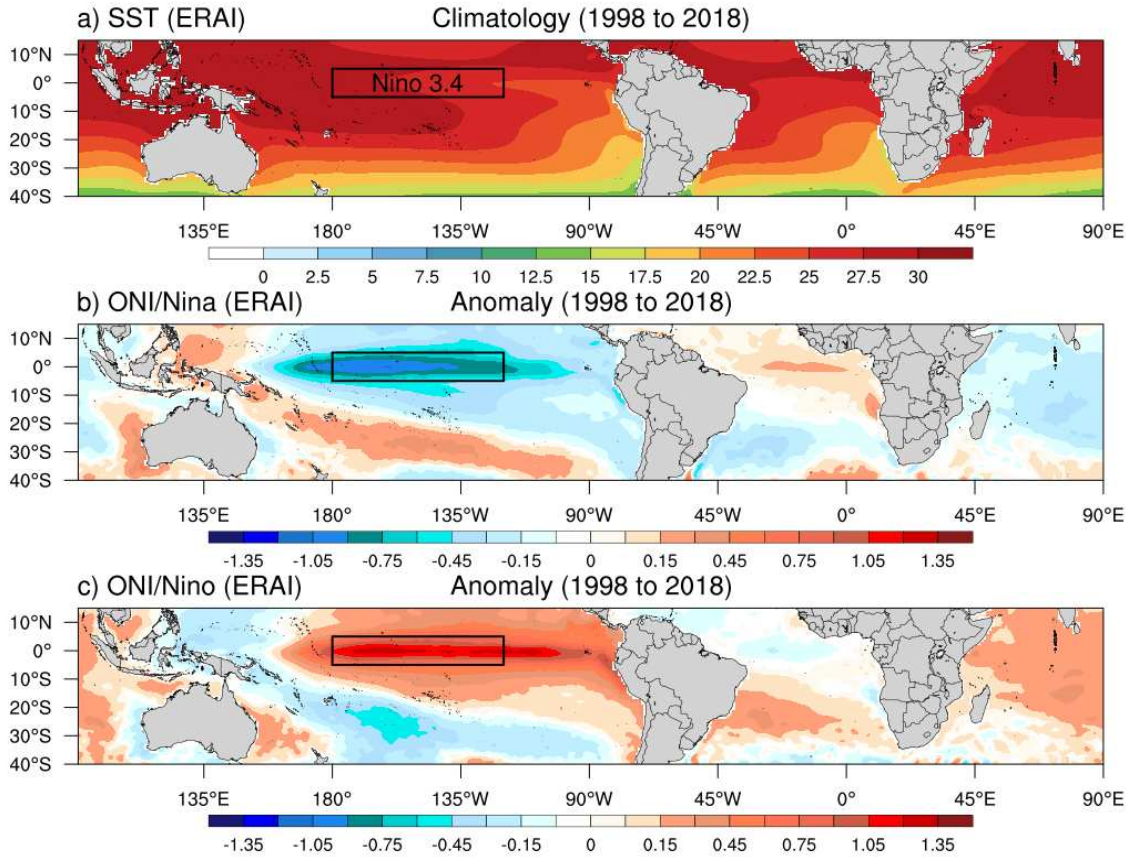

Figure 6.4. Sea Surface Temperature (SST) climatology in the 1998-2018 period *(a)*. *(b)* SST anomaly on La Nina events and; *(c)* SST anomaly on El Nino events. The black box shows the Nino3.4 region.

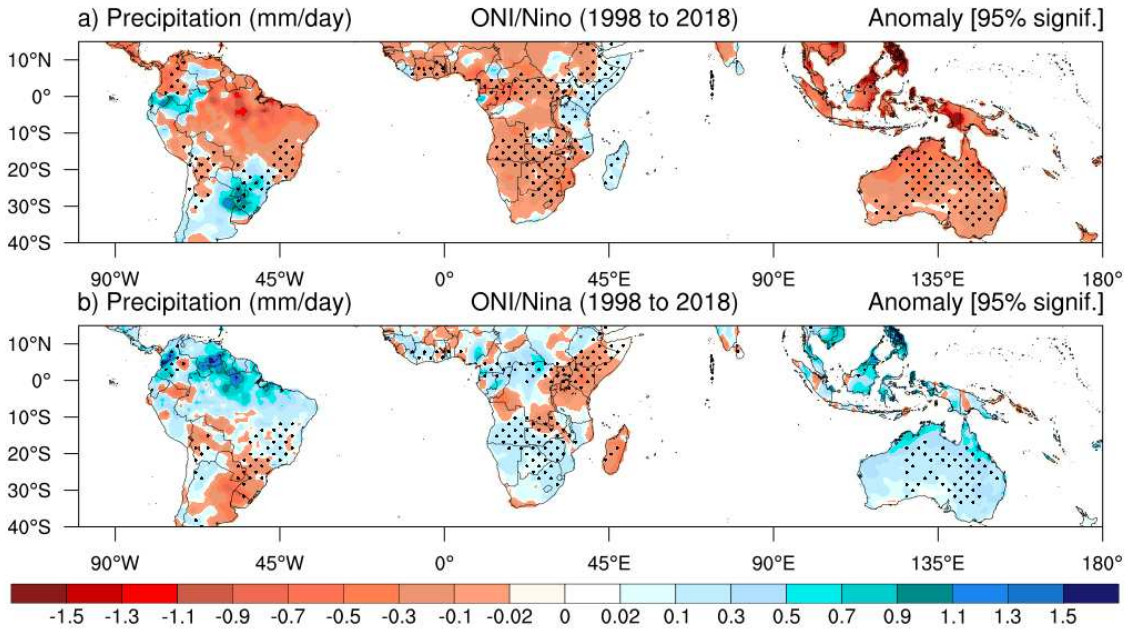

Figure 6.5. Anomalies in CPC precipitation for El Nino *(a)*; and La Nina *(b)* events in the 1998-2018 period. Black dots show statistically significant differences at 95%.

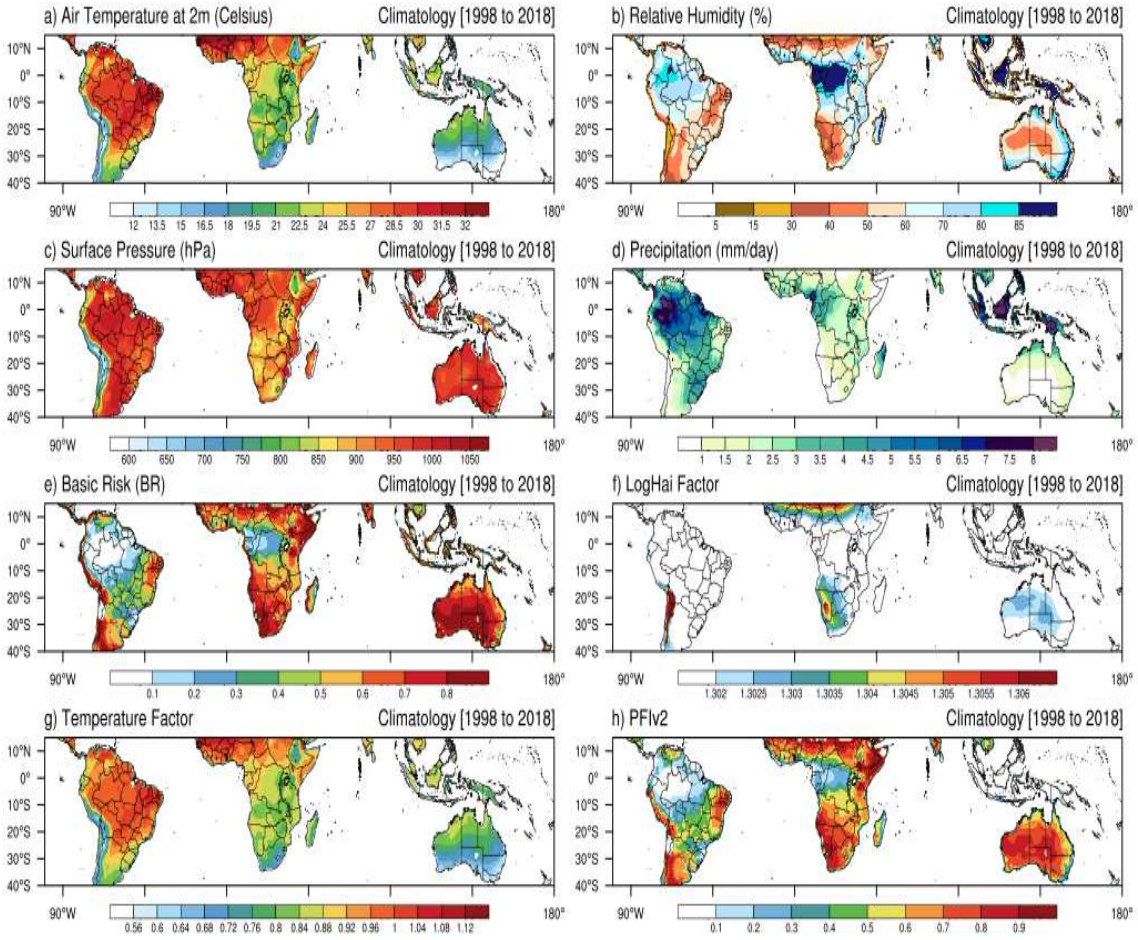

Figure 6.6. Present day (1998-2018) climatology. Maximum temperature at 2 m (*(a)*, °C), relative humidity *(b)*, surface pressure (*(c)*, hPa), precipitation (*(d)*, mm/day), PFIv2 factors *(e)-(g)* and, *(h)* PFIv2.

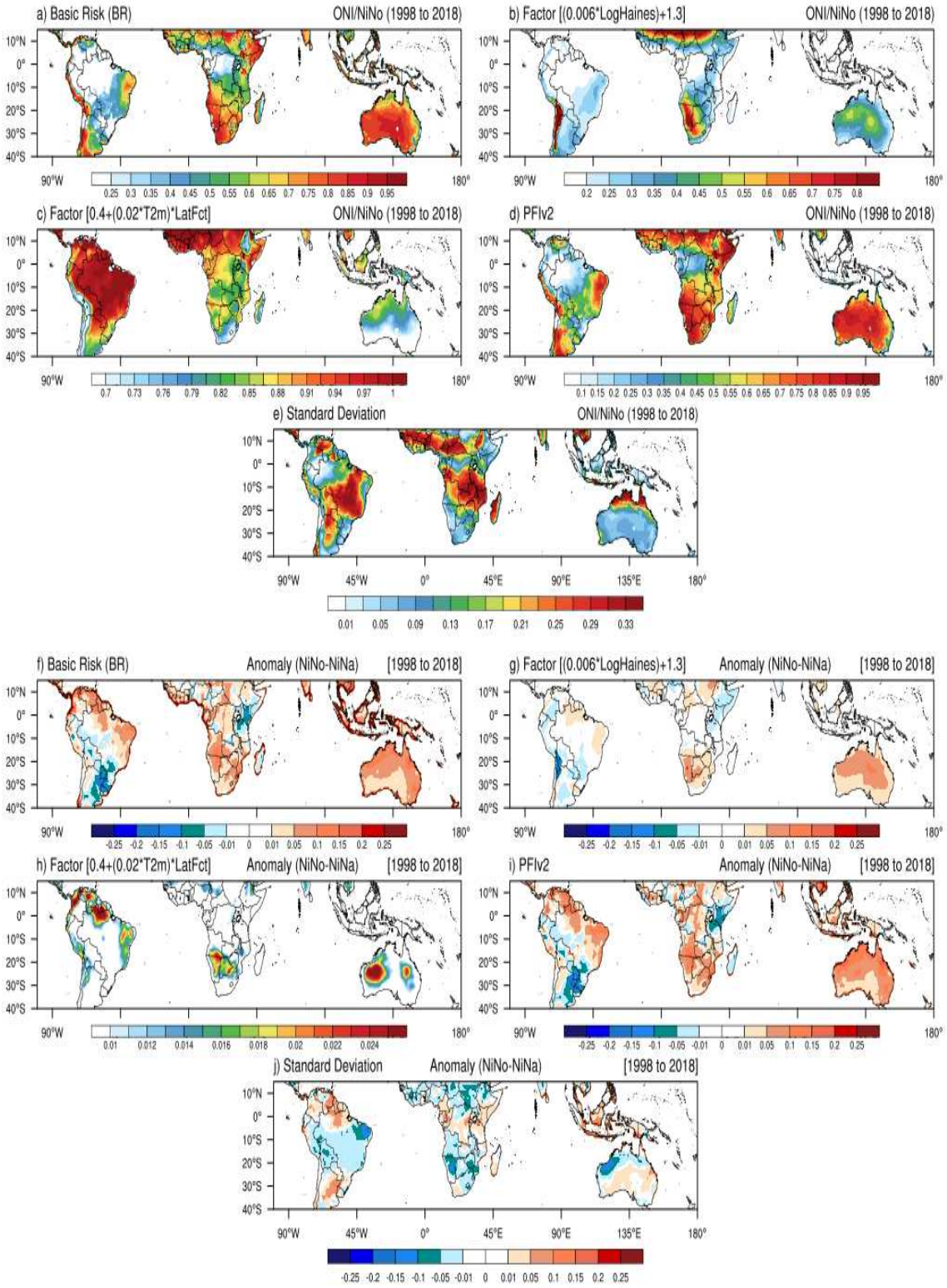

Figure 6.7. PFIv2 factors on El Nino events during the 1998-2018 period *(a)-(d)*. Figure *(e)* is the standard deviation. The same sequence is shown from *(f)-(j)*, but for the difference between El Nino and La Nina events.

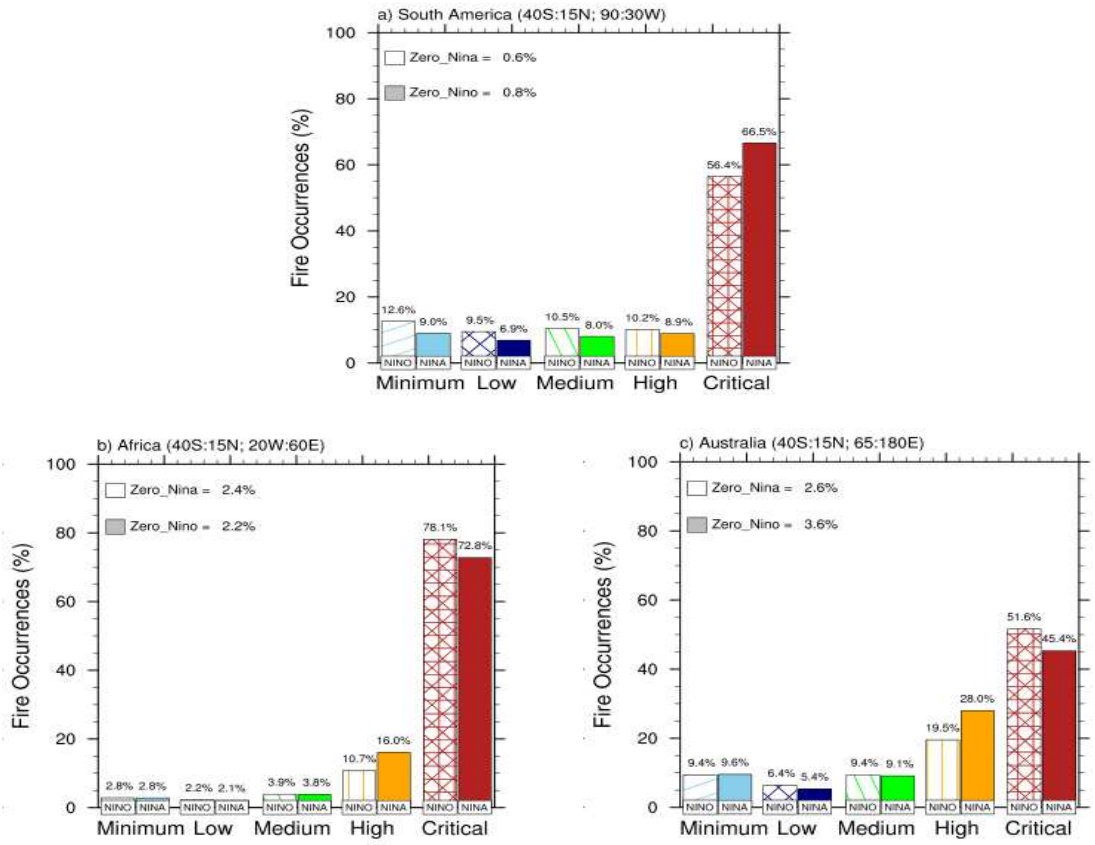

Figure 6.8. Percentage of accumulated daily fire at each PFIv2 for El Nino and La Nina events in *(a)* South America, *(b)* Africa, and *(c)* Australia in the 2001-2018 period. ZERO indices are the percentage of fire events that were observed in a level closest to zero by PFIv2 (displayed in the top left corner of each panel).

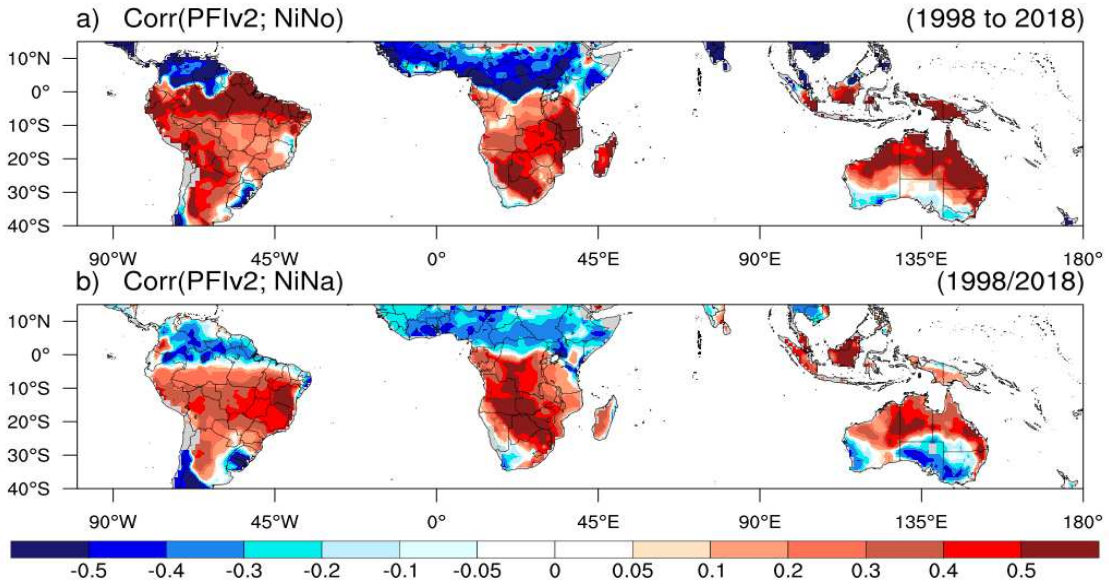

Figure 6.9. Correlation between the PFIv2 and ENSO for El Nino *(a),* and La Nina *(b)* events in the 1998-2018 period. Gridpoints that do not show statistically significant differences are shown in grey.

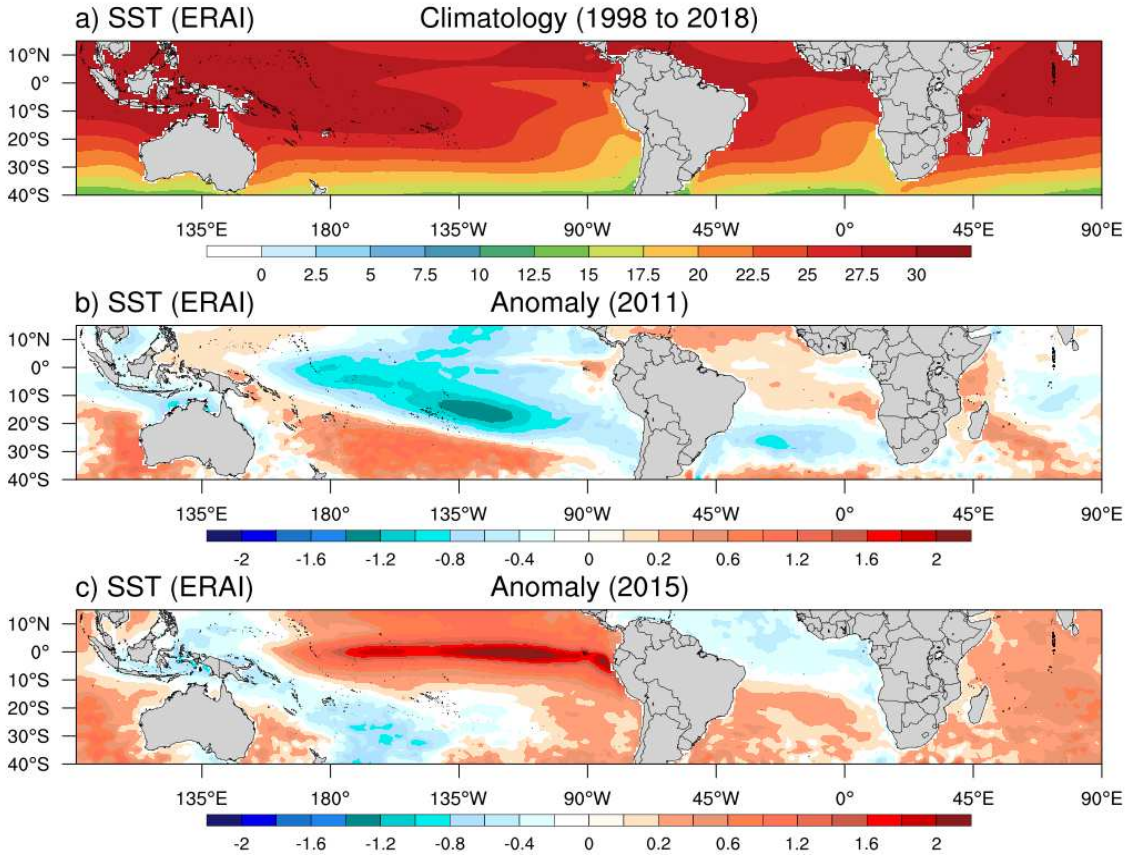

Figure 6.10. Sea Surface Temperature (SST) climatology in the 1998-2018 period *(a)*. *(b)* SST anomaly on a La Nina event (2011) and; *(c)* SST anomaly on an El Nino event (2015).

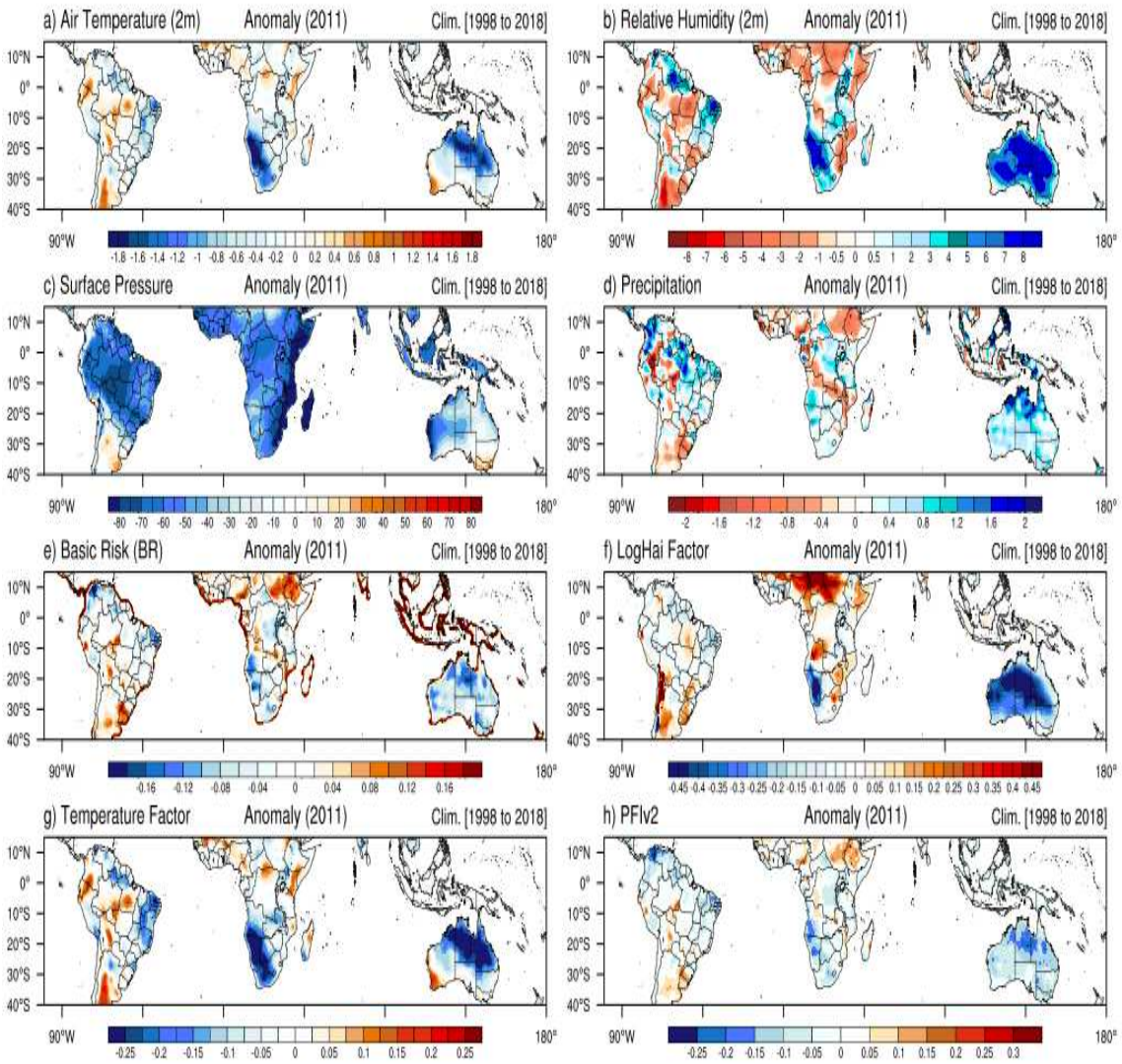

Figure 6.11. Anomalies in *(a)* maximum temperature at 2 m (°C), *(b)* relative humidity (%), *(c)* surface pressure (hPa), *(d)* precipitation (mm/day), *(e)-(g)* PFIv2 factors, and *(h)* PFIv2 distribution for 2011 (La Nina event) with respect to climatology from 1998 to 2018.

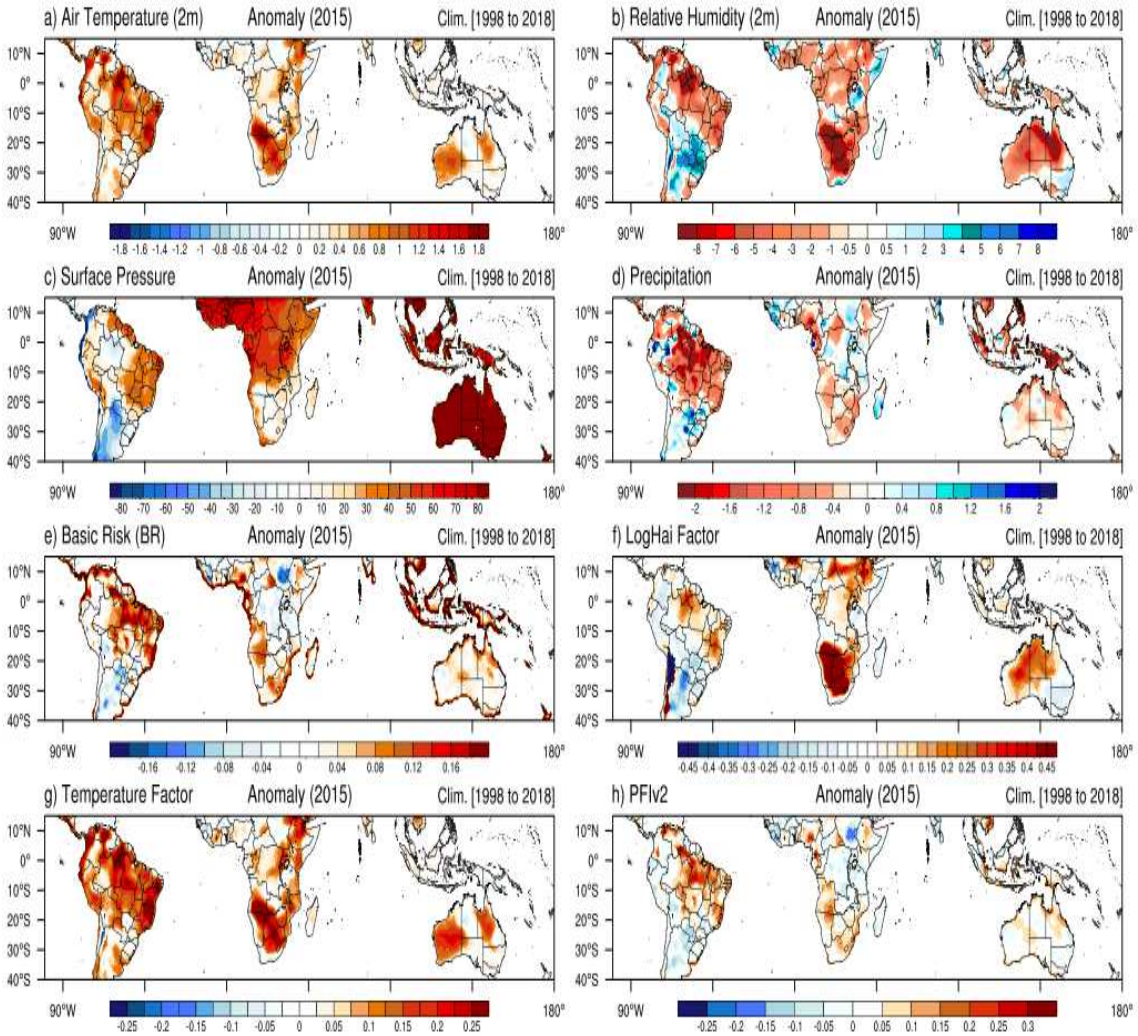

Figure 6.12. Anomalies in *(a)* maximum temperature at 2 m (°C), *(b)* relative humidity (%), *(c)* surface pressure (hPa), *(d)* precipitation (mm/day), *(e)-(g)* PFIv2 factors, and *(h)* PFIv2 distribution for 2015 (El Nino event) with respect to climatology from 1998 to 2018.

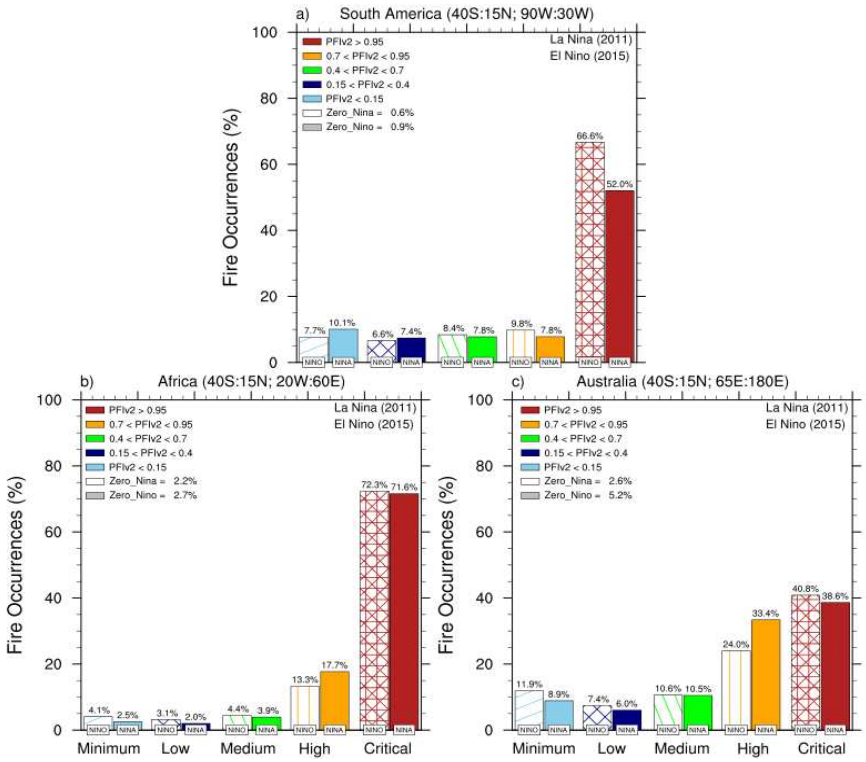

Figure 6.13. Percentage of accumulated daily fire at each PFIv2 level in *(a)* South America; *(b)* Africa; and *(c)* Australia on La Nina (2011) and El Nino (2015) events. ZERO indices are the percentage of fire events that were observed in a level closest to zero by PFIv2 (displayed in the top left corner of each panel).

CAPÍTULO 7
CONCLUSÕES E PERSPECTIVAS FUTURAS

Baseado no Índice de Risco Potencial de Fogo versão 2 (PFIv2), este trabalho avaliou a suscetibilidade da vegetação ao fogo, segundo as condições atmosféricas do presente. O índice revelou-se como uma ferramenta útil no entendimento da distribuição global do fogo em vegetação. Isso só foi possível devido à base já consolidada do PFI.

Demonstrou-se que a modificação proposta no PFIv2 pôde reproduzir as regiões com as maiores incidências de incêndios na Ásia, América do Norte e Europa. Embora o aprimoramento priorize as regiões extratropicais, o modelo também foi eficiente nos trópicos, cujas ocorrências de queimadas sazonais superaram a 400 mil eventos. A nova correção do fator de temperatura do ar, devido às variações da latitude e a função logística de Haines atuam em função de parâmetros locais, tais como: elevação da topografia e latitude.

A aplicação das novas variáveis com potencial de melhora apresentou desempenho superior a 11% na Europa, em relação ao PFI. Apesar do aprimoramento na metodologia do modelo, convém mencionar que fora dos trópicos e sob condições sazonais pouco propícias à ocorrência de queimadas, o modelo diverge em sua representatividade.

A construção do artigo intitulado "*IMPROVEMENT OF THE POTENTIAL WEATHER FIRE INDEX ON A GLOBAL PERSPECTIVE*" (Capítulo 5) mostrou que o modelo depende, principalmente, da variável de precipitação. Nos testes de sensibilidade do modelo, notou-se que o nível de complexidade em estimar a precipitação, pelos projetos de reanálises com ou sem assimilação de dados, limita o funcionamento completo do índice.

Os resultados do PFIv2, devido às diferentes fontes de precipitação foram superiores a 63% com o CPC (com assimilação de dados observados) e 52,8% com o ERAI (sem assimilação de dados observados). Isso é verificado principalmente na África, com níveis de acerto de 88,4% (CPC) e 78% (ERAI), nas classes máximas (alto e crítico) do PFIv2. Logo, pode-se considerar que o modelo é eficiente em sua representatividade. Pois sendo de complexidade intermediária, se equipara a modelos mais robustos, utilizando-se de poucas variáveis, que geralmente são de fáceis aquisições.

Vale ressaltar que nas regiões tropicais, as contribuições do PFIv2 foram de 73% e 75% nas classes máximas, durante eventos de La Niña e El Niño, respectivamente. Sabe-se que as queimadas, em sua grande maioria, possuem origens antropogênicas. Contudo, o modelo não visa a fonte de ignição, mas a verificação da suscetibilidade da vegetação aos incêndios. Implicitamente, pode-se afirmar que tais considerações estão inseridas na formulação do PFIv2, pois independentemente da fonte de ignição, as condições climáticas precisam ser propícias para a existência do fogo.

Como perspectivas futuras, projeta-se a combinação do PFIv2 com outros modelos, para verificar como a temperatura, precipitação, raios, densidade populacional e variações no uso da terra podem favorecer as condições de fogo, em condições de mudanças climáticas.